

Interactions of "Forever Chemicals" – Per and Polyfluoroalkyl Substances with Dissolved Organic Matter Extracted from Commonly Employed Soil Organic Amendments

by

John Lawhon

A thesis submitted to the Graduate Faculty of
Auburn University
in partial fulfillment of the
requirements for the Degree of
Master of Science

Auburn, Alabama
December 10, 2022

Copyright 2022 by John Lawhon

Approved by

Yaniv Olshansky, Chair, Assistant Professor, Crop, Soil, and Environmental Sciences
Yucheng Feng, Professor of Crop, Soil, and Environmental Sciences
Audrey Gamble, Assistant Professor of Crop, Soil, and Environmental Sciences

Abstract

Per- and polyfluoroalkyl substances (PFAS) are a large group of chemicals that are highly persistent and ubiquitous in the environment. These compounds, known for their adverse effects on humans and the ecosystem, reach farmlands with irrigation water and land application of biosolids. The fate and bioavailability of PFAS in the soil environment are fundamentally influenced by their interactions with dissolved organic matter (DOM), the concentration of which in soil solutions is elevated due to land application of organic amendments. The development of efficient risk assessment and treatment strategies requires an understanding of the underlying mechanisms of PFAS interactions with DOM and its effect on contamination spread in the soil and water medium.

This study examined the interactions of perfluorooctane sulfonate (PFOS) and perfluorooctanoic acid (PFOA) with DOM extracted from class B biosolids, animal manure, and plant derived composts, and a humic acid standard. The molecular structure of the DOM was analyzed using UV-vis absorbance, fluorescence excitation-emission matrices (EEM) coupled with Parallel Factor (PARAFAC) analysis, Fourier Transform Infrared (FTIR) spectroscopy, and size exclusion chromatography. The PFOS – DOM binding interactions were assessed using equilibrium dialysis and fluorescence quenching. Furthermore, to evaluate the impact of DOM on PFAS transport in soils, the adsorption and desorption of PFOS were measured using the B horizon of Gwinnett and Vaiden soil.

Results demonstrate distinct molecular properties of DOM extracted from the different types of organic amendments. The biosolids have a large proteinaceous content, lower aromaticity, and moderate molecular weight. In contrast, plant-derived compost and humic acid are composed of a larger aromatic molecular structure and lessened proteinaceous content. DOM obtained from

biosolid and manures exhibited the strongest interactions with PFOS ($K_{\text{DOC}} = 91,724 \text{ L kg}^{-1}$), while DOM of humic acid displayed the weakest ($K_{\text{DOC}} = 7,157 \text{ L kg}^{-1}$). Binding of PFOS to DOM was correlated with the proteinaceous content ($r = 0.71$), carboxyl group content ($r = 0.55$), aromaticity ($r = 0.70$), and negatively correlated with degree of humification ($r = -0.81$). Fluorescence quenching results indicated direct interactions of PFOA and PFOS with humic and proteinaceous fluorophores, where up to a 50% decrease in fluorescence intensity of humic and proteinaceous fluorophores was noted. Moreover, following reaction with PFOS and PFOA, fluorescence intensity increased by up to 50% for fluorophores associated with humic and proteinaceous DOM extracted from biosolids, poultry litter, and humic acid. These results suggest that DOM undergo structural and compositional changes when interacting with PFAS. In the presence of DOM from biosolids, aged poultry litter, and public works compost, the adsorption of PFOS on Gwinnett soil increased by up to 120%, whereas DOM extracted from humic acid and peat moss decreased adsorption by 52%. Similar results were observed for the Vaiden soil. However, the highest increase in adsorption (122%) was observed in the presence of aged poultry litter DOM. Adsorption-desorption isotherms indicated pronounced hysteresis behavior, dependent on the presence and type of DOM in the adsorption reaction step, implying the importance of PFOS-DOM-soil ternary complexes. This study demonstrated a strong potential for using DOM molecular descriptors as predictors for the behavior of anionic PFAS in the soil and water environment. Importantly, the use of DOM descriptors and distribution coefficients have potential for further use in modeling efforts to predict the transport of PFAS in the environment. Further research should focus on establishing DOM molecular descriptors and binding coefficients between short and longer chain PFAS as well as zwitterionic and cationic moieties rather than just anionic.

Acknowledgements

I owe a special thanks to my Chair, Dr. Yaniv Olshansky, without his guidance and support this research would have not been possible. My utmost gratitude goes out to Dr. Jianping Wang in the department of Crop Soil and Environmental Sciences for her unrelenting support in the lab throughout the duration of this project. Thank you to the United States Geological Survey and the Alabama Water Resources Research Institute for providing the funding and full research support. Finally, I would like to thank my family and friends for the continued support along the way throughout my studies here at Auburn University, their support cannot be understated.

Table of Contents

Abstract.....	2
Acknowledgments.....	4
List of Tables	6
List of Figures.....	8
List of Abbreviations	10
Chapter 1: Introduction.....	11
1.1 PFAS Contamination.....	11
1.2 Route of PFAS to the Environment.....	12
1.3 PFAS Health Concerns.....	15
1.4 PFAS Impact on the Environment.....	16
1.5 PFAS Fate in the Soil.....	18
1.6 Dissolved Organic Matter Characterization.....	20
1.7 PFAS Interactions with DOM.....	21
Chapter 2: Materials and Methods.....	26
2.1 Materials.....	26
2.2 DOM Extraction.....	27
2.3 Soils.....	29
2.4 DOM Characterization.....	31
2.5 Dialysis Equilibrium.....	33
2.6 Batch Sorption Desorption Experiments.....	33
2.7 Fluorescence Quenching Experiments.....	34
2.8 PFOS Quantification.....	35
2.9 Data Analysis.....	36
Chapter 3: Results.....	40
3.1 UV-VIS and Absorbance Indices.....	40
3.2 Fluorescence Indices.....	44
3.3 PARAFAC Derived Components.....	45
3.4 FTIR.....	49
3.5 DOM Molecular Weight.....	53
3.6 Dialysis Equilibrium Experiments with PFOS.....	55
3.7 Fluorescence Quenching.....	56
3.8 PFOS Adsorption on Soils.....	60
3.9 PFOS Adsorption and Desorption on Vaiden Soil	65
3.10 Pearson Correlation Coefficients between K_{DOC} , K_d , and DOM Descriptors.....	68
Chapter 4: Discussion and Conclusion.....	71
4.1 Differences in Chemical Properties of DOM Sources.....	71
4.2 PFOS Adsorption.....	74
4.3 Conclusion.....	78
Appendix.....	81

List of Tables

Table 1. Selected PFAS and their characteristics.....	26
Table 2. List of DOM and the solid organic amendments used for their extraction.....	28
Table 3. Selected physical and chemical properties of the soils.....	30
Table 4. UV absorbance and fluorescence indices of the selected DOM sources.	41
Table 5: Summary of excitation and emission wavelengths corresponding to fluorescence components observed in PARAFAC components.....	45
Table 6: Peak assignments used to evaluate the transmission FTIR spectra of DOM.....	49
Table 7. FITR indices of the selected DOM.....	52
Table 8: Reports molecular weight values found from HPSEC analysis of DOM sources. M_w refers to weight average molecular weight while M_n represents number average.....	53
Table 9: Freundlich fitting parameters of PFOS adsorption to Gwinnett and Vaiden soil and distribution coefficients calculated for C_e of 20 and 300 $\mu\text{g L}^{-1}$	61
Table 10. Freundlich coefficients for adsorption isotherms of PFOS on Vaiden soil (mean (standard deviation), $n = 3$).....	65
Table 11. Pearson Correlation matrix between DOM characterization indices, K_{DOC} , and K_d values found from batch sorption experiments employing the Gwinnett and Vaiden soils.....	69
Table A1. TOC (mg L^{-1}), texture, as well as PFOA and PFOS (ng g^{-1}) concentrations in DOM extracts.....	99

List of Figures

Figure 1. UV-Vis absorbance spectra of the selected DOM.	42
Figure 2. Fluorophores contours of components obtain from the PARAFAC model (top) and 2D representation of the component loading (bottom).....	46
Figure 3. Distribution of PARAFAC components (%) in each of the tested DOM.	47
Figure 4. Transmission FTIR spectra of freeze-dry DOM. DOM names in this image were named based on DOM abbreviations seen in Table-1. The symbol ν indicates stretching of the specified bonds in Table-5. Specifically, ν_{as} indicates asymmetric stretching, ν_s indicates symmetric, and $\nu >$ indicates broad stretching. The symbol δ indicates bending.....	50
Figure 5. Distribution coefficients (K_{DOC} , from highest to lowest value) of PFOS between aqueous solution and DOM.	55
Figure 6. Fluorescence quenching of the DOM fluorophores by PFOA and PFOS. The fluorophores intensity was normalized to PFAS free DOM solution. Fluorophores are described in Table	58
Figure 7. Impact of DOM on adsorption of PFOS on Gwinnett soils.....	62
Figure 8. Impact of DOM on adsorption of PFOS on Vaiden soils.....	63
Figure 9. Impact of DOM on adsorption and desorption of PFOS on Vaiden soil.....	66
Figure A1. Sorption of PFOS on Gwinnett using varying solution:soil ratios.....	80
Figure A2 Sorption kinetics of PFOS on Gwinnett.....	81
Figure A3. Sorption and desorption kinetics of PFOS on Vaiden.....	82
Figure A4. Represents outliers and leverage plot for resulting three component PARAFAC model.....	83

Figure A5-13. DOM samples residuals from derived PARAFAC model.....84-88

Figure A14. Resulting split-half analysis from validation of 3-component PARAFAC model.....89

Figure A15-30. 2-D Fluorescence quenching results for all DOM vs PFOA and PFOS at five concentrations.....90-97

Figure A31. Fluorescence distribution of PARAFAC components in each of the tested DOM.....98

Abbreviations

AEC	Anion Exchange Capacity
CEC	Cation Exchange Capacity
DOM	Dissolved Organic Matter
fDOM	Fluorescent Dissolved Organic Matter
cDOM	Chromophoric Dissolved Organic Matter
SOM	Soil Organic Matter
EEM	Excitation Emission Matrix
FTIR	Fourier Transform Infrared Spectroscopy
PARAFAC	Parallel Factor Analysis
K_d	Distribution Coefficient
PFAS	Per and Polyfluoroalkyl Substances
PFOA	Pentadecafluorooctanoic
PFOS	Perfluorooctanesulfonate
UV-Vis	Ultraviolet-Visible Spectroscopy
WEOC	Water Extractable Organic Carbon

Introduction

1.1 PFAS Contamination

Per- and polyfluoroalkyl substances (PFAS) represent a group of over 4000 anthropogenic organo-fluorine compounds. PFAS are a surfactant, containing a hydrophilic head (e.g., carboxylate, sulfonate) and alkyl chain where all (perfluoroalkyl) or some (polyfluoroalkyl) of the hydrogen substituents are replaced by fluorine, such that the perfluoroalkyl moiety contains $C_nF_{2n+1}-R$ (Buck et al., 2011). Due to fluorine's small atomic size and strong electronegativity, PFAS imparts enhanced properties to molecules such as higher surface activity at low concentrations and oil or water repellency (Sunderland et al., 2019). Such characteristics led to the extensive use of PFAS in industrial and commercial products such as waterproof clothing, food contact materials, non-stick cookware, household products, outdoor equipment, inks, oil production, pesticides, leather, textiles, cosmetics, and medical devices (Wang et al., 2017; Sunderland et al., 2019). In addition, PFAS is an active ingredient in aqueous film-forming foams (AFFF) used to extinguish flammable liquid fires such as fuel fires at airports and military installations for firefighting and training activities (Sunderland et al., 2019).

The unique and strong carbon-fluorine bond makes PFAS highly persistent against biological, chemical, and physical degradation under environmental conditions. Some PFAS such as perfluorotelomers may undergo chemical transformation under environmental conditions. However, the transformation end products are usually the resistant perfluoroalkyl or perfluoroalkyl(poly)ether acids (Wang et al., 2017). Therefore, PFAS are classified as persistent organic pollutants (POPs, Ahmed et al., 2015). Furthermore, unlike other non-polar HOC's, many stable PFAS are anionic under environmental conditions (Buck et al., 2011).

1.2 Route of PFAS to the Environment

Due to the wide use of PFAS in commercial products and industrial processes, PFAS can be released to the environment from a wide range of sources, including direct discharge of industrial wastes, land applied biosolids, and the use of AFFF (Sunderland et al., 2018; Costello and Lee, 2020). PFAS has a relatively high-water solubility, making water the main vehicle of transfer across environmental compartments and biota. PFAS have been found to be directly emitted to the environment next to chemical manufacturing facilities as well as industrial sites where PFAS is commonly used (Sunderland et al., 2019). Such pollution resulted in PFOA concentrations reaching 3550 ng L⁻¹ in one public water supply (Sunderland et al., 2019). In the United States, long-term use of AFFF has been proposed as a primary contributor of PFAS to groundwater near airports and military bases, where PFOA concentrations can be hundreds of orders of magnitude higher than the US EPA health advisory level of 0.002 ng L⁻¹ for drinking water (Hu et al., 2016; Cui et al., 2020; Johnson et al., 2022). Landfills in China were suggested as a primary source of groundwater contamination that may pose a high risk of contaminating drinking water supplies (Banzhaf et al., 2017). Electronic waste has been identified as additional source of perfluorooctane sulfonate (PFOS) to landfills and waste processing sites due to PFOS being a primary constituent in the production of metal plating, with PFOS being found to range from 0.07–0.43 µg kg⁻¹ in these e-products (Garg et al., 2020). The relatively high solubility of PFAS making them mobile in soils, surface and groundwater, and available to plant roots for uptake (Zhao et al., 2016; Ghisi et al., 2019). Volatile precursors such as FTOH, have been found to undergo atmospheric oxidation, leading to PFAS being transported to remote regions such as the High Arctic (Young et al., 2007; Kwok et al., 2013), where anthropogenic activities would not be expected to contribute substantial PFAS contamination.

Soils are an important reservoir of PFAS (Brusseau et al., 2020). Near military installations where AFFF had been used, soils were found to contain widespread contamination of 19 types of PFAS including short ($C < 7$) and long chain perfluorocarboxylic acids and sulfonates such as PFOA and PFOS, as well as ultra-short ($C < 3$) perfluoroalkyl sulfonic acids such as perfluoroethanesulfonate (PFES) and perfluoropropanesulfonate (PFPrS) (Barzen-Hanson and Field., 2015; Anderson et al., 2016). Furthermore, transport modeling conducted at contaminated sites also indicated soils to represent a long-term source of PFAS for the surrounding environment (Shin et al., 2011; Xiao et al., 2015; Weber et al., 2017). In some contaminated soils, the concentration of PFOS reached $160 \mu\text{g kg}^{-1}$ concentration (Brusseau et al., 2020). In agricultural environments, multiple pathways exist that lead to PFAS contamination in soils, such as land application of biosolids, irrigation with PFAS-contaminated water, leaching from landfilled wastes, and biosolid-based fertilizer application (Taniyasu et al., 2013; Blaine et al., 2014; Liu and Liu., 2016; Johnson et al., 2022). Specifically, 50% of US biosolids produced by wastewater treatment are disposed through land application, highlighting an important source of PFAS to agricultural soils (Lindstrom et al., 2011).

Although great attention has been given to persistent organic pollutants in wastewater treatment effluents and biosolids, only in the last decade have concerns arisen regarding PFAS in wastewater effluents and treatment by products (Lindstrom et al., 2011; Sunderland et al., 2019). Wastewater treatment plants tend to receive large PFAS quantities through influents such as landfill leachates and discharge from industrial and consumer point sources (Becker et al., 2008; Sunderland et al., 2019). Current standard wastewater treatment protocols do not actively remove PFAS. In addition, the transformation of precursors in the treatment processes results in increasing effluent concentrations of the more persistent perfluoroalkyl acids relative to influent (Hu et al.,

2016). As municipal wastewaters and biosolids are released into the environment or applied as soil organic amendments, PFAS can be directly added to surface waters and agricultural soils (Becker et al., 2008; Lindstrom et al., 2011; Venkatesan and Halden., 2013; Costello and Lee., 2020).

Alabama is a hotspot for PFAS contamination due to the presence of production facilities, military installations, and a large volume of streams and rivers (Vitikoski et al., 2022). Out of 74 riverine samples retrieved from ten river basins in Alabama, 65 were found to contain at least six of the seventeen types of PFAS tested, with the average concentration being 35 ng L⁻¹. The most common type of PFAS identified in surface water was for perfluoropentanoic acid (PFPeA). Furthermore, the Coosa River contained the largest PFAS concentration of 237 ng L⁻¹, which was attributed to large quantities of waste that are discharged from local carpet and textile industries that have their effluents treated by a municipal wastewater treatment plant in Dalton, Georgia, located at the headwaters of the Coosa River. Historical production of PFAS from fluorotelomer facilities in Decatur, AL also led to extensive PFAS contamination in soils as well as ground and surface waters near these facilities (Lindstrom et al., 2011; Newton et al., 2017). Samples taken from a local wastewater treatment plant that collected waste from these fluorochemical facilities contained PFOS and PFOA concentrations of up to 3000 and 244 µg g⁻¹ in sewage and 5 and 2 µg L⁻¹ in effluent water respectively (Newton et al., 2017). Over 34,000 dry metric tons of fluorochemical industry impacted biosolids, from this wastewater treatment plant, were supplied as organic amendments to local farmers on approximately 2000 ha of agricultural fields in Limestone, Lawrence, and Morgan counties in Alabama. This application of PFAS contaminated biosolids led to elevated PFOA concentration up to 6,410 ng L⁻¹ in well water and 11,000 ng L⁻¹ in surface waters (Newton et al., 2017). Downstream of Decatur in the West Morgan-East Lawrence Water Authority (approximately 12 miles SW from Decatur), PFOA and PFOS were

found to range as high as 130 and 100 ng L⁻¹ in drinking water supplies, respectively. This resulted in the West Morgan-East Lawrence Water Authority to advise 100,000 customers to not drink their tap water due to contamination exceeding the EPA health advisory level of 70 ng L⁻¹ (Newton et al., 2017; EPA., 2016). It was also demonstrated that these biosolids applications led to PFOS and PFOA concentrations reaching 410 ng g⁻¹ and 320 ng g⁻¹ in soils respectively, but the highest level of contamination was identified for perfluorodecanoic acid (PFDA) and perfluorododecanoic acid (PFDoA), which exceeded 950 ng g⁻¹ and 500 ng g⁻¹ respectively (Washington et al., 2010). Furthermore, contaminated biosolid application to agricultural soils even lead to accumulation of PFOA and PFOS in crops meant for human consumption, where concentrations in plant tissues were documented to reach 200 and 170 ng g⁻¹ respectively (Washington et al., 2010).

1.3 PFAS Health Concerns

Humans are chronically exposed to PFAS through consumption of contaminated foods and drinking water (Jogsten et al., 2009; Sunderland et al., 2019). Human exposure to PFAS has associated adverse health effects, including, high cholesterol (Nelson et al., 2010), thyroid disease (Lopez et al., 2012), pregnancy-induced hypertension (Darrow et al., 2013), ulcerative colitis (Steenland et al., 2013), developmental toxicity (Lau et al., 2004; 2007), cell membrane disruption and genetic damage (Gong et al., 2019), as well as kidney and testicular cancers (Barry et al., 2013). Specific PFAS moieties such as PFOS have been linked an increase in liver weight, liver cell hypertrophy, histopathological changes to lungs, decreased hormone levels, decreased reproductive outcomes, and development delays (Pizzurro et al., 2019). PFOA and PFOS have been detected in trace levels in human breastmilk, representing a significant pathway for infant exposure to PFAS (Antignac et al., 2013; Zheng et al., 2021). A study conducted from 2011–2012 by the U.S. National Health and Nutrition Examination Survey found that 97% of over 1600

individuals aged 12-60, had detectable PFAS concentrations in the blood serum (Grandjean et al., 2012). Due to PFASs biomagnification tendencies, increased levels of PFASs in animal-derived foods has been found, especially in fish (Kantiani et al., 2010). Migration of PFASs from food packaging is also a significant pathway of human exposure (Begley et al., 2005; Tittlemier et al., 2005). Due to the posing health risks, the United States Environmental Protection Agency (US EPA) established a lifetime advisory level of 0.004, 0.02, 10, and 2,000 parts per trillion (ppt) in drinking water for the concentrations of perfluorooctanoic acid (PFOA), perfluorooctane sulfonate (PFOS), hexafluoropropylene oxide (HFPO; GenX), and perfluorobutane sulfonic acid (PFBS) (PFBS, EPA., 2022) and has also developed a strategic plan aimed at researching PFAS exposure and toxicity, restricting PFAS entering the environment as well as the remediation of PFAS contaminated lands (PFAS Strategic Roadmap, US EPA., 2021). Starting in February of 2023, the European Union (EU) will begin phasing out and banning the use of over 200 PFAS, marking the first time that the EU has imposed bans on chemicals with similar structures and properties all at once.

1.4 PFAS Impact on the Environment

PFAS has been identified in several environmental matrices such as air, surface, and ground waters, as well as soil and sediments (Young et al., 2007; Newton et al., 2017; Brusseau et al., 2020; Vitikoski et al., 2022). Transport of PFAS in the environment occurs through aqueous and atmospheric media, abiotic solid-phase partitioning, and eventually leads to bioaccumulation in wildlife, plants, and humans. PFAS has a relatively high-water solubility, making water a main vehicle of transfer across environmental compartments and biota. In agricultural systems, PFAS-contaminated soils have been found to lead to PFAS accumulation in important crops meant for human consumption and livestock feed such as maize, wheat, potatoes, carrots, and cucumbers

(Ghisi et al., 2019; Wang et al., 2020). PFAS uptake by crops depending on PFAS concentration, chain length, and functional group, where short chain PFAS (C4-C6 compounds) accumulated in leaves and fruits while long chain PFAS were more concentrated in the roots of the selected plants (Ghisi et al., 2019). Furthermore, the abundance and characteristics of soil organic matter were considered one of the most important factors governing plant sorption of PFAS (Ghisi et al., 2019). Ghisi (2019) also recommended that plant residues, such as maize stover, be avoided in animal feeds since such practices were found to lead to contaminated food chains. Considering agricultural crops constitute a major portion of livestock and human diets, consumption of PFAS-laden food represents an important route responsible for the accumulation of PFAS in animals and humans (van Asselt et al., 2011; Blaine et al., 2014). Importantly, higher predatory organisms such as mammals contain larger amounts of PFOS than lower predatory organisms (Kannan et al., 2005). PFAS has been shown to be capable of bioaccumulation in organisms, and bioaccumulation generally increases with perfluoro-alkyl chain length (Martin et al., 2009). Studies investigating PFAS impact on Arctic marine food webs found substantial PFAS concentrations in seabirds, fish, and ice amphipods, ranging from 3.85-65.8 ng g⁻¹ of PFOS (Haukås et al., 2007). Importantly, Haukås (2007) also found PFOS concentrations up to 225 ng g⁻¹ in livers of glaucous gull's.

Earthworms are a common species used to evaluate the toxicity of compounds in the soil environment, and as an indicator for the overall health of a soil system (Baylay et al., 2012). Xu et al. (2013) noted decreased growth in *Eisenia fetida* following a 14 and 42-day exposure to 120 mg kg⁻¹ PFOS-contaminated soil, while reporting no changes on growth at 80 mg kg⁻¹. Furthermore, Zareitalabad et al. (2013) found survival was less than 40% out of a total of five adult earthworms (*Aporrectodea caliginosa*) when they were exposed to 100 mg kg⁻¹ of PFOA and PFOS. While both studies highlight the negative impacts PFAS have on these soil organisms, the concentrations

causing negative impacts occur at environmentally irrelevant concentrations, showing very low risk of PFOS and PFOA affecting earthworms at concentrations relevant to soils and soil-solution. However, adverse effects may persist under environmentally relevant conditions and concentrations where long term exposure to PFAS can occur. It is important to note that while PFAS may not pose a toxicological threat to terrestrial organisms, Zhao (2014) and Sunderland (2019) proposed that PFAS in soil can bioaccumulate in earthworms and plants.

1.5 PFAS Fate in the Soil

Following their introduction to soils, the fate and bioavailability of PFAS are controlled by its interactions with the soil's mineral and organic constituents, as well as retention in the air-water interfaces (Higgins and Luthy, 2006; Li et al., 2018; Lyu et al., 2018; Bolan et al., 2021). PFAS sorption to soils increases with increasing perfluoroalkyl chain length (Costello and Lee., 2020). Hydrophobic and electrostatic interactions with soil organic matter (SOM) have been suggested as the main modes of interaction governing PFAS adsorption in soils (Higgins and Luthy, 2006; Jeon et al., 2011; Du et al., 2014; Wei et al., 2017). Electrostatic repulsion forces between PFAS anionic head-group and negative charge of soil surfaces, tend to decrease PFAS adsorption. However, positive charges of organic matter moieties and Fe and Al bearing minerals may facilitate electrostatic attraction.(Li et al., 2018; Sigmund et al., 2022). Soils net negative surface charge tends to decrease with decreasing pH, therefore, anionic PFAS sorption to organic matter has been found to increase at low pH (Higgins and Luthy, 2007; Campos Pereira et al., 2018; Zhi and Liu, 2019). Ionic strength and divalent cationic species such as Ca^{2+} and Mg^{2+} also affect PFAS adsorption (Higgins and Luthy, 2007; Li et al., 2018). Increasing concentrations of Ca^{2+} and Mg^{2+} were found to directly increase PFAS sorption, where the effects of Ca^{2+} and Mg^{2+} on sorption were attributed to a reduction in the charge present on the organic matter (Higgins and

Luthy, 2007; You et al., 2010; Li et al., 2018). However, no evidence has been presented suggesting that monovalent cations such as K^+ and Na^+ significantly affect PFAS sorption (Higgins and Luthy, 2007; Wang et al., 2015). Under natural conditions, SOM carries a net negative charge resulting from the presence of dissociated carboxylic and phenolic acid groups (Kinniburgh et al., 1999). Such dissociated functional groups determine a soils ability to bind positively charged cations via cation exchange capacity (CEC). Anionic PFAS sorption to soils is expected to be inversely related to CEC. However, cationic and zwitterionic PFAS species tend to have a large affinity for soils with large CEC such as those in agricultural settings (Li et al., 2018; Costello and Lee, 2020). While numerous soil characteristics affect the fate of PFAS, a fraction of SOM, termed dissolved organic matter (DOM), has been identified as an important soil fraction directly influencing PFAS transport in soil. When present together, DOM enhances soil adsorption of PFAS (Liu and Lee., 2005), increases PFAS solubility (Carmosini and Lee., 2008), and even influences the bioavailability of PFAS (Xia et al., 2015). Importantly, DOM adsorption of PFAS has been identified to be affected by the concentration and composition of DOM (Liu and Lee., 2005; Carmosini and Lee , 2008; Longstaffe et al., 2016). However, DOM is often an overlooked soil component when it comes to the fate of PFAS in the environment, leading to limited research regarding DOM impact on PFAS sorption.

1.6 Dissolved Organic Matter Characterization

Dissolved organic matter (DOM) is operationally defined as any organic matter in the solution that passes through a $0.45\mu\text{m}$ filter (Bolan et al., 2011). Other definitions include 0.2 or $0.7\ \mu\text{m}$ thresholds (Zsolnay., 2003; Bolan et al., 2011). DOM is a heterogenous mixture of aggregated organic molecules composed of carbohydrates, proteins, lipids, plant, animal, and microbial remnants in addition to synthetic organic compounds such as surfactants (Bolan et al.,

2011). The chemical and physical properties of DOM greatly depend on input organic molecules, weather regimes, pH, ionic strength, and composition of biota surrounding the site (Bolan et al., 2011).

Plant litter and humus are the most important sources of DOM in soil, since the decomposition of litter and humus in surface-near, organic-rich soil compartments results in the production of soluble organic compounds (Bolan et al., 2011; Kaiser and Kalbitz, 2012). Plant residues also serve as a major source of DOM in soils (Bolan et al., 2011). Due to the heterogeneous composition of organic compounds derived from decomposition of plant materials, DOM can be grouped into "labile" and "recalcitrant" matter (Marschner and Kalbitz, 2003; Bolan et al., 2011) as well as separation into different molecular weight (MW) compounds. Labile DOM is composed of relatively low molecular size (< 1 nm) compounds such as amino sugars, low MW proteins, as well as simple carbohydrates such as glucose and fructose (Kaiser et al., 2009; Bolan et al., 2011), which is more commonly seen from DOM extracts of biosolids or raw poultry litters (Bolan et al., 2011). Recalcitrant DOM is composed of larger proportion of plant derived compounds such as lignin, polysaccharides and other plant biopolymers or their microbial transformation products (Marschner and Kalbitz, 2003; Bolan et al., 2011). Soil solutions however are comprised of both recalcitrant and labile DOM such as carbohydrates, low MW carboxylic acids and amino acids (Bolan et al., 2011), owing to their overall heterogeneous chemical composition.

The amount of DOM in soils depends on various factors, including vegetation type and land management practices such as lime, fertilizer, and application of organic amendments (Bolan et al., 2011). The application of organic amendments to improve soil properties and as partial or full substitutes to inorganic fertilizers, can rapidly increase DOM concentration in the upper 30

cm of the soil by more than 100 mg C kg soil⁻¹ (Rochette and Gregorich, 1997). While this increase is short-lived, due to transport and microbial degradation, long-term application of organic amendments has been shown to result in net increases of DOM concentration by 46% (Murphy et al., 2000; Chantigny, 2003; Boddy et al., 2007). In addition, the type of organic amendment will dictate the molecular structure and composition of the associated DOM (Bolan et al., 2011). For example, Brazilian Oxisols amended with biosolids resulted in DOM extracted from the soil to be composed of components of relatively small molecular size, with a low level of aromatic polycondensation and degree of humification when compared to the same soil without amendment (Bertoncini et al., 2005).

1.7 PFAS Interactions with DOM

PFAS can interact with DOM through electrostatic interactions, hydrogen bonding, hydrophobic adsorption and partitioning, as well as van der Waals forces (Longstaffe et al., 2016; Carmosini and Lee, 2008; Xiao et al., 2019; Du et al., 2014). The oxygen atoms present in the variable head group of PFAS (e.g., carboxylate, sulfonate) make hydrogen bonding possible with DOM (Schwarzenbach et al., 2003; Carmosini and Lee, 2008; Du et al., 2014). Such interactions will allow for PFAS to interact with specific functional groups contained in the DOM molecule, such as -NH, -OH, -COOH (Du et al., 2014). Electrostatic interactions have been identified as a primary acting force between PFAS molecules and DOM constituents (Du et al., 2014; Kothwala et al., 2017). DOM contains positively charged functional groups that electrostatically attract the anionic functional group heads of the PFAS molecule (Du et al., 2014; Kothwala et al., 2017). cation bridging mechanism can facilitate interactions of anionic PFAS with negatively charged DOM moieties (Schwarzenbach et al., 2003).

PFAS has also been shown to bind to negatively charged DOM sources, overcoming electrostatic repulsion (Du et al., 2014; Carmosini and Lee, 2008). Concerning a molecule of DOM, hydrophobic assemblages are present within its molecular structure (especially on the surface of DOM molecule), such hydrophobic domains allow for the hydrophobic C-F chain of PFAS to be distributed into the hydrophobic regions of the DOM molecule, even if the DOM surface contains a negative charge (Schwarzenbach et al., 2003; Du et al., 2014). Importantly, long-chain PFAS moieties such as PFOA and PFOS are capable of forming hemi-micelles and micelles in water via the hydrophobic aggregation of C-F chains (Yu et al., 2009). This aggregation of PFAS molecules can serve as an attractive source for more PFAS molecules (Du et al., 2014).

The binding of PFOA, PFOS pentafluoroaniline and pentafluorophenol to Pahokee Peat Humic Acid were quantitatively assessed with ^1H and ^{19}F Nuclear Magnetic Resonance (NMR) spectroscopy-based diffusion measurements (Longstaffe et al., 2016). The author found that in the presence of DOM, the organofluorine diffusivity decreased by 7 – 44% compared with the DOM-free solution. Based on compound solubility and the assessed interactions with DOM, the authors conclude that hydrophobic effect-derived desolvation was the main mode of interaction (extracted from Pahokee peat) for PFOS (Longstaffe et al., 2016). In addition to the hydrophobic effect, the authors used $^1\text{H}\{^{19}\text{F}\}$ Reverse-Heteronuclear Saturation Transfer-NMR to demonstrate that PFOA preferably interacts with proteinaceous binding sites. While this study provides relevant information on the binding mechanisms, the concentrations of PFAS and DOM required for the analysis are several orders of magnitude higher ($0\text{-}20,000\text{ mg L}^{-1}$ TOC, $0.003\text{-}0.03\text{ mmol mL}^{-1}$) than relevant concentrations in the environment. The predominance of proteinaceous binding sites was also demonstrated by comparing adsorption of a series of perfluorinated carboxylic acids and

PFOS to dissolved chicken egg albumin and Sigma-Aldrich HA (Xia et al., 2015). The distribution coefficients (K_d) between PFAS (perfluoroalkyl acids, and PFOS) and DOM from HA and albumin ranged from range between 10^4 to 10^6 L kg⁻¹. A significant higher K_d values obtained for albumin, indicating the preferential binding of PFAS to proteinaceous compounds (Xia et al., 2015). Liu (2022) also employed dialysis studies investigating the bioaccumulation of PFOA, PFOS, perfluorohexanesulfonic acid (PFHxS), and commercial chlorinated polyfluoroalkyl ether sulfonic acid (Cl-PFESAs, trade name F-53B) on dissolved bovine serum albumin and HA found similar results to Xia (2015). Both HA and albumin were found to significantly inhibit bioaccumulation and translocation of four PFAS moieties, where the impacts were greater for the dissolved albumin in comparison to the HA (Liu et al., 2022). FTIR and excitation-emission fluorescence spectroscopy also revealed that HA could bind with tryptophan residues of albumin, leading to competition with PFAS for binding sites on the surface of albumin, resulting in overall lower PFAS binding in a matrix containing both HA and albumin (Liu et al., 2022).

Carmosini and Lee (2008) showed significant interactions between fluorotelomer alcohols and DOM that was dependent of the C-F chain length. The K_{DOC} (i.e., K_d normalized by DOC concentration) of 8:2 fluorotelomer alcohols (FTOHs) was up to 10^4 L kg⁻¹ making the PFAS-DOM interactions meaningful at, at least, 10 mg L⁻¹ of DOC in soil solutions (i.e., producing a 10% extent of binding). Importantly, the differences between DOM types led to the 2 order of magnitude differences in the K_{DOC} values, exemplifying that not only the concentration but also the type of DOM controls the binding of PFAS. The authors further suggest that more significant PFAS binding was expected for DOM of certain types of waste materials (e.g., landfill leachates) due to their concentrations of total organic carbon (TOC). While insights were gained regarding FTOH-DOM interactions, this study failed to provide a relevant molecular characterization of

selected DOM sources and the ubiquitous anionic perfluoro- carboxylic and sulfonic acids. Importantly, under natural conditions, DOM has also been shown to directly impact the transport of PFAS where PFAS affinity with DOM was largely dependent on PFAS chain length (Li et al., 2022), which confirms the conclusions of previous lab investigations (Carmosini and Lee., 2008). It was also identified that the hydrophobic binding and cation bridging between PFAS and DOM was due to the hydrophobicity and number of free negatively charged functional groups of both the DOM and PFAS (Li et al., 2022).

The experimental data available for characterizing PFAS-DOM interactions is very limited by few sources. The lack of environmentally relevant DOM sources commonly applied to soils must be included in a comprehensive study rather than commercial humic substances since the co-introduction of PFAS and organic materials can directly impact PFAS mobility and bioavailability. Strong indications exist, showing the PFAS-DOM interactions are DOM nature dependent, but no approach exists allowing predicting interactions of PFAS with various types of DOM. The impact various DOM sources have on PFAS adsorption to soil is also unknown. Therefore, a systematic study of the interactions between PFAS and DOM from multiple sources and the DOM impact on soil sorption is essential for the development of efficient risk assessment of PFAS-impacted agricultural ecosystems.

Research Objectives

Major Research Goal:

This study aims to develop and identify molecular DOM descriptors that can be used as quantitative predictors for the interactions between PFOS and DOM and its impact on PFOS adsorption on soils.

Specific Research Objectives:

1. Elucidate the molecular characteristics of DOM extracted from common soil organic amendments.
2. Characterization of the binding between selected DOMs and PFOS.
3. Finding relationships between DOMs molecular composition and structure and interactions with PFOS.
4. Understand the impact DOM sources have on PFAS adsorption and desorption to soils.

Hypotheses and Rationales:

- Molecular characterization of DOM sources from different organic amendments will result in varying chemical compositions reflected in characterization results.

Rationale: Molecular composition of DOM sources has been shown to be directly influenced by environmental conditions as well as the quantity and quality of organic material. For instance, biosolids are expected to have a higher content of proteinaceous and fatty acid DOM in comparison to plant derived products (such as humic acid) that are more enriched with lignin like components. This difference is attributed to the provenance of the organic materials, where municipal wastewater treatment plants experience an income of high nutrient load materials that are rich in nitrogen where effluents contain relatively high C/N ratios, hence heightened protein and fatty acid composition is expected for a biosolid sourced DOM.

- Molecular composition of DOM sources will significantly impact binding affinity of PFOS to DOM.

Rationale: (a) The presence of hydrophobic aromatic and aliphatic groups presents great potential for hydrophobic interactions between the fluorinated tail and DOM. (b) PFOA and PFOS have been shown to preferentially interact with protein like fraction of DOM.

(c) Increased fractions of negatively charged DOM components will increase electrostatic repulsion of carboxylate and sulfonate head groups.

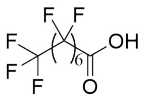
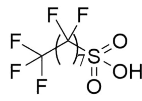
Materials and Methods

2.1 Materials

Ultrapure water (18.2 MΩ) was obtained using the Smart2Pure system (Thermo Scientific, Waltham, WI). KBr was purchased from Pike Technologies (Pike Technologies, Fitchburg, WI). HCl and NaOH were purchased from VWR (VWR, Randor, PA). Glucose Monohydrate was purchased from J.T. Baker (J.T Baker, Phillipsburg, NJ). Polystyrene sulfonate (Mw 1,600; 4,600; 7,420; 15,800 Da) was purchased from American Polymer Standards Cooperation (OH, USA), acetone (≥99.5 %) was purchased from VWR (OH, USA), and guanosine (≥98%) was produced by Thermo Fisher Scientific (UK).

Pentadecafluorooctanoic Acid (PFOA) and potassium perfluorooctanesulfonate (PFOS) were purchased from TCI America Inc. (TCI Inc, Portland, OR) and Matrix Scientific (Matrix Scientific, Columbia, SC) respectively (Table 1). Isotopically labeled Internal M8PFOS and M8PFOA standards were purchased from Wellington Laboratories (Guleph, ON).

Table 1. PFAS and selected physical and chemical properties.

Name	PFOA	PFOS
Formula	C ₈ HF ₁₅ O ₂	C ₈ HF ₁₇ O ₃ S
Structure		
pK _a *	<1	<1
Aqueous solubility* (mg L ⁻¹ 25°C)	3300	910
LogK _D *	1.58	3.05

* Values obtain from Chemcilze (<https://chemicalize.com/app/calculation>)

$$* \text{Log}D = \log \left(\frac{[\text{solute}]_{\text{octanol}}}{[\text{solute}]_{\text{water}}^{\text{ionized}} + [\text{solute}]_{\text{water}}^{\text{neutral}}} \right)$$

2.2 DOM Extraction

The organic amendments used for DOM extraction are listed in Table 2, and includes plant and animal wastes composts, biosolids from municipal wastewater treatment and humic acid standard. Immediately after sampling, the composts and sludge-based organic amendments were stored at 4°C until used for DOM extraction.

DOM was extracted from the organic amendments by mixing a homogeneous sample with ultrapure water (1:5 g g⁻¹). Fifty grams of air-dry organic amendment were added to 250 mL polypropylene Nalgene[®] (Rochester, NY) container with 125 mL of ultrapure water. The suspensions were placed on a reciprocal shaker (Lab-Line, Dubuque, Iowa) at 150 oscillations per minute for 24 hours at 25°C. Suspensions were transferred to polypropylene copolymer 50 mL tubes and centrifuged at 14,000 rpm for 10 minutes at 25°C using a refrigerated centrifuge (IEC, Chattanooga, TN). The supernatant was decanted to a clean precombusted glass beaker and the pH was adjusted to 7.0 using 0.1M HCl or NaOH. The solution was then filtered through a 0.45µm cellulose acetate membrane (Fisherbrand, Pittsburgh, PA). The DOM solutions were stored in precombusted glass Erlenmeyer flasks at 4°C for less than 24 hours before analysis or use for binding experiments.

Table 2. List of DOM and the solid organic amendments used for their extraction.

<i>DOM Name</i>	<i>DOM Source</i>	<i>Abbreviation</i>
Public Works Compost	Composted wood and yard wastes from Auburn Public Works (Auburn, AL). Compost was formed into a pile and turned once every month for 11 months.	PWC
Poultry Litter	Fresh poultry litter. Poultry litter was formed from additions of poultry excretion, feathers, feed, and bedding materials composed of pine shavings and sawdust. Prior to sample collection, the litter was placed into a pile on the soil surface for one month without turnover.	PL
Aged Poultry Litter	Poultry litter formed from additions of poultry excretion, feathers, feed, and bedding materials composed of pine shavings and sawdust. Prior to sample collection, the litter was placed into a pile on the soil surface for eight months without turnover.	APL
Green Compost	Evergreen® commercial compost of pine, hardwood, cattle manure, and sand.	GC
Cattle Manure	Commercial Composted cattle manure (Blak Kow®, Oxford FL). This sample is composed of raw cattle manure that was composted on a soil surface for three months with weekly turnover.	CM
Peat Moss	Sphagnum peat moss (Miracle Grow®, Marysville OH) Organic amendment formed from sphagnum peat moss and fertilizer consisting of polymer coated ammonium nitrate, ammonium phosphate, calcium phosphate, and potassium sulfate (0.19-0.11-0.15), .	PM
Biosolid	Class B biosolid produced under aerobic conditions at the Veolia Water Services (Auburn, AL).	BIO
Humic Acid	Humic acid sodium salt standard (Beantown Chemical, Hudson, NH)	HA

2.3 Soils

Soil samples were collected from B horizons of Gwinnett and Vaiden soils. The Gwinnett soil was collected from a forest located in Auburn, AL and classified as clayey, kaolinitic, subactive, thermic Rhodic Kanhapludult. The Vaiden soil was taken from the Auburn University Blackbelt Research and Extension Center in Marion Junction, AL (32.47145, -87.23097) and was classified as clayey, smectitic, subactive, thermic Aquic Dystrudert. Soils were air-dried and sieved to remove particles greater than 2 mm. Selected physical and chemical properties of the soils are listed in Table 3. Particle size analyses of the sand, silt, and clay fractions were determined by the hydrometer method (Bouyoucos., 1962). The pH was measured in water of a 1:2 soil:solution suspension. Water extractable organic carbon (WEOC) was measured by suspending 2 g of air-dried soil and 10 g of ultrapure water for 8 hours on a reciprocal shaker at 25°C in the dark. The supernatant was separated by centrifuge (25°C 4000 g 20 min), and WEOC was measured by a TOC-L analyzer (Shimadzu, Kyoto, Japan). Cation exchange (CEC) and anion exchange capacity (AEC) were measured using the unbuffered salt extraction method described by Sumner and Miller (1996). Briefly, 5 g of soil was mixed with 30 g of 0.2M NH₄Cl and shaken on an end-over-end shaker for 5 minutes. The solution was then centrifuged (25°C 4000 g 20 min) and decanted into a 100 mL volumetric flask. This process was repeated two more times, where the final volume of 100 mL was reached by filling the remaining volume with 0.2M NH₄Cl. The solution was then filtered with a 0.45 µm polypropylene filter (Fisher Scientific, Waltham, MA) and Na, K, Mg, and Al were analyzed by inductively Coupled Plasma Optical Emission spectroscopy (ICP-OES, Spectro Ciros, Spectro Analytical Instruments Inc. Mahwah, NH). Then, the excess of Cl⁻ and NH₄⁺ entrained in the soil pores were washed with ethanol. Finally, 0.2M

KNO₃ was added to exchange the adsorbed Cl⁻ and NH₄⁺, which were measured by ion chromatography (IC, Spectro Ciros, Spectro Analytical Instruments Inc. Mahwah, NH) and colorimetric ammonium assay analysis (Sumner and Miller, 1996).

Table 3. Selected physical and chemical properties of the soils. Values represent average of three replicates with standard deviations in parentheses.

	Gwinnett	Vaiden
% Sand (>2 mm)	37	38
% Silt (< 2 - >0.002 mm)	18	12
% Clay (< 0.002 mm)	45	50
Textural Class	Clay	Clay
pH	5.72 (0.05)	5.21 (0.03)
WEOC ¹ (mg L ⁻¹)	1.11 (0.02)	1.48 (0.26)
CEC ² (meq 100g ⁻¹)	2.73 (0.10)	6.06 (0.89)
AEC ³ (meq 100g ⁻¹)	1.00 (0.05)	0.34 (0.01)

¹ Water extractable organic carbon; ² cation exchange capacity; ³ anion exchange capacity

2.4 DOM Characterization

Dissolved organic carbon (DOC) concentrations were measured by a TOC-L analyzer (Shimadzu, Kyoto, Japan). Standard calibrations for organic carbon were created with glucose monohydrate at concentrations ranging from 0 to 200 mg C L⁻¹. Electrical conductivity and pH were measured using Accumet Basic AB30 Conductivity Meter (Fisher Scientific, Waltham, MA) and SevenCompact S220-Basic, pH/Ion benchtop meter (Mettler Toledo, Columbus, OH) respectively.

Molecular spectroscopy methods were used to characterize the chemical structure and composition of the DOM. To analyze the composition of chromophoric DOM (cDOM), UV-vis absorbance was measured from 250 to 700 nm at 0.5 nm intervals, on a UV-1800 spectrophotometer (Shimadzu, Kyoto, Japan), using 1.0 cm quartz cuvette. Fluorescence excitation–emission matrices (EEMs) were obtained with a FP-8500 spectrofluorometer equipped with 150W Xe excitation source (JASCO, Easton, Maryland). The EEMs were acquired with

excitation (Ex) from 250 to 585 nm, 5 nm interval, and emission (Em) from 260 to 600 nm, at 2 nm interval using 1.0 cm quartz cuvette. To minimize inner filter effects, samples were diluted with ultrapure water to UV-absorbance at 254 nm < 0.15 (Lakowicz 2006). Ultrapure water blanks were measured daily, for background subtraction and Raman normalization and correction for Rayleigh scattering. Importantly, fluorescence EEM measurements can only capture the fluorescence components contained in a molecule of DOM (fDOM).

Transmission Fourier-transform infrared spectroscopy (FTIR) spectra were collected on an FTIR-6800 spectrometer (Jasco, Easton, Maryland) with a KBr beam splitter and a deuterated triglycine sulfate (DTGS) detector. Aliquots of DOM solutions were freeze-dried, diluted with 200 mg KBr (0.5%), and compressed into pellets. For each sample, 120 scans were collected over the spectral range of 400–4000 cm^{-1} at a resolution of 4 cm^{-1} . Three replicates were collected for each DOM. Before each analysis, the sample compartment was purged with $\text{N}_{2(\text{g})}$ for 10-minutes to minimize the signal from atmospheric CO_2 and H_2O . KBr blank was subtracted from each sample using SpectraManager (Jasco, Easton, Maryland). Peak positions were determined using the second order Savitzky–Golay method and peak assignment.

Weight average molecular weight (Mw) and number average molecular weight (Mn) were determined by high-performance liquid chromatography (Agilent 160 Infinity system II, USA) equipped with size-exclusion column and fluorescence and UV detector (HPLC-SEC-FLD/UV). Samples were diluted with ultra-pure water to a concentration of 25 mg C L^{-1} , and 100 μL of each sample was injected by autosampler and pumped through a size-exclusion column (Protein-Pak 125, 10 μm , 7.8x300 mm, Waters, USA). A solution of sodium chloride (100 mM) and phosphate buffer (K_2HPO_4 , NaH_2PO_4 , 2 mM) were used as a mobile phase at the rate of 1 ml min^{-1} . Each

sample was injected twice. The FLD was set for excitation and emission wavelength at λ_{Ex} : 260, λ_{Em} :450 and λ_{Ex} : 275, λ_{Em} : 340, and UV absorbance was measured at 245 nm.

2.5 Dialysis Equilibrium

Dialysis equilibrium studies were employed to investigate the binding between selected DOM sources and PFOS. Spectra-por/6 dialysis bags (Repligen, Waltham, MA) with a 1 kDa molecular weight cutoff (MWCO) were washed with ultrapure water for one hour to remove excess NaN_3 . 10 mL of the selected DOMs (750 mg C L^{-1}) was sealed within the dialysis bags. Homoionic DOM was prepared by dialyzing dialysis bags against 1 M NaCl for 24 hours and then another 48 hours against 50 mM NaCl in 4 L glass beakers. The equilibrating solutions were replaced every 4 hours. This process also removed the DOM fraction smaller than 1 kDa which was measured to be lower than 5% of total DOC. The bags were then transferred to 50 mL polypropylene centrifuge tubes (VWR, Radnor, PA) containing 30 mL of $500 \mu\text{g L}^{-1}$ PFOS and 50 mM NaCl at pH 7. The tubes were agitated in the dark at 90 rpm and 25°C for 72 hours on a reciprocal shaker (Lab-Line, Dubuque, Iowa). Following equilibration time, 5 mL aliquots were taken from outside and inside the dialysis bags for PFOS and DOC quantification. Two types of control were used in dialysis experiments, (i) blank with no DOM to test that PFOA and PFOS can diffuse freely through the dialysis membrane, and (ii) blank with no PFOA or PFOS to show that DOM cannot move outside of the dialysis bag.

2.6 Batch Sorption Desorption Experiments

The impact of DOM on PFOS adsorption on soils was measured using the batch adsorption method. Soil suspensions were prepared by mixing 1 g of soil with 30g of 5 mM CaCl_2 aqueous solution, in 50 mL polypropylene centrifuge tubes. Solutions of DOM, and PFOS were added to

obtain an initial DOM concentration of 100 mg C L⁻¹ and PFOS concentration ranging from 1 to 1000 µg L⁻¹. The solution volume was adjusted to 30 mL with 5 mM CaCl₂ aqueous solution. The solid-to-solution ratio (1:30, w:w) was determined in a preliminary experiment to enable 30 – 70% PFOS removal from the solution (Figure A1). The pH of all solutions was adjusted to 5.5 (similar to the native soil pH) with 0.1 M of HCl or NaOH solutions. A total of seven duplicates were prepared for each batch experiment. The tubes were agitated on a reciprocal shaker (90 rpm) in the dark at 25°C for 48 hours. The time required for apparent equilibrium was established in a preliminary kinetic experiment (Figure A2). Following equilibration, tubes were centrifuged at 14,000 rpm for 10 minutes at 25°C using a refrigerated centrifuge. 5 mL of each supernatant was collected for PFOS and DOM quantification.

Desorption experiments were conducted immediately after the adsorption experiments only for the Vaiden soil. At the end of the adsorption step, 25 mL of the supernatant was replaced with 5 mM CaCl₂ aqueous solution. The tubes were further agitated under the same conditions (as described above) for 48 hours to reach apparent equilibrium. The apparent desorption equilibrium was measured in a preliminary experiment (Figure A3).

2.7 Fluorescence Quenching Experiments

PFOA and PFOS titration experiments were used to examine the fluorescence quenching of DOM. DOM solutions were diluted with 50 mM NaCl to obtain initial UV absorbance of 0.2 at 254 nm in pre-combusted (500°C, 3 hours) glass beakers and 10 mL aliquots were transferred to pre-combusted 20 mL vials with polypropylene caps (Fisherbrand, Pittsburgh, PA). Then 10 mL of PFOA or PFOS aqueous solutions (50 mM NaCl, pH 7) were added to each vial. Triplicates of PFAS concentration of 0, 20, 100, 500, 1000, and 2000 µg L⁻¹ were prepared. The vials were incubated for 24 hours on a reciprocal shaker (90 rpm) in the dark at 25°C. Then, 6 mL from each

vial was transferred for fluorescence and UV-Vis analysis. Two sets of controls were used, (i) DOM-free PFOA or PFOS solution to confirm that these analytes have no fluorescence and UV-Vis signal, and, (ii) PFAS-free DOM solution to demonstrate that no significant change was measured during the experiment.

2.8 PFOS Quantification

PFOS quantification was performed with a Vanquish Flex Binary ultra-performance liquid chromatography (UPLC) system (Thermo Scientific) fitted with a PFC-free kit (P/N 80100-62142) coupled to a quadrupole orbitrap mass spectrometer (Orbitrap Exploris 120, Thermo Scientific) with heated electrospray ionization (H-ESI) in negative mode using Xcalibur software (V4.4.16.14). A delay column was placed between the pump and autosampler (HypersilGOLD, 1.9 μm , 175 \AA , 3 x 50 mm) to separate any PFAS in the LC system and solvents from the analytes. The standard or sample (10 μL) was injected onto a C18 column (Waters BEH C18 1.7 μm , 2.1 x 50 mm with VanGuard 2.1 x 5 mm pre-column) maintained at 40°C with a 200 $\mu\text{L min}^{-1}$ flow rate of mobile phase of solution A (2 mM ammonium acetate in water) and solution B (100% acetonitrile) beginning at 15% B for the first 0.3 minute to 95% B at 9 min, held at 95% B for 2 min, back to 15%B at 12 min, and with re-equilibration of 3 min. The MS scan range was 200-1000 m/z with resolution of 120,000, standard automatic gain control (AGC) target, 70% RF lens, maximum injection time auto, with EASY-IC run-start on. The spray voltage was 2500 V, ion transfer tube temperature was 320 °C, and the vaporizer temperature was 275 °C and mild trapping was off. The sheath gas was 30 and aux gas 5 (arbitrary units). Xcalibur 4.4 Quan Browser was used for data analysis with a 5-ppm mass error window. Mass spectrometer parameters were as follows: the collision energy of -15 V; and a source and desolvation temperature of 700 °C.

Precursor and product ions (m/z) were 506.95 and 498.92, respectively. The method limit of detection (LOD) was 100 ng L⁻¹.

2.9 Data Analysis

The specific UV-absorbance (SUVA₂₅₄) was calculated by normalizing the absorbance at 254 nm by the DOC concentration (L mg-C⁻¹ cm⁻¹). SUVA₂₅₄ is used as an indicator of aromatic content per unit of organic carbon concentration (Fellman et al., 2008). E2:E3 is the ratio between the UV- absorbance at 250 and 365 nm and is indicative of molecular weight and proportional to the amount of aromatic material in the sample (Minor et al., 2014). E4:E6 is the ratio between UV-absorbance at 465 and 665 nm. This ratio is indicative of aromaticity from condensed aromatic rings, molecular weight, and O:C atomic ratio (Chen et al., 1977).

Fluorescence EEM data pre-processing included subtracting EEM of the ultrapure water blank, treating the first and second-order Rayleigh scattering and inner filter effects as well as Raman normalization following the procedure described by Murphy et al., (2013), using the staRdom package in R (Purcher 2019, R Core Team 2020).

The humification index (HIX, Ohno et al., 2002) was calculated using Eq. 1:

$$\text{HIX} = \frac{\sum(I_{\text{em}}^{435 \rightarrow 480})}{\sum(I_{\text{em}}^{300 \rightarrow 345})} \quad [\text{Eq. 1}]$$

where $\sum I_{\text{em}}^{435-480}$ is the emission intensity in the 435 to 480 nm region and $\sum I_{\text{em}}^{300-345}$ refers to the sum of the emission intensity in the 300 to 345 nm range. HIX quantifies the fluorescence red shift between samples. Higher HIX values are indicative of increased carboxylic functional group content and the presence of larger molecular weight fragments of assemblage (Ohno., 2002).

Fluorescence index (FI, McKnight et al., 2001) was calculated by Eq. 2:

$$FI(ex370) = \frac{em450}{em500} \quad [Eq. 2]$$

Where em450 refers to the emission intensity at 450 nm and em500 refers to the emission intensity at 500 nm emission wavelength at 370 nm-excitation. FI values between 1.2 – 1.5 are associated with DOM enriched with lignin-like aromatic moieties derived from plant materials (McKnight et al., 2001). Microbially derived DOM contains more nitrogen and aliphatic functional groups, and is associated with FI values > 1.5 (McKnight et al., 2001).

The EEMs were further decomposed to their underlying chemical components (i.e., protein and humic-like fluorophores) using parallel factor analysis (PARAFAC). The PARAFAC model was obtained using the staRdom package in RStudio (Pucher 2019, R Core Team 2020). In addition to the eight selected DOM (Table 2), DOM extracts of commercial Miracle Gro® compost, O horizon of soils collected from Auburn University Old Rotation experimental station (32.593728, -85.485686), as well as B horizon of soils collected from a coastal forest at Weeks Bay National Estuarine Research Reserve (30.416210, -87.834019) were also included into the PARAFAC model. All samples were measured in triplicate, totaling 65 individual EEM measurements used for developing the PARAFAC model.

Input data was preprocessed according to best practices recommended by Murphy et al. (2013) as well as a tutorial from Pucher et al. (2019). EEM spectral correction was conducted using a range of calibration standards, including broad-spectrum xenon light sources and Rhodamine B, such corrections allowed us to remove instrument-specific influences on the EEMs (Resch-Genger and DeRose, 2010). Inner filter effects were then corrected using a separate UV-vis spectra, where EEMs are multiplied by a correction matrix that corresponds to each wavelength pair (Kothawala et al. 2013; Pucher et al., 2019). EEM's were normalized to a standard scale of Raman Units by

dividing all intensities by the area of the Raman peak of an ultrapure water blank measured on the day of analysis (Murphy et al., 2013; Pucher et al., 2019). Rayleigh scattering was removed then interpolated to replace the removed scatter areas (Murphy et al., 2013; Pucher et al., 2019). To explore the data set and determine the correct number of PARAFAC components, eight PARAFAC models were obtained with 2-9 components where all models were calculated with 1000 iterations, a tolerance of 10^{-8} , and 50 random starts. Leverage plots (Figure A4) were employed to visualize outliers in resulting PARAFAC models, outlier EEM measurements that skewed the model were removed, and the models were then re-calculated (Pucher et al., 2019). Residuals were also visualized for each EEM measurement contained in all eight PARAFAC models (Figure A5-13). This allowed us to examine the residuals in each PARAFAC model to not only select the correct number of components but see that the systematic variation in the dataset was captured by the PARAFAC model, ensuring there is only random error present in residuals (Murphy et al., 2013; Pucher et al., 2019). Residual analysis identified that a three component PARAFAC model to be suitable for the data set. The three-component model was further validated through split-half analysis (Figure A14), by using the split-half function, where the model is applied independently to two halves of the dataset, then compared for identical spectral properties (Stedmon & Bro, 2008).

Two indices were calculated by the ratio of absorbance at specific wavenumbers in FTIR spectra. Index I, Eq. (3) was used as a metric of the ratio of aromatic to aliphatic functional groups (Margenot et al., 2016). Increases in aromaticity (in the presence of phenolic functional groups) could be indicative of an enhanced possibility of hydrogen bonding or a decrease in hydrophobic interactions due to a lack of aliphatic assemblages. Index II, represented by Eq. (4), is the ratio of C- to O- functional groups (Margenot et al., 2016). Ratios of C- to O- would indicate the presence

of molecular oxygen or carboxylic acids that are capable of cation bridging with PFAS moieties (Kothwala et al., 2017).

$$\mathbf{Index\ 1} = \frac{1650+920+840}{2924+2850+1740+1405} \quad [\text{Eq. 3}]$$

$$\mathbf{Index\ 2} = \frac{2924+2850+650+1470+1405+920+840}{3400+1270+1110+1080} \quad [\text{Eq. 4}]$$

PFOS distribution coefficients (K_{DOC}) between aqueous solution and DOM was calculated by Eq. (5).

$$K_{\text{DOC}} = \frac{([C_{\text{in}}] - [C_{\text{out}}])}{[C_{\text{out}}] * [\text{DOC}]} \quad [\text{Eq. 5}]$$

where C_{in} is the PFOS concentration ($\mu\text{g L}^{-1}$) inside the dialysis bag and C_{out} is the PFOS concentration outside the dialysis bag (mg L^{-1}). DOC is the dissolved organic carbon (mg L^{-1}) inside the dialysis bag.

The adsorbed concentration of PFOS on the soils ($q_e \mu\text{g g}^{-1}$) was calculated by Eq. (6).

$$q_e = \left(\frac{C_o - C_e}{1000} \right) * \frac{V}{m} \quad [\text{Eq. 6}]$$

Where C_o is the initial PFOS concentration ($\mu\text{g L}^{-1}$), C_e is the equilibrium PFOS concentration ($\mu\text{g L}^{-1}$), V is the total volume of the sample (L), and m is the mass of soil (g) added to the sample.

The adsorption isotherms were fitted to Freundlich Eq. (7) below:

$$q_e = K_f C_e^n \quad [\text{Eq. 7}]$$

Where q_e is the adsorbed concentration ($\mu\text{g g}^{-1}$), K_f is the Freundlich constant (L g^{-1}), and n is the isotherm curvature (dimensionless).

Adsorption desorption Hysteresis Index (HI) was calculated following Huang et al., (1998), and is represented by Eq. (8):

$$HI = \frac{q_e^d - q_e^s}{q_e^s} \Big|_{C_e} \quad [\text{Eq. 8}]$$

Where q_e^d and q_e^s ($\mu\text{g g}^{-1}$), represent adsorbed concentrations of the adsorption and desorption experiments, respectively, at constant C_e .

Statistical analyses were performed with the Origin Pro® and Microsoft Excel®. Normality tests using Kolmogorov-Smirnov one sample tests ($\alpha = 0.05$) were employed to examine if DOM molecular indices were normally distributed. The differences in each molecular index between the DOM types were evaluated with a fixed effect analysis of variance (ANOVA) and Tukey's honestly significant difference (HSD) test ($\alpha = 0.05$). Relationships between PFOS sorption and DOM molecular indices were determined using Pearson's correlation. Correlations were described as moderate ($r = 0.31-0.69$) and strong ($r = 0.70-0.99$).

Results

3.1 UV-vis Absorbance Indices

The indices of UV-vis absorbance and fluorescence are summarized in Table 4. $SUVA_{254}$ values range from 0.638 to 1.721, which correlates to aromaticity of 7.3-16.5% (Weishar et al., 2003). $SUVA_{254}$ increased in the following order $CM < BIO < GC < PM < PL = PWC < HA < APL$. The differences between DOM types were statistically significant (Table 4, $p = 0.05$, ANOVA, Tukey's HSD). E2:E3 values ranged from 1.84 to 2.39, increasing in the order of $HA, = PWC, < APL, = PL, < GC, < CM, = PM = BIO$. The E2:E3 is negatively correlated with aromaticity and correlates with molecular size (Peuravuori and Pihlaja 1997). Hence, HA, PWC, and APL DOM contain the largest aromatic content of all DOM sources. E4:E6 ratios range from 6.47-8.86, which increased in the order of $HA < PWC < APL \sim GC < PL = BIO = CM$, where only PWC and HA were found to have significant values ($p = 0.05$, ANOVA, Tukey's HSD). E4:E6 is

positively correlated with oxygen containing functional groups, and inversely related to molecular weight (MW; Chen et al., 1977). HA and PWC DOM exhibited the lowest E4:E6 values while also representing the only statistically significant means ($p = 0.05$, ANOVA, Tukey's HSD), indicating higher MW and larger proportion of oxygenated groups in HA and PWC with respect to other DOM. It is important to note that the lack of E4:E6 ratios for the PM DOM source was due to the low absorbance for this DOM at 665 nm. Another study reported lower E4:E6 values for DOM extracted from biosolids, poultry litter, and cattle manures (3.7, 3.0, and 5.2, respectively; Riffaldi et al., 1983). Conversely, E4:E6 reported here for commercial humic standards (6.48) is within the range of what is reported in literature for Suwanee River and Sigma Aldrich HA (7.59, 5.58, 4.48 McCarthy et al., 1989; Chin et al., 1994; Zhang et al., 2009). $SUVA_{254}$ for animal waste DOM reported here was similar to values reported in literature for DOM extracted from raw and composted animal manures (Wang et al., 2013; 2014). Specifically, $SUVA_{254}$ values for cattle manure, poultry litter, and biosolids ranged from 1.27, 1.5, and 0.53 $L\ mg^{-1}\ cm^{-1}$, respectively. $SUVA_{254}$ for HA was lower when compared to studies examining the optical properties of DOM extracted from various commercial HA (Weishar et al., 2003). Importantly, all three absorbance indices ($SUVA_{254}$, E2:E3, and E4:E6) indicate the HA, PWC, and APL DOM to be high MW DOM composed of a large proportion of aromatic assemblages while DOM such as BIO and CM are low MW DOM with lower contents of aromatic carbon compared to HA, PWC, and APL DOM.

Table 4. UV-Vis absorbance and fluorescence indices of the selected DOM. Values represent the means (N = 3) and values in parentheses represent standard deviation.

Sample Name	SUVA ₂₅₄ (L mg ⁻¹ cm ⁻¹)	E2:E3	E4:E6	Fluorescence Index (FI)	Humification Index (HIX)
Cattle Manure	0.643 (0.01) ^g	2.26 (0.07) ^b	8.87 (0.02) ^a	1.90 (0.00) ^d	0.892 (0.00) ^b
Biosolid	0.874 (0.01) ^f	2.39 (0.31) ^a	8.72 (0.00) ^a	1.94 (0.01) ^{cd}	0.457 (0.01) ^g
Green Compost	1.05 (0.01) ^e	2.19 (0.59) ^c	8.38 (0.03) ^c	1.99 (0.00) ^{bc}	0.886 (0.00) ^d
Peat Moss	1.20 (0.02) ^d	2.35 (0.11) ^a	NA	1.72 (0.01) ^e	0.920 (0.00) ^c
Poultry Litter	1.25 (0.03) ^c	1.99 (0.17) ^d	8.64 (0.02) ^b	2.06 (0.01) ^a	0.810 (0.00) ^e
Public Works Compost	1.29 (0.01) ^c	1.91 (0.29) ^e	7.23 (0.01) ^d	1.50 (0.00) ^f	0.910 (0.05) ^c
Humic Acid	1.53 (0.02) ^b	1.84 (0.25) ^f	6.48 (0.11) ^e	0.991 (0.00) ^g	0.974 (0.00) ^a
Aged Poultry Litter	1.72 (0.03) ^a	1.98 (0.35) ^d	8.28 (0.03) ^c	2.05 (0.05) ^b	0.781 (0.01) ^f

* Letters display differences between means within a column examined using ANOVA and Tukey's-HSD at $\alpha = 0.05$.

The normalized UV-Vis absorbance spectra for the eight DOM samples are presented in Figure 1. All spectra exhibited a steep decrease in absorbance from 240 to 260 nm. Spectra of PL, APL, BIO, and GC samples produced a shoulder in the 260–270 nm range, consistent with strong absorbance by amino acids (Birdwell and Engel., 2010). All spectra exhibited limited absorbance at higher wavelength (>600 nm).

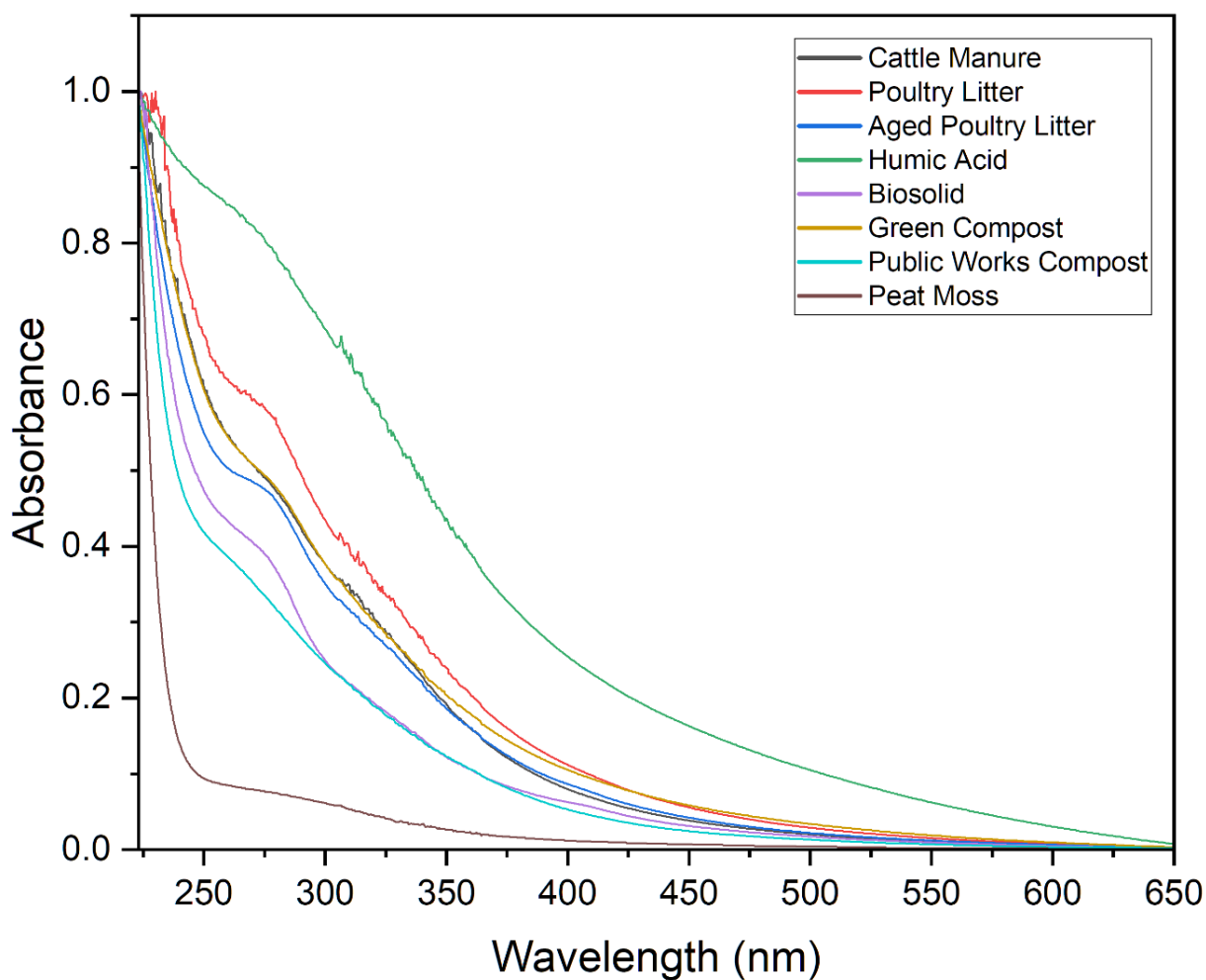


Figure 1. UV-Vis absorbance spectra for all 8 extracted DOM sources. Measurements presented here are the average of three measurements from the same DOM solution. All spectra were normalized to a value of 0-1 to compare intensities.

3.2 Fluorescence Indices

FI values between 1.2 and 1.5 are indicative of DOM derived from plants and are expected to have a higher proportion of aromatic moieties from plant lignin. Microbial-derived DOM have FI values ranging between 1.5 and 2.0. Microbially derived DOM consists of a larger proportion of aliphatic carbon and nitrogen-containing functional groups (McKnight et al., 2001). In this study, all DOM excluding PWC and HA exhibited FI values between 1.7 and 2.0, indicative of microbial-derived DOM (Table 4).

Humification index (HIX) quantifies red shift (Eq. 1) between the fluorescence spectra of the different types of DOM. This shift (i.e., higher HIX) is indicative of increased carboxylic and N-containing functional group content, and the presence of larger molecular weight fragments of assemblages (Ohno., 2002). The measured HIX values ranged from 0.80 to 0.98 (Table 4), excluding BIO, which was significantly lower HIX (0.46) ($p = 0.05$, ANOVA, Tukey's HSD). These HIX values, are lower than previously reported for values of DOM extracted from waste-derived organic amendments such as cattle manure and poultry litters (Ohno, 2002; Ohno et al., 2007; Hunt and Ohno., 2007). The low HIX value for BIO is corroborated with the low $SUVA_{254}$ and higher E2:E3 and E4:E6 values, indicating a smaller molecular size and low degree of oxygen and nitrogen-containing functional groups. The HA and PWC exhibited the highest HIX values (0.97 and 0.92), respectively.

3.3 PARAFAC Derived Components

The PARAFAC model developed in this study contained three components (Figure 2 and Table 5). Component 1 (C1, λ_{Ex} : 250-465 λ_{Em} : 390-456) was previously described as a humic like fluorophore of terrestrial origin (Borisover et al., 2012; Coble et al., 1996; Ohno and Bro, 2006). C1 is commonly found in DOM dominated by terrestrial precursor materials, such as soil solution, forested streams, and wetlands (Borisover et al., 2012; Coble et al., 1996; Ohno and Bro, 2006). Fluorescence signals in the region of C1 are generally absent from DOM of wastewater (Stedmon and Markager 2005). Based on large peak excitation wavelengths and correlation with ultrahigh-resolution mass spectrometry analysis, fluorophores of the C1 region are expected to be relatively high MW (Ohno et al., 2010). Component 2 (C2, λ_{Ex} : 260-400 λ_{Em} : 314-490) is similar to previously reported anthropogenic humic fluorophores observed in water extracted of soils amended with animal manures and biosolids and wastewater (Borisover et al., 2012; Stedmon and Markager, 2005; Fellman et al., 2008). Compared to C1, C2 has a blue-shifted emission and is related to lower MW hydrophobic compounds (Ishii et al., 2012; Gao et al., 2017; Qin et al., 2020). C2 lacks terrestrial fluorescence signals found in PARAFAC components similar to C1, identifying C2 to be independent of terrestrial humic fluorophores (Gao et al., 2017). Component 3 (C3, λ_{Ex} : 250-335 λ_{Em} : 270-374) is associated with proteinaceous fluorophores (tyrosine-like) and is directly related to the content of proteinaceous DOM (Stedmon and Markager., 2005; Fellman et al., 2008; Coble et al., 1997; Ohno and Bro, 2006; Yamashita et al., 2008). While other amino acids are found in DOM, only protein signals from tryptophan, tyrosine, and phenylalanine can fluoresce (Lakowicz., 2006). The fluorescence of these specific amino acids is due to the presence of an indole group or some other aromatic ring structure in which electrons are shared (Hudson et al., 2007; Lakowicz., 2006). Both tyrosine and phenylalanine lack the presence of an

indole group, in turn containing aromatic rings with shared electrons (Hudson et al., 2007). Protein fluorescence is generally excited at the absorption maximum near 280 nm or at longer wavelengths (Lakowicz., 2006). However, phenylalanine is not excited in most experiments and is not observed in many studies evaluating DOM, leading to absorption in the region of 280 nm owing to the presence of tyrosine and tryptophan like signals (Lakowicz., 2006). Tryptophan is typically excited at longer wavelengths in comparison to tyrosine, studies have shown that tryptophan can be selectively excited from wavelengths of 295-305 nm (Kierdaszuk et al., 1995). The signals seen in C3 center at Ex/Em maxima of 270/300 nm further support that this fluorescence signal has similar characteristics to that of tyrosine.

Table 5. Summary of excitation and emission wavelengths corresponding to fluorescence components observed in PARAFAC model.

Component	Excitation Wavelength	Emission Wavelength	Character	References
1	250-465	390-456	Terrestrial Humic Like	Borisover et al., 2012; Coble et al., 1996; Ohno and Bro, 2006
2	260-400	314-490	Anthropogenic Humic Like	Borisover et al., 2012; Stedmon and Markager, 2005; Fellman et al., 2008
3	250-335	270-374	Proteinaceous (Tyrosine-like)	Coble et al., 1997; Ohno and Bro, 2006; Yamashita et al., 2008

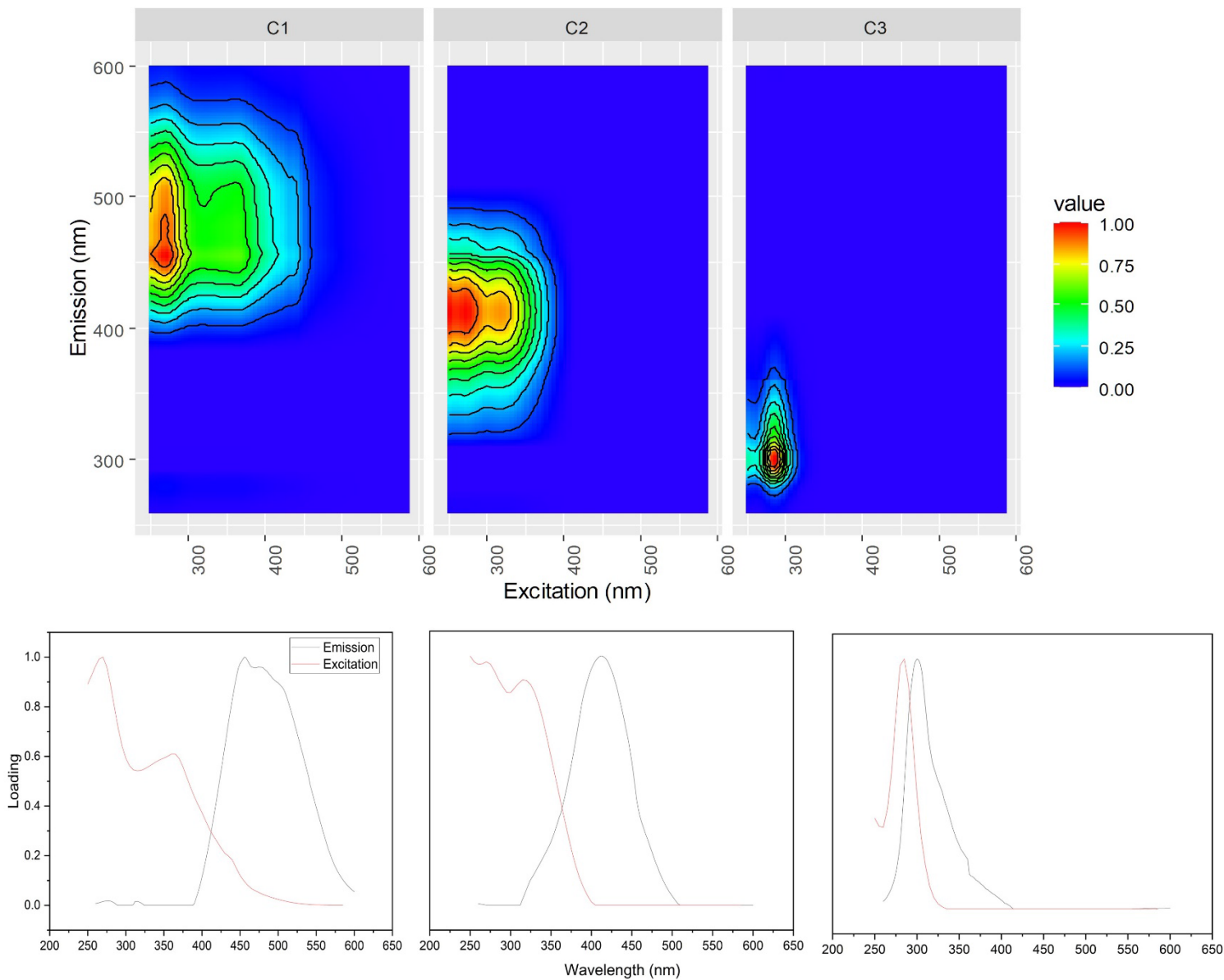


Figure 2. Fluorophores obtained from the PARAFAC model constructed from 65 individual DOM samples. 3D EEM (top) and 2D representation of the three-component loading (bottom). C1 represents humic like fluorophores, C2 represents anthropogenic humic fluorophores, and C3 represents proteinaceous fluorophores.

The relative distribution of each fluorophore obtained for the PARAFAC model varied between the selected DOM (Figure 3). The highest proportion of C1 was found in PWC (74%) and HA (47%), with lower contribution of this component to BIO (8%) and PL (27%). C2 was most pronounced in PM C2 (68%) and by PL (53%) but was absent from the PWC EEM. The highest proportion of proteinaceous like fluorophore (C3) was observed in BIO making 71%, with substantial lower values (<36%) for other DOM samples. For peat moss derived DOM C3 consists only 4% of the fDOM. It is important to note that the BIO DOM not only contains the largest fluorescence contribution to C3 but also contributes the least to the terrestrially C1.

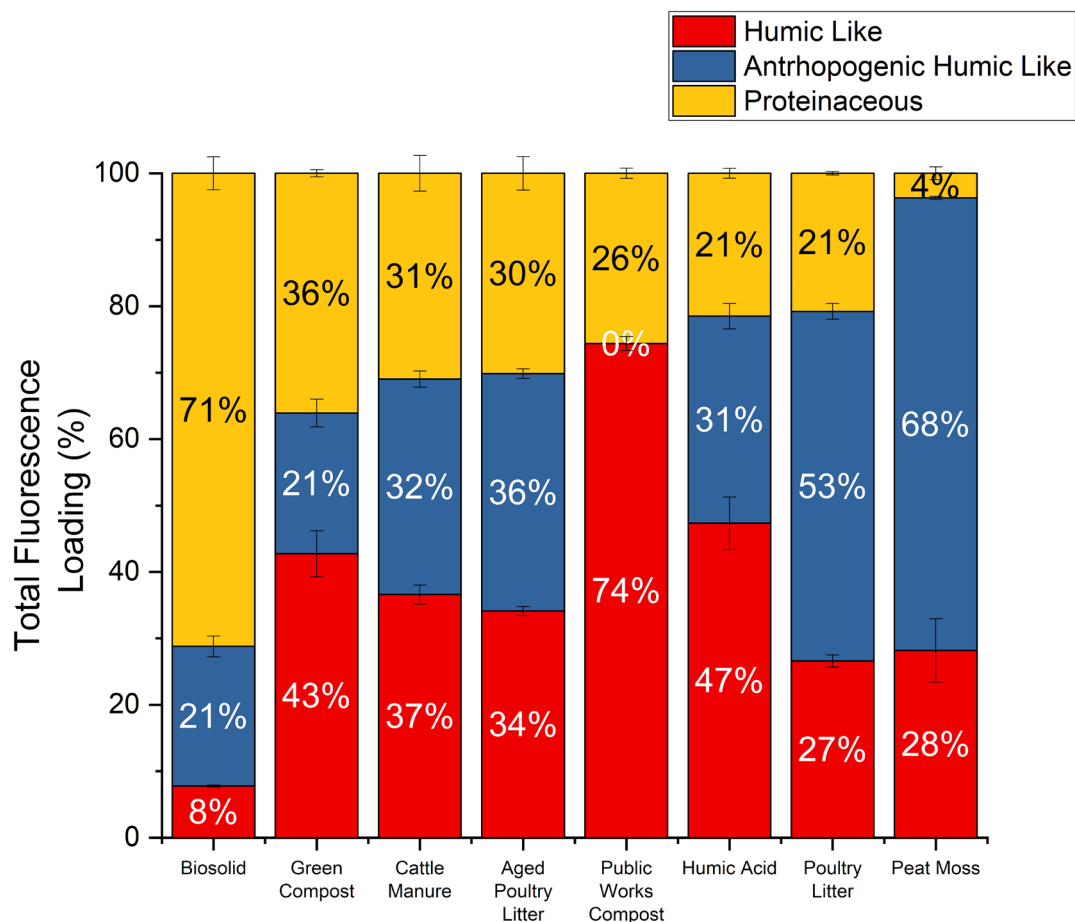


Figure 3. Distribution of PARAFAC components (%) in each of the tested DOM. Image is shown with loadings and standard deviations between replicates in error bars. Loadings with absolute fluorescence values are located in Figure A31.

3.4 FTIR Characterization of DOM Sources

Transmission FTIR spectra of the freeze-dry DOM samples, and their peak assignments are presented in Figure 4 and Table 6. A weak and narrow band at 3960 cm^{-1} was recorded for HA, PWC, CM, and PM. This band is assigned to OH stretches from primary alcohols (Coates, 2006). Broad band between wavenumbers 3000 and 3500 cm^{-1} was present in all spectra and assigned to -OH or -NH stretches (Leenheer., 1981). All samples other than the HA DOM displayed pronounced bands around 2950 and 2850 cm^{-1} , assigned to C–H symmetric and asymmetric stretches (Coates, 2006), indicating the presence of aliphatic moieties in these samples. A strong band of carbonyl C=O stretches (1731 cm^{-1}) in ester functional group (Gauthier et al., 1987) was present in the spectra of HA, CM, PWC, and PM. Carboxylic acid band at 1700 cm^{-1} (Coates et al., 2006) were observed in spectra of HA, PWC, and CM. The spectra of GC, PL, APL, and BIO exhibited broad absorption at 1650 cm^{-1} which is attributed to C=O stretches of amides (amide I vibration) associated with proteins (Omoike and Chorover, 2005). The BIO DOM exhibited pronounced amid II peak (C=N stretch and N–H band at 1540 cm^{-1}) which confirms a greater relative prevalence of proteinaceous material as shown by fluorescence analysis. GC, PM, and BIO spectra presented band at 1610 cm^{-1} assigned to the asymmetric stretch of carboxylate (COO^-) with smaller contributions from the C=C stretch of aromatics (Smith, 2000; Coates, 2006). The carboxylate symmetric stretching at 1400 cm^{-1} is also seen for all DOM sources other than GC and BIO (Smith, 2000; Coates, 2006). PWC, PL, APL and GC spectra exhibited peaks at 1429 cm^{-1} ascribed to C–H banding of CH_2 or CH_3 (Chefetz et al., 1998). Weak bands in all spectra at 1390 – 1406 cm^{-1} assign to symmetric stretches of C–O in carboxylate (Omoike and Chorover, 2006). Shoulders present at 1259 cm^{-1} indicate an asymmetric stretch of C–O stretch associated with the presence of the phenol from carboxylic acid (Omoike and Chorover., 2006). Only PWC and GC

samples produced absorption at 1094 cm^{-1} which is assigned to C–O stretching of aliphatic groups (O-alkyl; Sparks et al., 1996). C–O stretches present at 1100 cm^{-1} was observed in the spectra of HA, GC, and PWC, indicating the presence of secondary alcohols (Coates., 2006). Sample PM was the only DOM to exhibit C–O–C stretching between 1140 and 1070 cm^{-1} which shows sample PM to contain ether (Coates., 2006). Finally, C–O stretches present at 1032 cm^{-1} indicate that samples HA, PWC, APL, and PL contain primary alcohol groups (O–H) (Coates., 2006; Smith., 2000).

Table 6. Peak assignments used to evaluate the transmission FTIR spectra of freeze-dry DOM.

Wave number (cm^{-1})	Peak assignment	References
3700 – 3200 (broad)	νOH , Hydroxy group, H-bonded	Coates (2006)
2970 – 2915 2880 – 2845	ν_{as} (C–H ₃ and C–H ₂), ν_s (C–H ₃ and C–H ₂)	Coates (2006)
1725 - 1700	$\nu C=O$, <i>Carboxylic Acid</i>	Gauthier (1987)
1650 - 1590	νNH ,	Coates (2006)
1680 - 1610	$\nu C=C$, <i>Aromatic Carbon</i>	Coates (2006)
1610	$\nu_{as}(RCOO^-)$	Coates (2006); Smith (2000)
1650 - 1550	$\nu > NH$, <i>Secondary Amine</i>	Coates (2006)
1485 – 1445	$\delta(CH_2)$, <i>Methylene</i>	Chefetz, Hadar, and Chen (1998)
1429	$\delta(CH_2)$, $\delta(CH_3)$	Chefetz (1998)
1406	$\nu_s(C-O)$, $\delta(COO^-)$	Omoike and Chorover (2006)
1400	$\nu_s(CO_2)$	Smith (2000)
1259	$\nu(C-O)$, <i>Phenol</i>	Coates (2006); Smith (2000)
1190-1130	$\nu(C-N)$, <i>Secondary Amine</i>	Coates (2006)
1140-1070	$\nu C-O-C$, <i>Ether</i>	Coates (2006)
1100	$\nu C-O$, <i>Secondary Alcohol</i>	Coates (2006)
~1050	$\nu C-O$, <i>Primary Alcohol</i>	Coates (2006)

Note: The symbol ν indicates stretching of the specified bonds in Table-5. Specifically, ν_{as} indicates asymmetric stretching, ν_s indicates symmetric, and $\nu >$ indicates broad stretching. The symbol δ indicates bending.

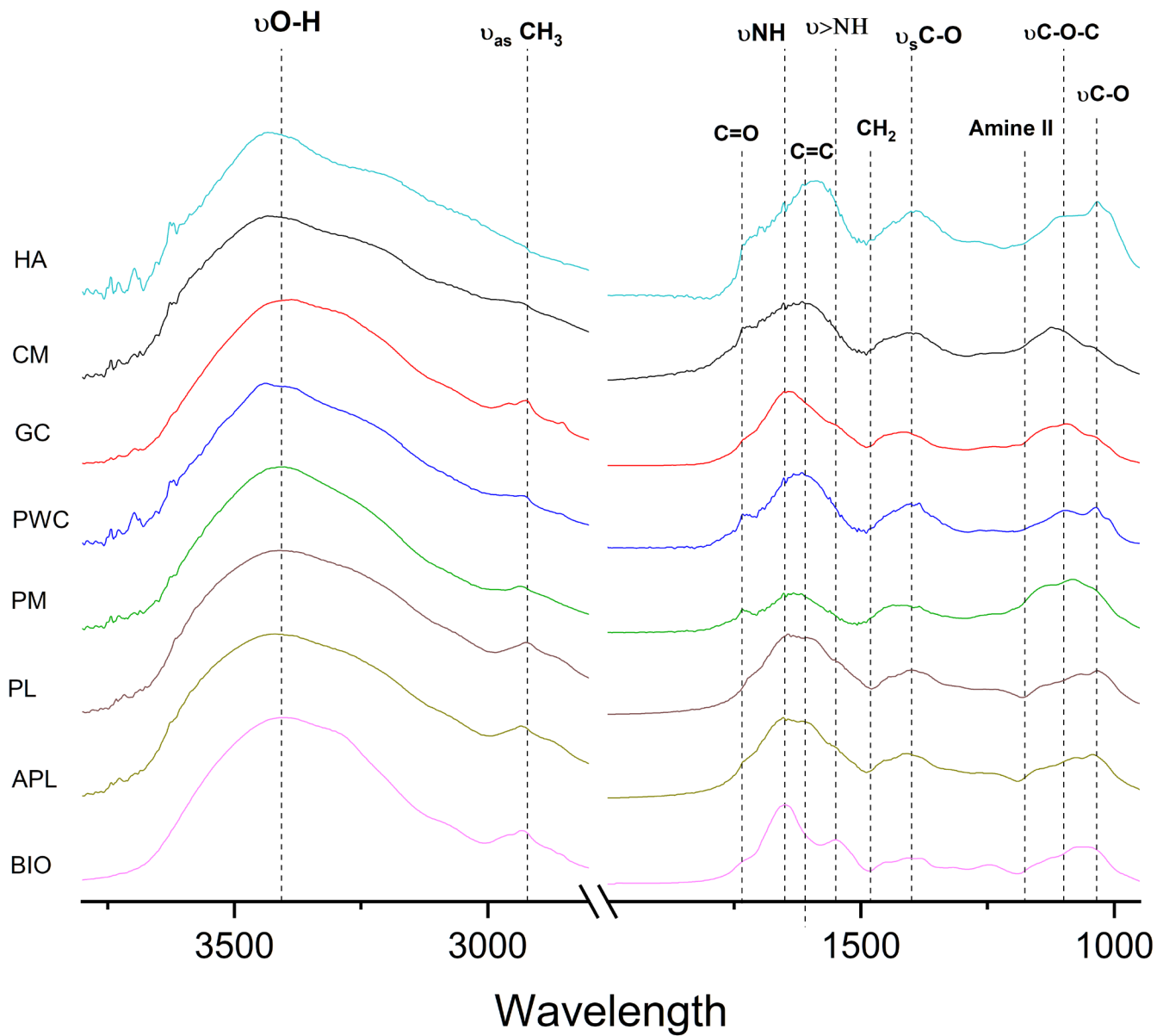


Figure 4. Transmission FTIR spectra of freeze-dry DOM. The symbol ν indicates stretching of the specified bonds in Table 6. Specifically, ν_{as} indicates asymmetric stretching, ν_s indicates symmetric, and $\nu >$ indicates broad stretching. The symbol δ indicates bending. Humic acid (HA), cattle manure (CM), green compost (GC), public works compost (PWC), peat moss (PM), poultry litter (PL), aged poultry litter (APL) and biosolid (BIO) DOM sources are represented by abbreviations.

Values of the two FTIR indices (Eq. 3 and 4) were calculated for each spectrum and are presented in Table 7. Index I is a ratio of aromatic to aliphatic functional groups. This ratio has been shown to increase with increasing degree of decomposition of DOM sources (Veeum et al., 2014; Margenot et al., 2016). PM, GC (0.31), BIO (0.42), and CM (0.45) exhibited the lowest values for Index I (Table 7), indicating relatively lower content of aromatic carbon as well as low degree of decomposition. Conversely, samples HA (0.882), APL (0.858), and PL (0.563) have the largest values for Index I. The differences in molecular composition between the DOM as indicated by FTIR Index I, are in good agreement with results from UV-vis absorbance ($SUVA_{254}$, E2:E3, and E4:E6). Therefore, suggesting that HA and APL are relatively more aromatic while BIO, GC, and CM have the least aromatic content.

FTIR Index II is the ratio of carbon to oxygen-containing functional groups (Margenot et al., 2016). Hence, indicating the relative degree of oxidation. Higher values of Index II are associated with greater DOM recalcitrance (Margenot et al., 2016). GC (1.47), APL (1.27), and PWC (1.16) have the largest values for Index II, indicating a lower degree of oxygen-containing functional groups (Table 7). Conversely, samples PM (0.47), CM (0.87), and BIO (1.00) have the lowest Index II values. Previous studies reported a similar range from 0.66- to 1.91 for Index I, and for Index II between 1.1 and 2.6 (Chefetz et al., 1998).

Table 7. FITR indices (Eq. 3 and 4) of the selected DOM. Each value represents a mean, and the standard deviation in parentheses, of three individual measurements.

Sample Name	Index I	Index II
Cattle Manure	0.450 (0.00) ^d	0.870 (0.04) ^a
Biosolid	0.420 (0.12) ^{cd}	1.00 (0.01) ^d
Green Compost	0.310 (0.04) ^a	1.47 (0.17) ^{de}
Peat Moss	0.300 (0.00) ^e	0.470 (0.07) ^e
Poultry Litter	0.563 (0.00) ^{ab}	1.10 (0.01) ^c
Public Works Compost	0.403 (0.00) ^{bc}	1.16 (0.01) ^d
Humic Acid	0.882 (0.00) ^{bc}	1.12 (0.15) ^b
Aged Poultry Litter	0.860 (0.00) ^{bc}	1.27 (0.01) ^b

* Letters display differences between means within a column examined using Tukey's-HSD at $\alpha = 0.05$.

3.5 DOM Molecular Weight

The weight average molecular weight (M_w) values obtained for cDOM at a UV absorbance of 254 nm range from 847 to 1851 Da, and the number average molecular weight (M_n) ranged between 792 and 1691 Da (Table 8). However, only the value of M_w and M_n for the cattle manure DOM was significantly higher compared with other cDOM ($p < 0.05$ ANOVA, Tukey's HSD). M_w and M_n were also measured for fDOM fluorophores by selecting the center of C1 (λ_{Ex} : 260, λ_{Em} :450) and C3 (of λ_{Ex} : 275, λ_{Em} : 340). The M_w C1 fDOM for PWC, GC and CM ranged between 1237 and 1571 Da and were significantly larger than all other sources which ranged from 791 to 1311 Da ($p < 0.05$ ANOVA, Tukey's HSD). M_n C1 fDOM also noted similar trends to M_w where samples PWC, GC, and CM ranged between 1134 to 1448 Da and were significantly larger than all other sources which ranged from 740 to 1189 Da ($p < 0.05$ ANOVA, Tukey's HSD). It is important to note that PWC exhibited the largest C1 proportion (Figure 3) amongst the tested

DOM, which, as previously mentioned, is associated with a larger humic-like molecular structure. The C3 fDOM of PL, APL, and HA was associated with relatively low M_w and M_n (763-772 and 715-723 Da, respectively), while M_w and M_n value of BIO, CM, and GC were significantly ($p < 0.05$ ANOVA, Tukey's HSD) larger (47556 - 38679 and 39552-32338 Da, respectively). These values further support findings from fluorescence analysis, demonstrating the largest proportion of C3 fDOM in BIO, GC, and CM. The HPSEC analysis demonstrated that the selected DOM exhibited range size fraction that is associated with the specific molecular fraction of each DOM. Overall, lower variability was observed for cDOM compared with fDOM.

Table 8. Weight average molecular weight (M_w) and number average molecular weight (M_n) obtained for cDOM and fDOM. Values are the average of two replicates, standard deviation is represented in brackets.

Sample Name	UV ₂₅₄		$\lambda Ex: 260 \lambda Em: 450$		$\lambda Ex: 275 \lambda Em: 340$	
	M_w (Da)	M_n (Da)	M_w (Da)	M_n (Da)	M_w (Da)	M_n (Da)
Cattle Manure	1592 (1.47) ^{ab}	1461 (1.31) ^{ab}	1505 (8.34) ^b	1388 (7.44) ^b	47431 (132) ^b	39346 (106) ^b
Biosolid	1566 (7.96) ^{ab}	1437 (7.09) ^{ab}	1359 (4.39) ^c	1255 (3.93) ^c	47556 (264) ^a	39522 (212) ^a
Green Compost	1301 (15.6) ^{bc}	1120 (13.9) ^{bc}	1237 (12.6) ^e	1135 (11.3) ^e	38679 (1858) ^c	32338 (1509) ^c
Peat Moss	1223 (393) ^{bc}	1130 (353) ^{bc}	1409 (8.47) ^c	1292 (7.57) ^c	NA	NA
Poultry Litter	1239 (0.00) ^{bc}	1145 (0.00) ^{bc}	815 (0.00) ^f	762 (0.00) ^f	771 (2.50) ^d	722 (2.27) ^d
Public Works Compost	1851 (24.8) ^a	1691 (22.2) ^a	1571 (10.9) ^a	1448 (9.70) ^a	NA	NA
Humic Acid	1459 (10.7) ^{ab}	1342 (9.63) ^{ab}	1311 (30.9) ^d	1189 (27.6) ^d	763 (16.57) ^d	715 (15.1) ^d
Aged Poultry Litter	847 (0.39) ^c	792 (0.36) ^c	791 (0.00) ^f	740 (0.00) ^f	772 (2.00) ^d	723 (2.00) ^d

* Letters display differences between means within a column examined using Tukey's-HSD at $\alpha = 0.05$.

3.6 Dialysis Equilibrium Experiments with PFOS

Dialysis equilibrium experiments were employed to investigate the binding between selected DOM and PFOS (Figure 5). K_{DOC} was found to range from 7,157 to 91,729 L kg⁻¹. From highest to lowest value, K_{DOC} was in the order of BIO > GC > APL > CM > PM > PL > HA respectively. When compared to K_{DOC} values of the HA standard, the binding abilities of PFOS with BIO were 122 % larger, indicating a significantly stronger binding affinity to human waste-derived DOM ($p < 0.05$, ANOVA Tukey's HSD). Also, compared to other dialysis studies involving DOM and PFOS, K_{DOC} values for the HA standard at the same free concentration of PFOS reported here were found to be larger than two studies, Xia (2015) and Liu (2022), where K_{DOC} was found to be 4738 and 4486 (L kg⁻¹) respectively. However, values reported here for the BIO DOM are 22% higher than those reported for bovine serum albumin (Xia et al., 2015), implying BIO binds more strongly with PFOS in comparison to bovine serum albumin. While high uncertainty was found between replicates, clear trends of enhanced PFOS interactions with human and animal waste DOM arose.

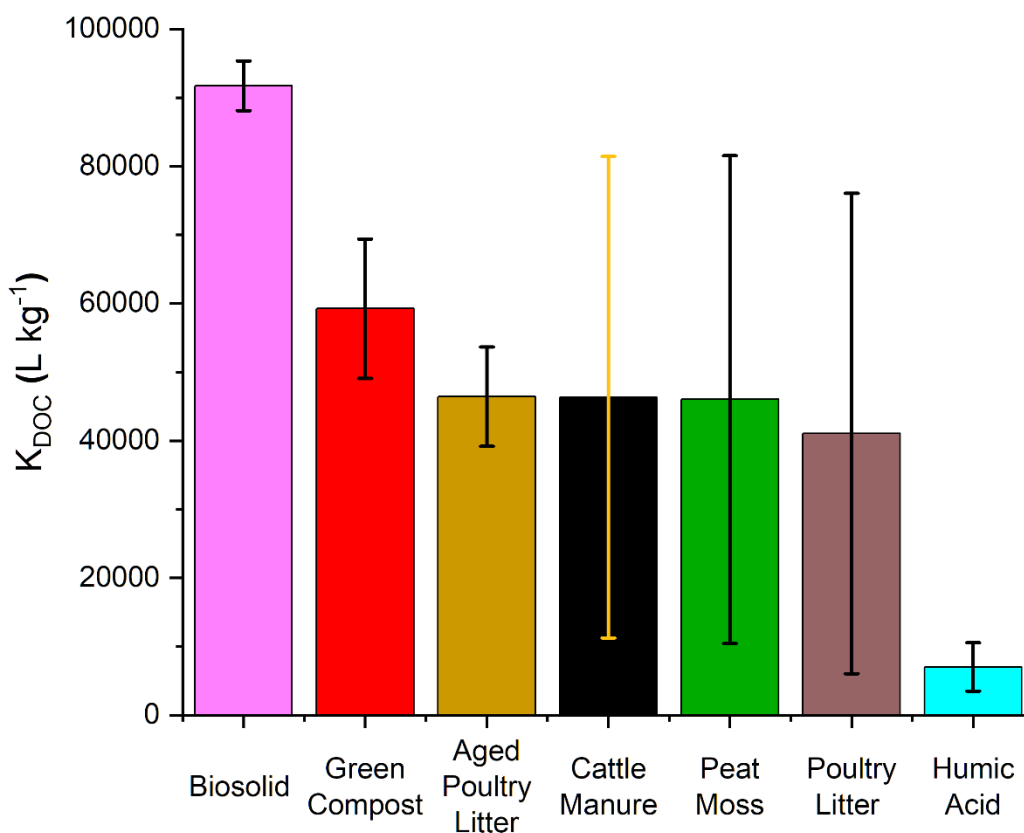


Figure 5. PFOS distribution coefficients (K_{DOC}) between aqueous solution and DOM. Error bars represent the standard deviation between replicate measurements.

3.7 Fluorescence Quenching

The fluorescence quenching of DOM by interaction with increasing concentrations of PFOS or PFOA is presented in Figure 6. Significant changes in the relative fluorophores' intensity was observed for BIO, GC, HA, PL, and APL (Figure 6). Only limited changes were observed for CM, PM, and PWC. The strongest impact of PFOA on fluorophores intensities was observed for APL, BIO, and GC (Figure 6). The C1's fluorescence decreased by 24% with the increase in PFOA concentration from 0 to 20 $\mu\text{g L}^{-1}$ for APL, HA, and GC. Therefore, suggesting preferential binding of PFOA to humic-like moieties of these DOMs. In contrast, the intensity of C1 of BIO and PL did not decrease. Further increase in PFOA concentration resulted in minimal changes in

the intensity of C1 of HA and GC. Whereas C1 intensity continued to decrease with an increase in PFOA concentration for APL. At the highest PFOA concentration ($1000 \mu\text{g L}^{-1}$), the intensity of C1 of APL decreased by 50%. In the presence of PFOS, the C1's fluorescence decreased for all DOM sources, but the most distinct changes occurred for APL, HA, and GC. The three DOM C1's fluorescence decreased by 20, 18, and 16%, respectively, with the increase in PFOS concentration from 0 to $20 \mu\text{g L}^{-1}$. At the highest PFOS concentration ($1000 \mu\text{g L}^{-1}$), C1's fluorescence decreased by 20% for GC, while a decrease of only 15% was noted for HA and APL. Changes in C1 fluorescence indicate that PFOA and PFOS may preferentially bind with humic-like moieties of the DOM sources, where such interactions were most pronounced for APL, GC, and HA.

Like C1 fluorophores, PFOA strongly impacted C2 fluorophores for sources GC, APL, and HA. In the presence of $20 \mu\text{g L}^{-1}$ PFOA, the C2 fluorophores of GC and APL were quenched by 15 and 10%, respectively. At the same concentration of PFOA, HA exhibited a 25% enhancement of C2 fluorophores. However, further increase in PFOA concentration did not result in further enhancements of C2 signals. This is an unexpected result, typically, as a quencher interacts with DOM fluorophores, the overall fluorescence intensity of the DOM decreases. Such an enhancement of fluorescence signals may indicate PFOA to alter the structure of the anthropogenic humic like moieties of the HA fDOM, resulting in enhanced fluorescence intensity (Ifon et al., 2022). At the highest PFOA concentration ($1000 \mu\text{g L}^{-1}$), the C2 intensity of GC and APL decreased by 15 and 25%. In the presence of PFOS, C2 fluorophores were impacted strongly for sources APL, PL, GC, and HA. In the presence of $20 \mu\text{g L}^{-1}$ PFOS, C2 fluorophores of GC, APL, and PL were quenched by 25, 20, and 22%, respectively. At the same PFOS concentration, C2 fluorophores of HA increased by 20%, but further increases in PFOS concentration did not result in further enhancements. Upon addition of $1000 \mu\text{g L}^{-1}$ PFOS, C2 fluorophores were quenched by

29, 25, and 5% for sources PL, GC, and APL. It is evident from these trends that at larger concentrations, C2 fluorophores of GC were impacted more strongly by PFOA in comparison to PFOS. However, PL exhibited much stronger interactions with PFOS than PFOA throughout all concentration levels. C2 fluorophores of APL were also found to have strong interactions with both PFOA and PFOS in all concentration ranges. Changes in C2 fluorescence indicate that PFOA and PFOS may preferentially bind with anthropogenic humic-like moieties of the DOM sources, where such interactions were most pronounced for APL, GC, and PL.

C3 fluorophores for PL and GC were quenched by 55 and 15% with the increase in PFOA concentration from 0 to 20 $\mu\text{g L}^{-1}$. At the highest PFOA concentration (1000 $\mu\text{g L}^{-1}$), C3 was quenched by 30 and 15% for PL and GC. Source BIO was found to exhibit a 5% increase in fluorescence intensity as 100 $\mu\text{g L}^{-1}$ PFOA was added, this trend further progressed, as 1000 $\mu\text{g L}^{-1}$ PFOA resulted in BIO C3 fluorophores to be enhanced by 12%. In the presence of 20 $\mu\text{g L}^{-1}$ PFOS, C3's fluorescence decreased by 25% for HA while limited changes were noted for other DOM types. At the largest concentration of PFOS, a 50% decrease in fluorescence was noted for HA while PL C3 fluorophores were enhanced by 50%. As with HA fDOM in the region of C2, C3 fluorescence enhancements were noted for both BIO and PL, this is an unexpected result and may indicate PFAS to alter the structure of proteinaceous fDOM in sample PL and BIO (Lackowicz, 2006). Overall, changes in C3 fluorescence indicate that PFOA and PFOS may preferentially bind with protein like moieties of the DOM sources, where such interactions were most pronounced for APL, GC, and PL. These results suggest that C3 fluorophores of PL interacted more strongly with PFOA but HA had the strongest interactions in the presence of PFOS.

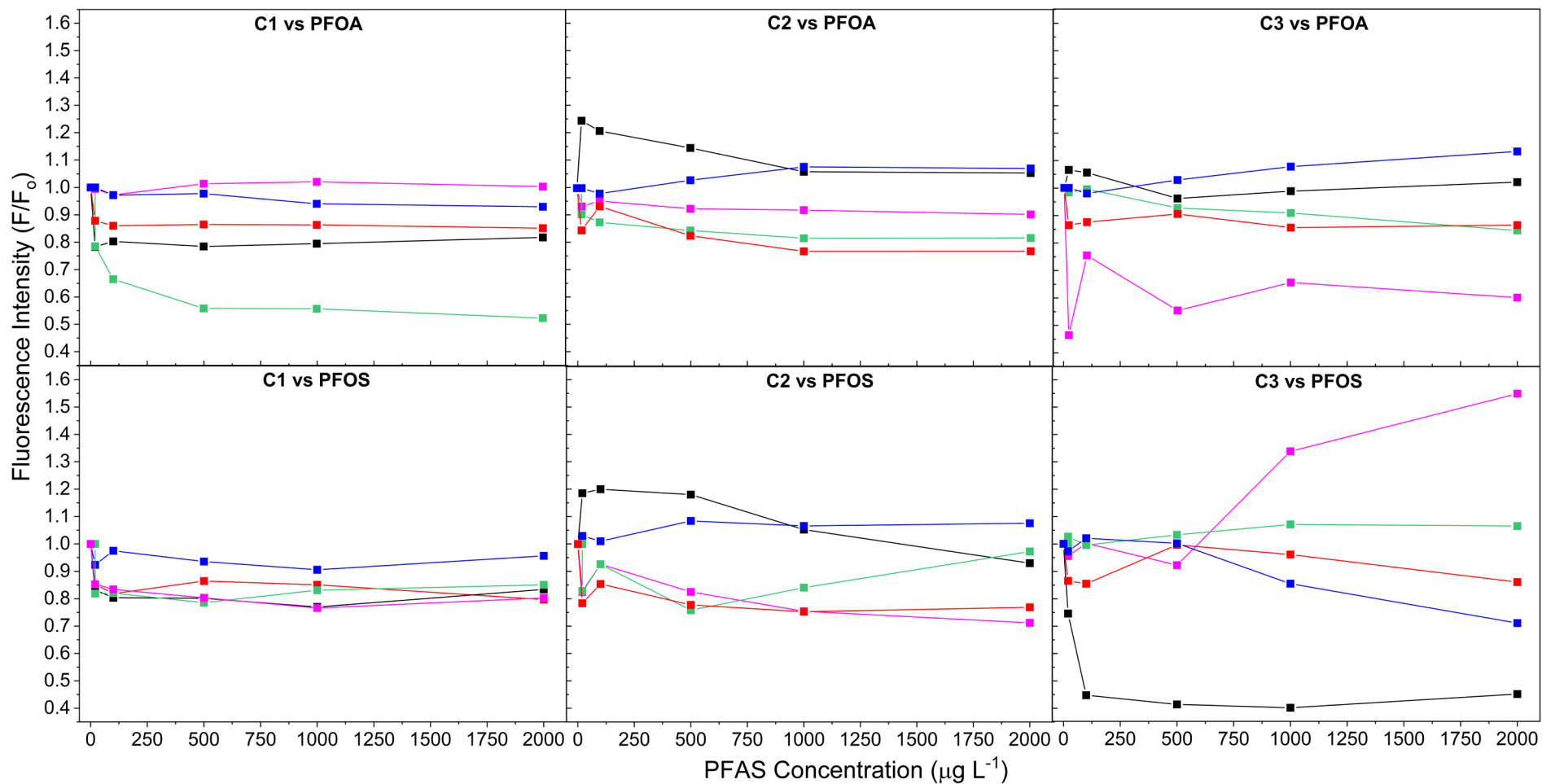


Figure 6. Fluorescence quenching of the DOM fluorophores by PFOA (top panel) and PFOS (bottom panel). The fluorophores intensity was normalized to PFAS free DOM solution. Fluorophores are described in Table 5. C1 – humic like fluorophores, C2 – anthropogenic humic fluorophores, and C3 – proteinaceous fluorophores.

3.8 PFOS Adsorption

The adsorption isotherms of PFOS on the two soils exhibited nonlinear and linear trends depending on the presence and type of DOM (100 mg C L⁻¹) in the aqueous solution (Figures 7 and 8). All isotherms fit well to Freundlich models (Table 9). The Freundlich parameters for the Gwinnett and Vaiden soils (Tables 9) were not directly comparable due to the various curvature of the isotherms, where the Freundlich exponent (n) ranged from 0.5 - 1.1, indicating that the DOM greatly impacted the diversity of free energies associated with the adsorption of the solute (Schwarzenbach et al., 2003). Therefore, PFOS adsorption in the presence of different DOM was compared by the K_d values calculated from the Freundlich fitting parameters (Table 9). The K_d values were calculated at low and high C_e concentrations (20 and 300 $\mu\text{g L}^{-1}$, respectively). Adsorption of PFOS to DOM free soils was higher by up to 66% for the Gwinnett compared to the Vaiden. The addition of 100 mg C L⁻¹ DOM to the reaction solution affected the adsorption of PFOS on both soils. However, the effect was both soil and DOM type dependent.

At low C_e (K_d 20), all DOM excluding PM increased the adsorption of PFOS on the Gwinnett soil, where increased adsorption was most prominent for sources APL, PL, and BIO. Both APL and PL increased the adsorption of PFOS onto the Gwinnett by 120%, while BIO increased adsorption by 106%. At high C_e (K_d 300) pronounced increasing effect in adsorption of PFOS on Gwinnett was observed upon the addition of BIO and APL DOM. Specifically, BIO and APL increased the adsorption of PFOS onto the Gwinnett by 62 and 45%, respectively. Conversely, sources PWC, CM and GC only had minor effects on PFOS adsorption. Furthermore, sources PM, HA, and PL substantially decreased the adsorption of PFOS to the Gwinnett where adsorption was seen to decrease by 11 and 52% for HA and PM, respectively.

DOM sources besides GC and HA slightly decreased PFOS adsorption onto the Vaiden soil at a low C_e (K_d 20). GC, CM, and HA increased PFOS adsorption by 23, 7, and 29% on the Vaiden soil, respectively. However, all other sources resulted in a decrease of ca. 20%, excluding BIO which decreased adsorption by 45% at the low C_e . At high C_e (K_d 300), DOM-Vaiden systems exhibited pronounced increasing effect upon the addition of APL, PWC, and GC DOM, where adsorption increased by 114, 41, and 44% respectively. Conversely, BIO, CM, PL and HA only had minor effects on PFOS adsorption to the Vaiden. Only PM resulted in substantially decreased PFOS adsorption, where adsorption decreased by 26% upon the addition of PM to the Vaiden system. A decrease in adsorption suggests that DOM act as a competitor on PFOS adsorption sites. In contrast, the increases observed in PFOS adsorption suggest the DOM adsorption on soils introduce additional adsorption sites for PFOS. Freundlich isotherms indicate that PFOS adsorption depends on the soil type and the sources and composition of DOM added to the system.

Table 9. Freundlich fitting parameters of PFOS adsorption to Gwinnett and Vaiden soil and distribution coefficients calculated for C_e of 20 and 300 $\mu\text{g L}^{-1}$. Standard errors are provided in parentheses.

Sample Name	Gwinnett					Vaiden				
	K_f (L g^{-1})	n	r^2	K_d 20 (L kg^{-1})	K_d 300 (L kg^{-1})	K_f (L g^{-1})	n	r^2	K_d 20 (L kg^{-1})	K_d 300 (L kg^{-1})
DOM Free Soil	0.0226 (0.03)	1.04 (0.20)	0.932	26.0 (0.18)	28.8 (0.10)	0.145 (0.07)	0.601 (0.07)	0.985	43.9 (0.05)	14.9 (0.19)
Cattle Manure	0.177 (0.06)	0.724 (0.05)	0.990	77.6 (0.19)	36.8 (0.12)	0.150 (0.07)	0.614 (0.07)	0.987	47.1 (0.12)	16.5 (0.10)
Biosolid	0.220 (0.19)	0.759 (0.15)	0.889	107 (1.37)	56.0 (0.54)	0.056 (0.03)	0.766 (0.08)	0.990	27.6 (0.04)	14.6 (0.05)
Green Compost	0.144 (0.04)	0.759 (0.05)	0.990	69.9 (0.17)	36.5 (0.10)	0.142 (0.02)	0.683 (0.02)	0.999	55.0 (0.06)	23.3 (0.01)
Peat Moss	0.0321 (0.02)	0.891 (0.09)	0.977	23.2 (0.13)	17.3 (0.04)	0.111 (0.02)	0.601 (0.03)	0.998	33.5 (0.06)	11.4 (0.07)
Poultry Litter	0.440 (0.17)	0.522 (0.06)	0.970	105 (0.32)	26.5 (0.17)	0.114 (0.05)	0.640 (0.06)	0.992	38.8 (0.24)	14.6 (0.03)
Public Works Compost	0.0262 (0.01)	0.0913 (0.09)	0.984	30.4 (0.15)	34.7 (0.06)	0.061 (0.01)	0.827 (0.04)	0.998	36.2 (0.01)	22.6 (0.21)
Humic Acid	0.237 (0.08)	0.616 (0.05)	0.983	75.1 (0.20)	26.5 (0.11)	0.233 (0.05)	0.539 (0.04)	0.995	58.7 (0.06)	16.8 (0.05)
Aged Poultry Litter	0.178 (0.08)	0.759 (0.08)	0.977	84.6 (0.39)	43.3 (0.21)	0.022 (0.04)	1.16 (0.31)	0.963	35.2 (0.10)	54.4 (0.12)

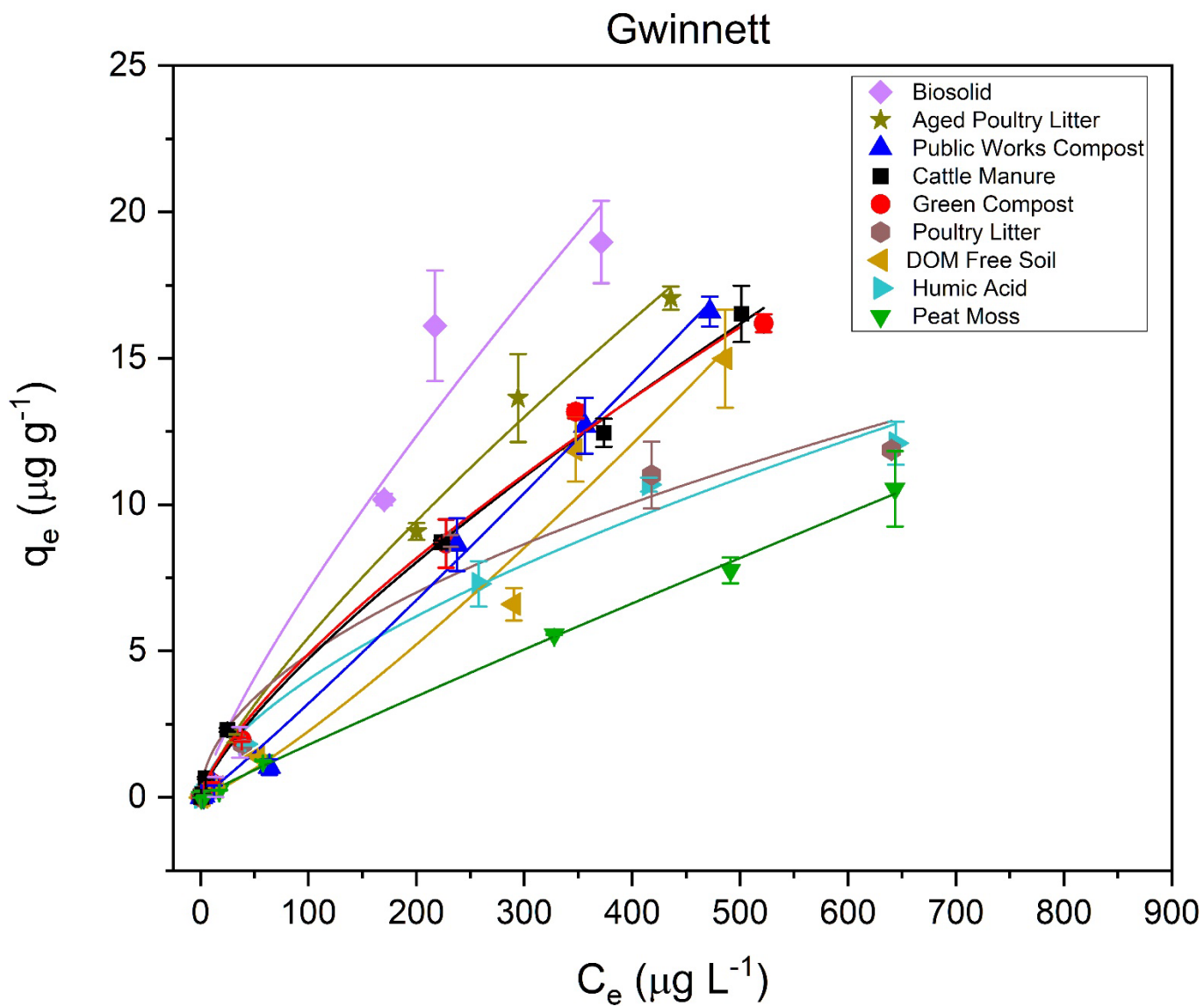


Figure 7. Impact of DOM on adsorption of PFOS on Gwinnett soils. Solids lines represent best fits to the Freundlich equation.

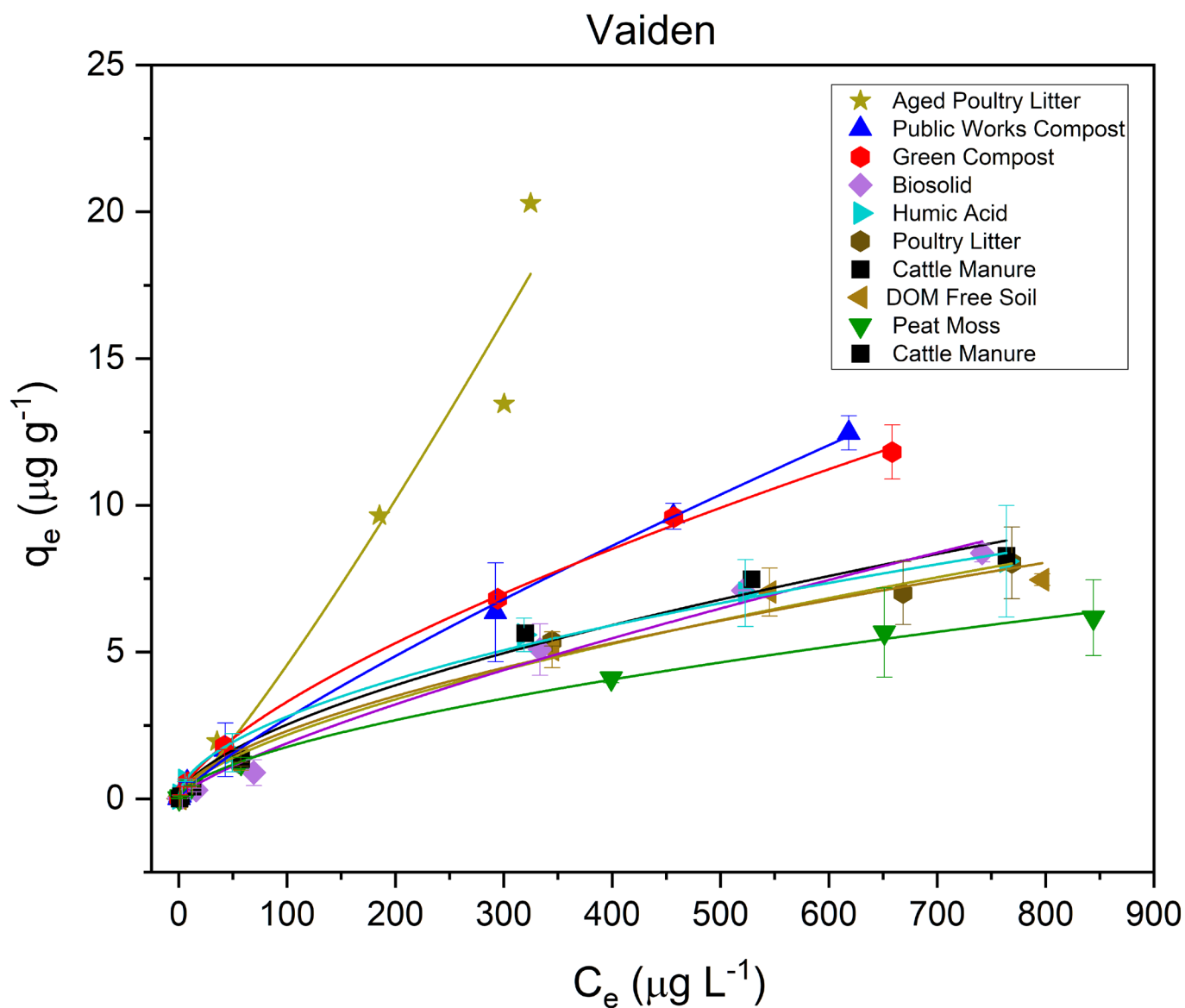


Figure 8. Impact of DOM on adsorption of PFOS on Vaiden soils. Solid lines represent best fits to the Freundlich equation.

3.9 PFOS Desorption

To further evaluate the impact of DOM on PFOS mobility in soil, the desorption of PFOS from the Vaiden soil was measured (Figure 9). Pronounced hysteresis was measured between PFOS adsorption and desorption on the DOM free Vaiden soil (Figure 9 and Table 10). On the DOM free Vaiden soil, HI increased with increasing of PFOS equilibrium concentration from 0.141 at $25 \mu\text{g L}^{-1}$ to 0.963 at $300 \mu\text{g L}^{-1}$, respectively (Figure 9). In the presence of 100 mg C L^{-1} of CM and APL in the reaction solution, the hysteresis was diminished. Other DOM types, including BIO and PWC, increased hysteresis, while PL did not affect the hysteresis between PFOS adsorption and desorption. It is important to note that in the desorption step, the replacing background solution did not contain DOM, which may compete with PFOS on adsorption surface sites. Importantly, these results indicate hysteresis to be concentration and DOM-dependent. High hysteresis between adsorption and desorption indicate strong PFOS-DOM-soil ternary complex.

Table 10. Freundlich coefficients for adsorption isotherms of PFOS on Vaiden soil (mean (standard deviation), n = 3). Hysteresis indexes were interpolated at C_e of 25, 100 and 300 $\mu\text{g L}^{-1}$ from Freundlich desorption isotherms.

<i>Sample Name</i>	<i>Desorption Fit</i>			<i>Hysteresis Indices</i>		
	$K_f (\text{L g}^{-1})$	n	r^2	$C_e = 25 \mu\text{g L}^{-1}$	$100 \mu\text{g L}^{-1}$	$300 \mu\text{g L}^{-1}$
DOM Free Soil	0.043 (0.01)	0.933 (0.05)	0.997	-0.141 (0.02)	0.362 (0.04)	0.963 (0.12)
Cattle Manure	0.275 (0.17)	0.515 (0.11)	0.962	0.335 (0.15)	0.165 (0.04)	0.0451 (0.01)
Biosolid	0.130 (0.02)	0.755 (0.08)	0.980	1.26 (0.16)	1.23 (0.26)	1.20 (0.26)
Green Compost	0.204 (0.03)	0.760 (0.04)	0.999	0.842 (0.14)	1.05 (0.17)	1.23 (0.13)
Peat Moss	0.212 (0.08)	0.606 (0.07)	0.986	0.944 (0.10)	0.957 (0.10)	0.967 (0.13)
Poultry Litter	0.0350 (0.05)	0.985 (0.27)	0.950	-0.0590 (0.05)	0.518 (0.09)	1.22 (0.09)
Public Works Compost	0.171 (0.01)	0.765 (0.01)	1.000	1.31 (0.04)	1.12 (0.04)	0.984 (0.03)
Humic Acid	0.337 (0.06)	0.587 (0.03)	0.995	0.685 (0.14)	0.802 (0.15)	0.900 (0.09)
Aged Poultry Litter	0.175 (0.09)	0.735 (0.10)	0.979	1.05 (0.09)	0.136 (0.03)	-0.288 (0.08)

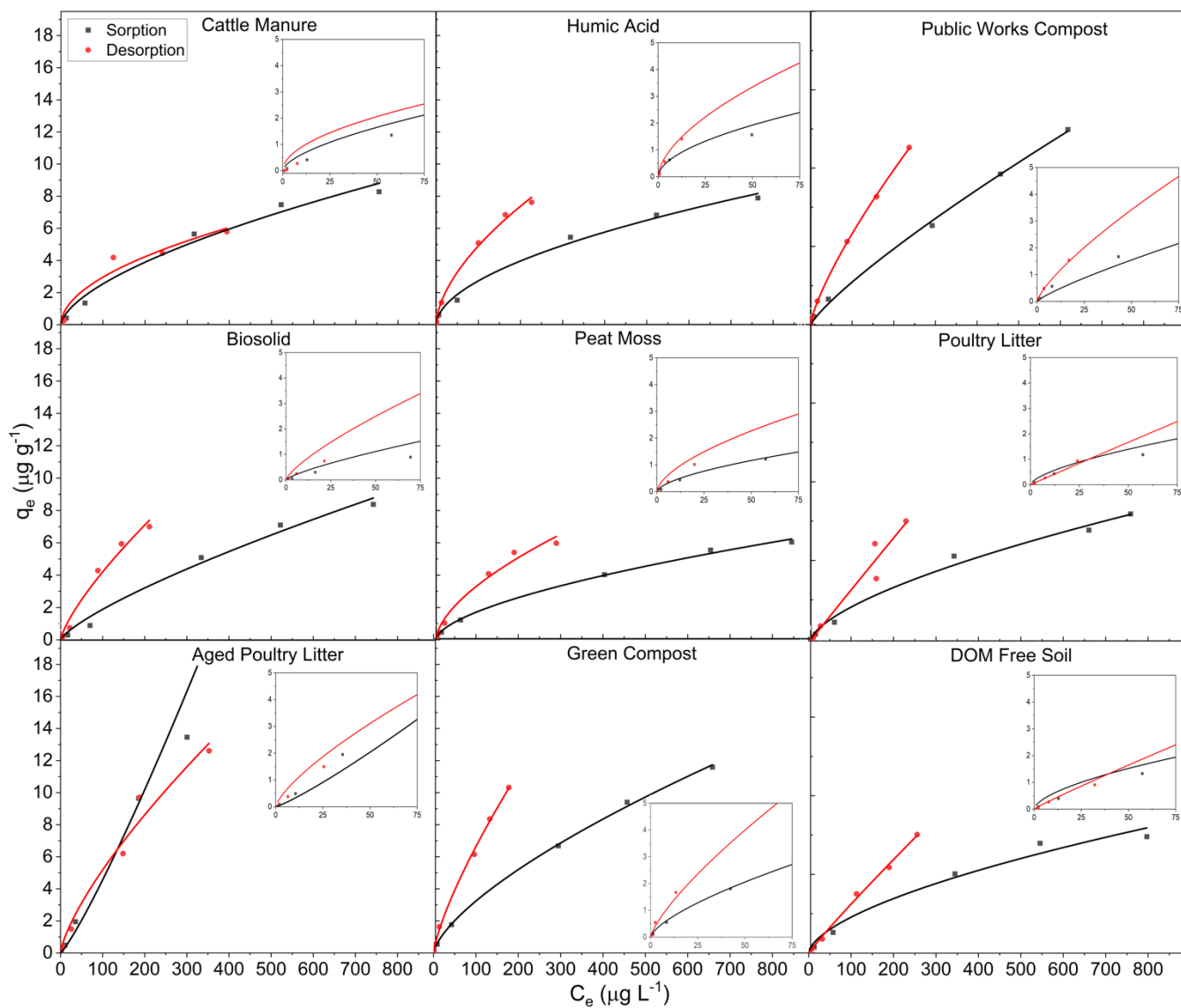


Figure 9. Adsorption and desorption of PFOS on Vaiden soil. 100 mg C L^{-1} was added to the adsorption reaction solution. The aqueous solution of the adsorption and desorption contained 50 mM CaCl_2 and the pH was 5.5. Black and red solid lines are the Freundlich fit for adsorption desorption isotherms, respectively.

3.10 Pearson Correlation Coefficients between K_{DOC} , K_d , and DOM Descriptors

Toward the goal of developing DOM predictive descriptors for PFOS adsorption, the Pearson correlation coefficients were calculated between K_{DOC} , K_d , and DOM molecular indices (Table 11). All adsorption experiments indicated that the content of proteinaceous fluorophores directly impacted PFOS adsorption. K_{DOC} ($r = 0.712$) as well as K_d derived from Freundlich isotherms employing the Gwinnett (Table 11, $r = 0.608$, $K_d 20$; $r = 0.840$, $K_d 300$) and Vaiden (Table 11, $r = 0.647$, $K_d 20$; $r = 0.019$, $K_d 300$) soils indicated strong positive correlations between C3 fluorescence signals and PFOS adsorption. Such results coincide with previous studies, indicating that PFAS binds strongly to DOM of higher proteinaceous contents (i.e., BIO) than those DOM with lessened protein content (i.e., humic acid) (Longstaffe et al., 2016). MW in the region of C3 fluorophores further corroborated this conclusion, where K_{DOC} ($r = 0.705$) and K_d (Gwinnett, $r = -0.044$, $K_d 20$; $r = 0.565$, $K_d 300$; Vaiden, $r = 0.884$, $K_d 20$; $r = -0.033$, $K_d 300$) exhibited strong positive correlations with PFOS adsorption. Furthermore, DOM aromaticity was also found to impact PFOS adsorption in all experiments. K_{DOC} ($r = 0.695$), as well K_d (Gwinnett, $r = 0.779$, $K_d 20$; $r = 0.542$, $K_d 300$; Vaiden, $r = 0.107$, $K_d 20$; $r = 0.560$, $K_d 300$) exhibited positive correlations with $SUVA_{254}$. These results coincide with other studies where $SUVA_{254}$ was found to be positively correlated to PFOS adsorption, however, such correlations were weak in these studies (Kothwala et al., 2017). Here, we present strong positive correlations between PFOS adsorption and $SUVA_{254}$, indicating heightened DOM aromaticity to enhance PFOS adsorption. Positive correlations were also identified between E4:E6 values, K_{DOC} ($r = 0.838$), and K_d (Gwinnett, $r = 0.563$, $K_d 20$; $r = 0.517$, $K_d 300$; Vaiden, $r = 0.719$, $K_d 20$; $r = 0.084$, $K_d 300$). E4:E6 has been found to be positively correlated with carboxyl group content (Chen et al., 1977), implying DOM with heightened carboxyl moieties to interact more strongly with PFOS.

Further correlations between DOM composition and PFOS adsorption were identified. Specifically, FI and HIX were found to be correlated to PFOS adsorption across all experiments. K_{DOC} ($r = 0.802$) as well as K_d derived from batch experiments employing the Gwinnett ($r = 0.379$, $K_d 20$; $r = 0.400$, $K_d 300$) and Vaiden ($r = 0.618$, $K_d 20$; $r = 0.286$, $K_d 300$) soils found FI to be positively correlated to PFOS adsorption. Such a correlation would indicate that DOM with larger FI values (or those that are microbially derived) interacts with PFOS more strongly. Furthermore, HIX is a general indicator of DOM decomposition, where there is a positive relationship between DOM properties, such as the presence of larger molecular weight fragments as HIX becomes larger (Ohno., 2002). Negative correlations were found between K_{DOC} ($r = -0.806$) as well as K_d (Gwinnett, $r = -0.581$, $K_d 20$; $r = -0.787$, $K_d 300$; Vaiden, $r = -0.604$, $K_d 20$; $r = -0.127$, $K_d 300$) and HIX. These correlations indicate that less humified DOM (i.e., BIO) have significantly stronger interactions than those DOMs that are more humified, such as commercial humic acids, corroborating correlations seen with FI values. These indices support the conclusion that human and animal waste DOM more strongly interacted with PFOS than DOM that is more humified and of terrestrial origin (i.e., HA).

Table 11. Pearson correlation matrix between DOM characterization indices, K_{DOC} , and K_d found from adsorption experiments in Figures 5, 7 and 8. Highlighted blue cells represent moderate correlations ($r = \pm 0.3-0.699$) while green represents strong ($r = \pm 0.7-0.999$).

Pearson Correlation Matrix					
DOM Molecular Indices	K_{DOC} ($L\ kg^{-1}$)	Gwinnett K_d 20 ($L\ kg^{-1}$)	Gwinnett K_d 300 ($L\ kg^{-1}$)	Vaiden K_d 20 ($L\ kg^{-1}$)	Vaiden K_d 300 ($L\ kg^{-1}$)
$UV_{254}\ M_w$ (Da)	-0.193	-0.16	0.47	0.052	-0.497
$UV_{254}\ M_n$ (Da)	-0.192	-0.23	0.107	0.204	-0.586
<i>Ex:Em</i> 260:465 M_w (Da)	-0.265	-0.564	-0.09	0.138	-0.555
<i>Ex:Em</i> 260:465 M_n (Da)	-0.265	-0.564	-0.09	0.139	-0.555
<i>Ex:Em</i> 275:340 M_w (Da)	0.705	-0.042	0.565	0.884	-0.033
<i>Ex:Em</i> 275:340 M_n (Da)	0.705	-0.044	0.565	0.886	-0.033
$C1$ ($RU\ L\ mg\ C^{-1}$)	0.093	0.055	0.131	0.409	0.365
$C2$ ($RU\ L\ mg\ C^{-1}$)	0.68	0.232	0.05	0.206	0.127
$C3$ ($RU\ L\ mg\ C^{-1}$)	0.712	0.608	0.84	0.647	0.019
$SUVA_{254}$ ($L\ mg\ cm^{-1}$)	0.695	0.779	0.542	0.107	0.56
$E2:E3$	0.716	0.02	0.244	0.673	-0.311
$E4:E6$	0.838	0.563	0.517	0.719	0.084
FTIR Index 1	-0.271	0.313	0.106	-0.129	0.155
FTIR Index 2	0.034	0.461	0.339	0.233	0.33
FI	0.802	0.379	0.4	0.618	0.286
HIX	-0.806	-0.58	-0.787	-0.604	-0.127

Discussion

4.1 Differences in chemical properties of DOM samples

The selected DOM demonstrates a broad range of chemo-physical characteristics. Hence, supporting the hypothesis that organic amendments from different sources will produce DOM with distinct properties. DOM of PWC and HA, which are extracted from solids primarily consisting of degraded plant materials, were characterized by a high degree of humification, low nitrogen content and higher content of aromatic, phenolic, and carboxyl constituents. Conversely, GC, BIO, PL, APL, and CM were characterized by lower aromatic moieties and a larger proportion of nitrogen-containing functional groups. Such DOM were extracted from organic amendments derived from animal wastes and biosolids from a municipal wastewater treatment facility.

As indicated by HIX, HA and PWC sources were found to be the most mature of all DOM (Table 4). It is expected that the long-term decomposition of organic matter has led to a significantly lower number of compounds with lignin structures (Santos et al., 2021). Such large HIX values (Table 4) when compared to the other DOM show that both PWC and HA are enriched in carboxyl group content and indicate properties such as total exchangeable acidity to be large in the two DOM. Furthermore, HA and PWC were found to have relatively higher SUVA₂₅₄ and low E4:E6, indicating larger proportion of aromatic materials and large MW assemblages when compared to the other DOM. This is also supported by larger M_w and M_n measured for these DOM by HPSEC analysis. FTIR Index I confirmed that both DOM sources are enriched with aromatic moieties, which was more pronounced for HA. This difference is likely due to the lessened degree of humification found for the PWC DOM compared to the more stable standard source. Finally, the fluorescence analysis demonstrated that HA and PWC fDOM were composed of mainly the terrestrial humic-like C1. Furthermore, the anthropogenic humic-like C2 was absent from PWC,

which is consistent with the absence of animal waste in the compost used for its extraction. The lack of evidence for nitrogen-containing functional groups compared to other DOM's is also evident for both PWC and HA samples since less than 25% of their total fluorescence was attributed to C3 fluorophore. HA and PWC also lacked signals from FTIR spectra which relate to the presence of amides (Figure 4) while also lacking shoulders in absorbance spectra (Figure 1) that would indicate the presence of nitrogen groups. FTIR spectra (Figure 4) presented the most pronounced carboxylates and phenolic bands for HA and PWC with respect to other type of DOM. Overall, PWC and HA were found to be highly humified, and terrestrially derived, with their compositions enriched in aromatic, carboxyl, and phenolic constituents.

The other DOM were extracted from organic amendments derived from either (1) municipal wastewater materials (BIO), (2) animal wastes that have been composted (PL, APL, CM, and GC), or (3) plant wastes that have been ameliorated with synthetic and inorganic fertilizers (PM). Due to their origin, BIO, APL, PL, CM, GC, and PM were expected to contain larger proportions of alkyl moieties, proteinaceous assemblages, and a lack of aromatic carbon when compared to the HA and PWC DOM. Fluorescence characterization showed BIO, GC, and CM to have the largest proportion of C3 proteinaceous fluorophores (Figure 3), where BIO contained the largest proportion of all DOM sources. This was further supported by the presence of amide I bands in their FTIR spectra and the presence of amide II bands in the spectra of the BIO DOM. These results are consistent with previously reported studies indicating higher proteinaceous content in DOM extracted from animal wastes and biosolids or soils amended with these materials (Ohno and Bro, 2006; Hunt and Ohno, 2007). In addition, the significantly larger ($p < 0.05$ ANOVA, Tukey's HSD) MW of BIO, GC, and CM was associated with C3 fDOM. Municipal wastewater treatment plants experience an income of high nutrient load materials that

are rich in nitrogen (despite undergoing de-nitrification processes) where effluents contain relatively high C/N ratios, hence the significantly greater prevalence of proteinaceous signals from FTIR and fluorescence analysis for the BIO source can be explained by its provenance. CM, BIO, and GC produced the three lowest SUVA₂₅₄ values respectively, indicating an aromatic content half of what is seen in the HA and PWC sources (Weishaar et al., 2003). Such a low aromatic content is expected for less mature DOM sourced from wastewater or animal wastes (Hunt and Ohno, 2007). HIX was also seen to be lowest in these three DOM, where values increase in the order of BIO < CM = GC.

Poultry wastes consist of excretion, feathers, feed, and bedding materials composed of pine shavings and sawdust. The composted poultry wastes were taken from the same composting pile but at different time intervals, one month for PL, and eight months for the APL. In general, the aromatic and alkyl compounds increase with composting time, as demonstrated by the FITR index I, HIX, and SUVA₂₅₄ values (Caricasole et al., 2010; Wang et al., 2014). Similar increases in aromatic and aliphatic signals were observed for poultry litters composted for 60 days (Wang et al., 2014) as well as plant based materials composted for 90 days (Caricasole et al., 2010). The aromatic content of APL was 16.5% (Weishaar et al., 2003) and was 32% larger than PL as indicated by the SUVA₂₅₄ values (Table 4). The fDOM of APL demonstrated a lower proportion of anthropogenic humic-like C2 and higher proportion of C1, which indicate an increase in the terrestrial humic like fDOM signals with longer composting time. Both APL and PL exhibited absorbance bands associated with amine I and II. However, fluorescence analysis indicated that the proteinaceous content of APL's fDOM was 24% higher than PL. It is important to note these differences since the APL DOM represents a transition in chemical characteristics where it

contains similar protein content to the animal waste-derived sources. At the same time, its aromaticity is similar to the mature plant derived DOM (i.e., PWC and HA).

As evident in the above characterizations, DOM molecules are highly heterogeneous. Their composition is heavily influenced by the source material and origin. Hence, supporting the hypothesis that the source of DOM will be reflected by unique chemical structure and composition. Therefore, justifying the need to investigate the effect of DOM type on the binding of PFAS. Furthermore, these DOM enable the examination of multiple possible interactions with PFAS and help identify DOM molecular indices that could be used as quantitative predictors for the interactions between PFAS and DOM.

4.2 PFOS Adsorption

In the soil environment, the fate of PFAS is controlled by its interactions with the soil's mineral and organic constituents, where DOM is of utmost importance regarding the fate, bioaccumulation, and translocation of PFAS (Xia et al., 2015; Lyu et al., 2018; Bolan et al., 2021). In this study, adsorption experiments identified PFOS adsorption to be DOM and soil type dependent. Furthermore, the distribution and range of K_{DOC} and K_d demonstrate the fundamental role of DOM molecular structure and composition on PFOS adsorption and, therefore, fate in the environment.

Dialysis equilibrium and batch sorption experiments identified a strong positive correlation between proteinaceous DOM content, size (C3 signals and M_w), and PFOS binding to DOM (K_{DOC}). BIO and PM contained the and lowest content of proteinaceous DOM, respectively. The PFOS K_d value for the Gwinnett soil increased by 91% when the GC was present in the reaction solution compared with DOM free solution. In comparison, K_d decreased by 52% in the presence of PM in the reaction solution compared with DOM free solution. These trends were also similar

in batch adsorption experiments employing the Vaiden soil. Hence, it is evident that the proteinaceous content of DOM facilitates stronger binding of PFOS and enhancing co-adsorption to soil. These findings agree with previous studies reported on the proteinophilic nature of PFOS, where PFOS was found to preferentially bind with protein compounds (Longstaffe et al., 2016; Liu et al., 2022). Furthermore, correlations indicated that less humified DOM have stronger interactions with PFOS. This was further supported by the positive correlation between FI and K_d as well as K_{DOC} values. Both correlations imply that DOM sourced from human and animal wastes, such as BIO, have stronger interactions with PFOS than those DOM sourced from degraded plant materials (PWC etc.,).

All experiments identified a strong positive correlation between $SUVA_{254}$ and PFOS adsorption. This indicates that heightened DOM aromaticity resulted in stronger interactions with PFOS. Correlations between $SUVA_{254}$ and PFOS binding have been identified in other studies, but such correlations were weak (Kothwala et al., 2017). Research has supported that a highly aromatic DOM structure can promote a hydrophobic backbone of the DOM molecule, which can facilitate hydrophobic interactions between the PFOS tail and DOM (Kothwala et al., 2017). DOM sources such as APL, which contained the largest composition of aromatic assemblages, increased PFOS K_d values for the Vaiden soil by 114% when the APL was present in the reaction solution compared with DOM free solution. This was consistent across all experiments with the APL DOM. Other DOM sources with high degrees of aromaticity, such as PWC, also resulted in enhanced PFOS adsorption. However, sources such as BIO, which were found to have the lowest degree of aromaticity of all DOM, resulted in enhanced PFOS binding in dialysis experiments as well as when added to the reaction solution of the Gwinnett soil. While correlations between PFOS adsorption and molecular indices indicate DOM with lessened aromaticity to undergo weaker

interactions with PFOS, the heightened interaction between BIO and PFOS is explained by BIO containing the largest composition of proteinaceous DOM of all sources. It is evident that while DOM aromaticity influences PFOS adsorption, multiple modes of interaction exist between DOM and PFOS, highlighting the complexity of the interactions between the two molecules and further indicate that PFOS adsorption was dependent on the source of DOM (Du et al., 2014; Qin et al., 2022).

Hydrogen bonding has been proposed as a form of interaction between PFOS hydrophilic head and phenolic and carboxyl moieties on the DOM molecule (Du et al., 2014; Ifon et al., 2022; Qi et al., 2022). Samples APL, GC, and PWC enhanced soil adsorption of PFOS with both the Gwinnett and Vaiden soil and were the only DOM sources that consistently enhanced soil adsorption of PFOS in both systems. Hence, it is evident that the molecular composition of these DOM presented consistent modes of interaction with the PFOS molecule. When analyzing FTIR spectra for the DOM sources, all three sources exhibited C–O stretch associated with the presence of phenol from carboxylic acid (Omoike and Chorover., 2006). Such molecular components would promote hydrogen interactions and possibly explain the enhanced interactions exhibited for the three DOM sources in all adsorption experiments. Furthermore, a positive correlation was identified between E4:E6, K_d , and K_{DOC} values, indicating increased DOM content of carboxyl moieties to enhance PFOS interactions with DOM. With this information, it is justified to conclude that PFOS adsorption is affected by the presence of phenolic and carboxyl moieties contained in the DOM molecule.

The Vaiden soil has similar physical and chemical characteristics to the Gwinnett soil. Both were found to have similar size distributions (clay textural class), pH, and WEOC. The primary measured difference between the two soils is the capacity to interact with negatively-charged

molecules, which is evident in the significantly lower AEC for the Vaiden soil (0.33 meq 100 g⁻¹) compared to the Gwinnett (0.99 meq 100 g⁻¹). Therefore, stronger electrostatic repulsion can explain the lower PFOS adsorption on the Vaiden soil. However, when DOM was added to these systems, soil adsorption of PFOS was seen to be impacted by DOM molecules in similar ways. Positive correlations were identified between K_d and proteinaceous signals, SUVA₂₅₄, E4:E6, FI values as well as an inverse relationship with degree of humification (HIX). These results indicate that PFOS sorption is in fact controlled by the properties of the soil, but also suggest that DOM source and composition can strongly influence PFOS adsorption.

APL, BIO, and GC exhibited the strongest quenching of fluorophores by PFOS and PFOA. These changes in fluorescence intensity agree with the strong interactions identified for the three DOM in dialysis experiments with PFOS. Importantly, PL and HA exhibited fluorescence enhancements when interacted with PFOA or PFOS. Similar increases in fluorescence intensity by interactions with PFOS was observed for humic substances (Ifon et al., 2022). It has been suggested that changes in the DOM tertiary structure due to interactions with PFOS can facilitate this enhanced fluorophore intensity. It would be important that further studies focus on fluorescence titrations and include the use of HPSEC to test if the DOM structure is changing upon the introduction of PFAS. Overall, fluorescence quenching experiments showed that when titrated with PFAS, DOM fluorophores underwent changes, highlighting that PFAS can in fact interact with DOM fluorophores.

Of all eight DOM, only the addition of APL and CM reduced the hysteresis between adsorption and desorption of PFOS to the Vaiden soil. It was previously demonstrated that PFAS with longer chain length (i.e., PFOS), are more difficult to desorb from natural sediments, soil, and organic matter than those PFAS with shorter chain length (Zhao et al., 2012, You et al., 2010, Jia

et al., 2010). It is important to note that hysteresis can be identified in systems with experimental artifacts such as hysteresis attributed to degradation, an insufficient time allowed for mass transfer to reach an equilibrium condition, and solute losses to vessel materials and components (Site et al., 2001). Such artifacts can be eliminated in the present study. Control experiments were run simultaneously with adsorption experiments, revealing adsorption to vessel was negligent. Likewise, preliminary studies identified sufficient time for the experimental system to approach apparent sorption desorption equilibria. Hysteresis caused by degradation can be excluded since PFOS is highly stable under the experimental conditions. Adsorption-desorption depended on the source and composition of DOM and the concentration of PFOS. This finding suggests that DOM can inhibit transport of PFOS through the soil subsurface. Moreover, the extent of this inhibition depends on the type of DOM. Hence, the selection of organic amendment may be critical in PFAS contaminated sites.

Conclusion

Eight sources of DOM were extracted from commonly employed soil organic amendments to evaluate the effects of DOM on PFOS adsorption. DOM sources were not only found to be heterogenous, but their source material directly impacted the inherent chemo-physical composition of the DOM, supporting our hypothesis that DOM sources from different organic amendments (i.e., green compost vs biosolid) will result in varying chemical compositions. PFOS adsorption was dependent on the source and composition of DOM and soil type, where the DOM proteinaceous content was the strongest indicator of PFOS adsorption. Furthermore, aromaticity, degree of humification, carboxyl group content, and the presence of phenolic functional groups strongly impacted PFOS adsorption. Therefore, the results support the hypothesis that the molecular composition of DOM influences the binding of PFAS. Fluorescence quenching results

revealed PFOA and PFOS to interact with DOM fluorophores. However, PL and HA exhibited increases in fluorescence intensity when titrated with PFAS. These fluorescence enhancements could imply DOM to undergo structural and compositional changes when interacted with PFAS. PFOS adsorption on soils was substantially affected by the presence of various DOM, where the most pronounced increases in PFOS adsorption were denoted for DOM extracted from human and animal wastes. Sorption-desorption isotherms also indicated pronounced hysteresis behavior, which may limit the transport of PFOS in soils. Moreover, adsorption-desorption depended on the source and composition of DOM and the concentration of PFOS, indicating the potential of DOM to inhibit the transport of PFOS through the soil subsurface. The extent of this inhibition depends on the type of DOM. Hence, the selection of organic amendments used in soil application may be critical in PFAS contaminated sites.

Limited research has focused on PFAS-DOM interactions. The studies that have focused on this topic have primarily employed DOM sourced from commercial humic and fulvic acids, which are not representative of organic materials applied to soils. Findings presented here show that soil organic amendment derived DOM can substantially influence the fate of PFAS in soils. With this information, consideration should be taken to the types of organic amendments applied in agricultural settings since the co-introduction of PFAS-DOM (i.e., use of biosolids) has been identified. This study demonstrated a strong potential for using DOM molecular descriptors as predictors for the behavior of anionic PFAS in the soil and water environment. Notably, the use of DOM descriptors and binding coefficients/parameters have potential for further use in modeling efforts to predict the transport of PFAS in the environment. Further research should focus on establishing DOM molecular descriptors and binding coefficients between short and longer chain PFAS as well as zwitterionic and cationic PFAS. It would also be of interest to examine PFAS

adsorption-desorption mechanisms with a broader range of soil types. Such research would allow for a complete analysis of the DOM molecular components that influence PFAS adsorption while further developing DOM molecular indices and binding parameters into a robust model that can predict the fate of PFAS in the soil and aquatic environment.

Appendix

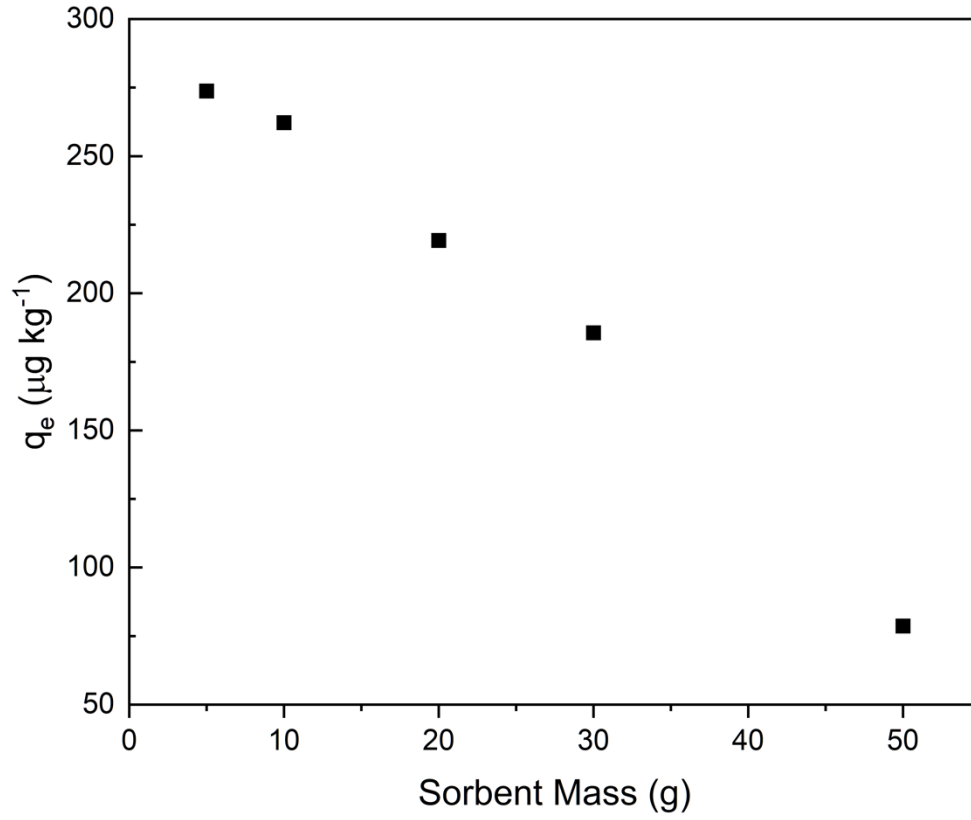


Figure A1. Sorption of PFOS on Gwinnett using varying solution:soil ratios. The solution volume was 30 mL and the equilibration time was 76 hours.

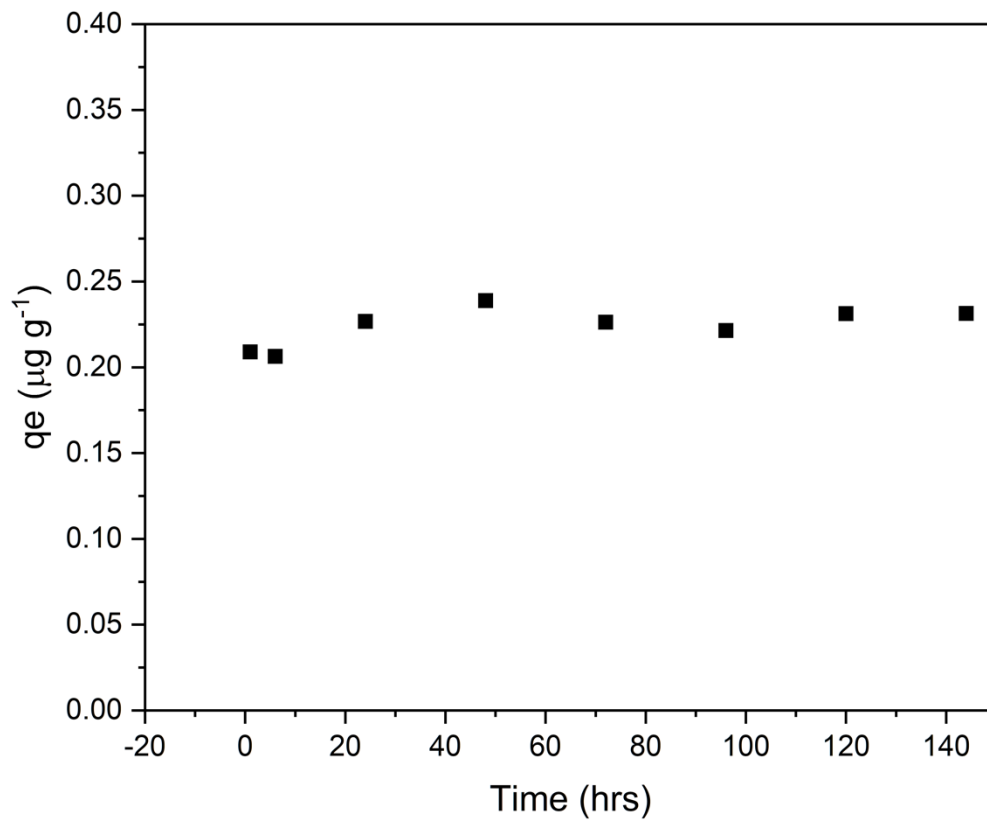


Figure A2. Sorption kinetics of PFOS on Gwinnett.

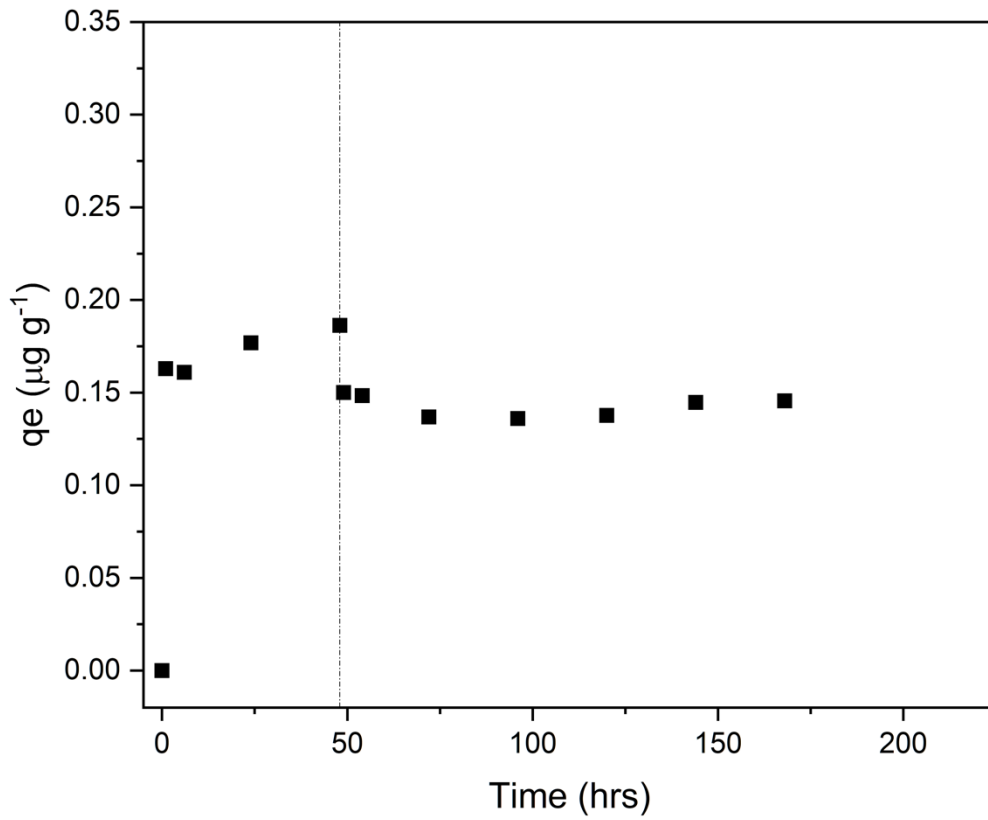


Figure A3. Sorption and desorption kinetics of PFOS on Vaiden. The desorption step started after 48 hours (dashed line).

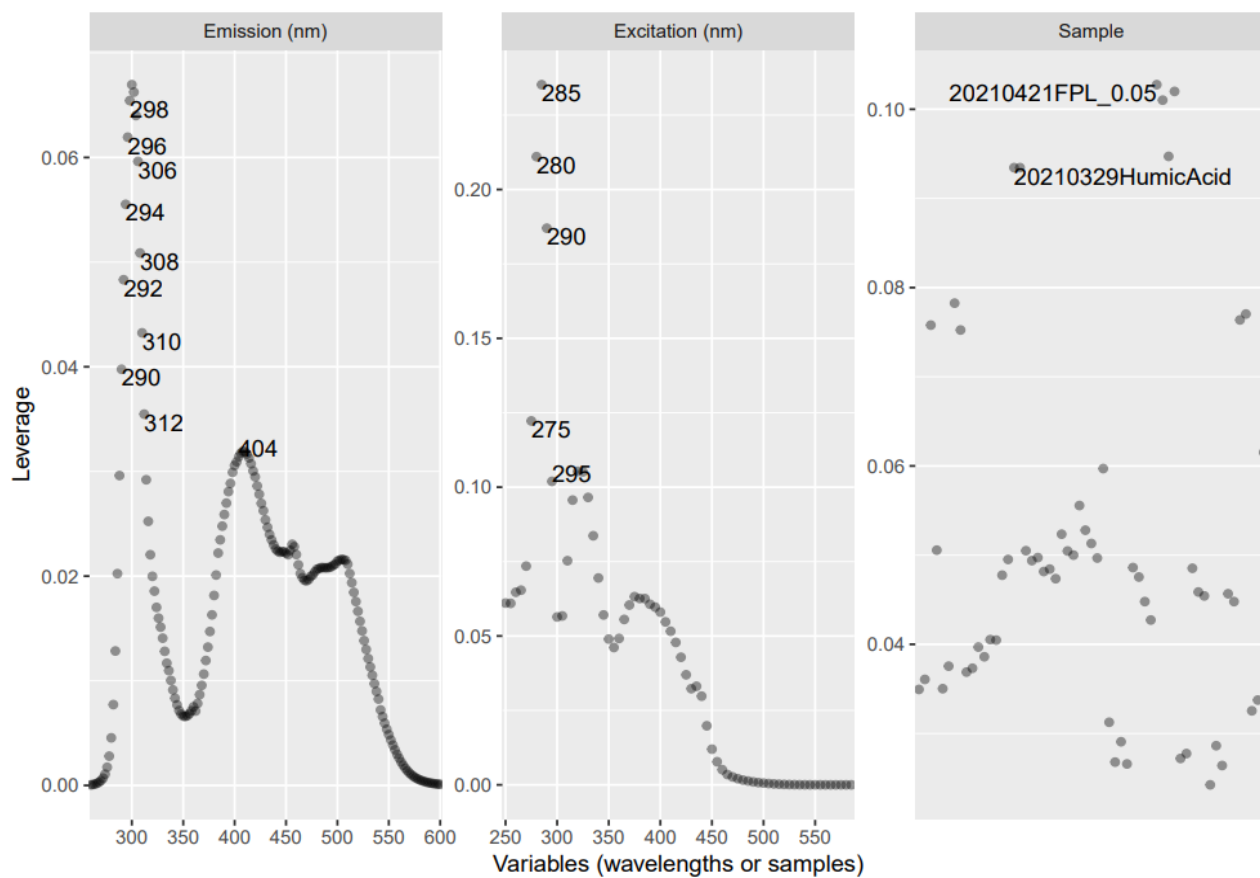


Figure A4. Represents outliers and leverage plot for resulting three component PARAFAC model.

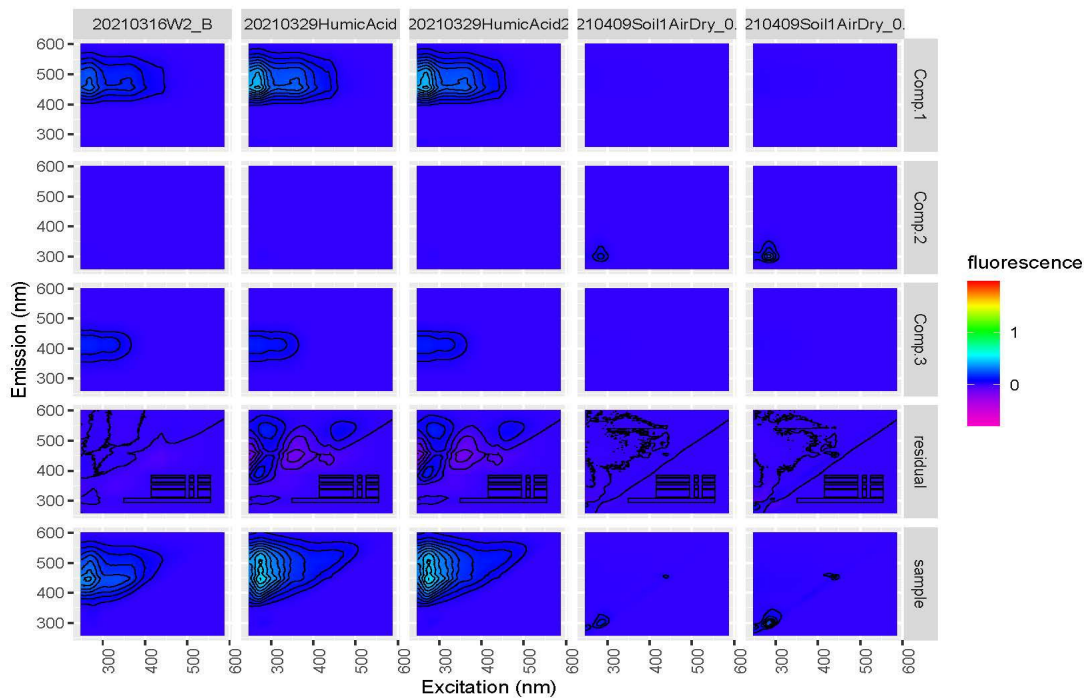


Figure A5. Represents plot of five DOM samples residuals from derived PARAFAC model.

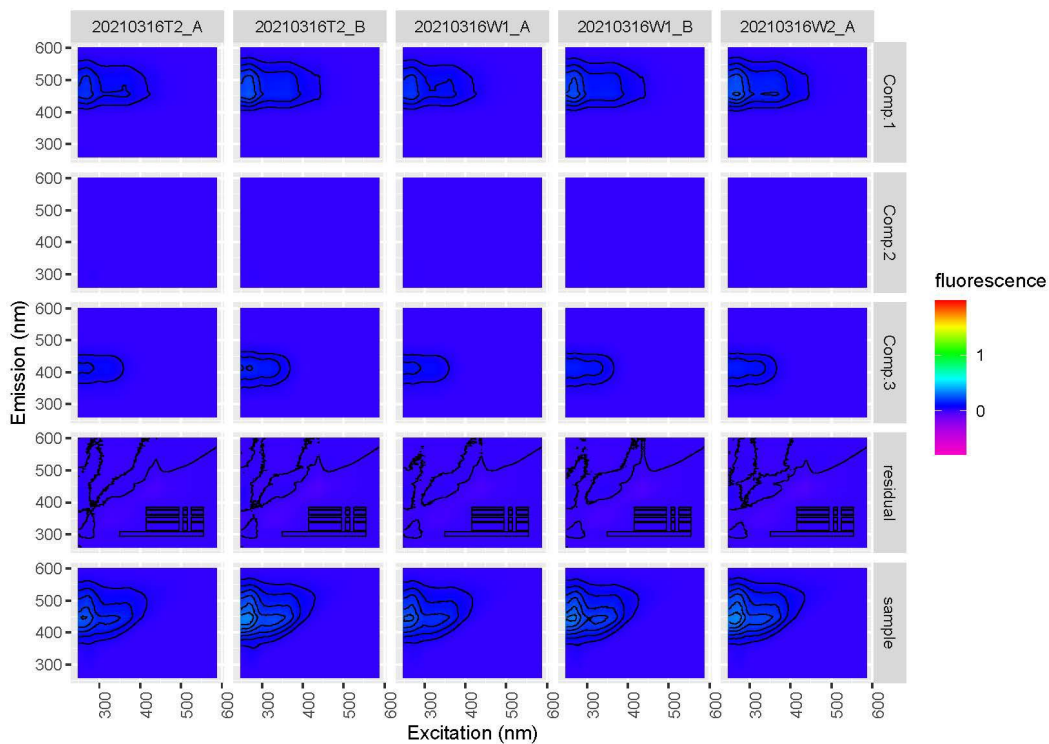


Figure A6. Represents plot of five DOM samples residuals from derived PARAFAC model.

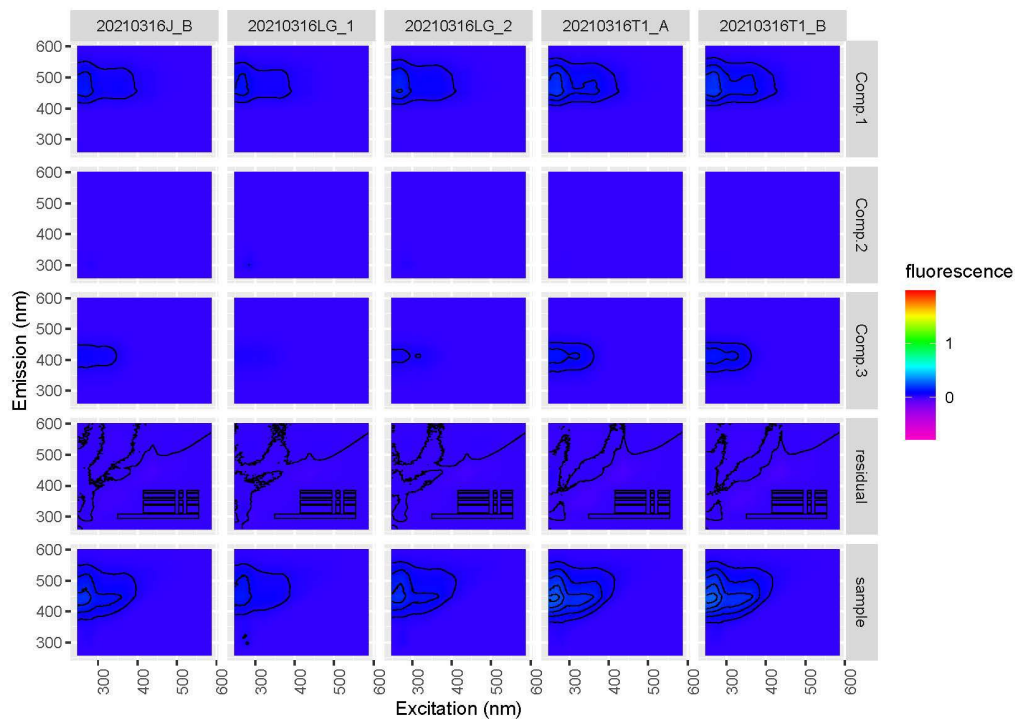


Figure A7. Represents plot of five DOM samples residuals from derived PARAFAC model.

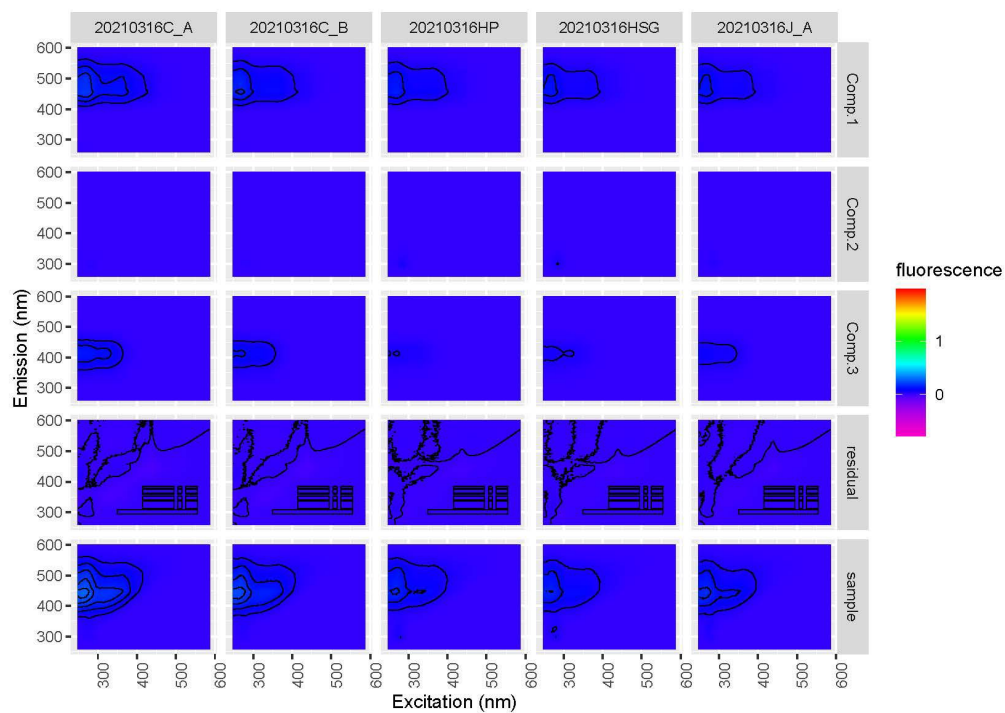


Figure A8. Represents plot of five DOM samples residuals from derived PARAFAC model.

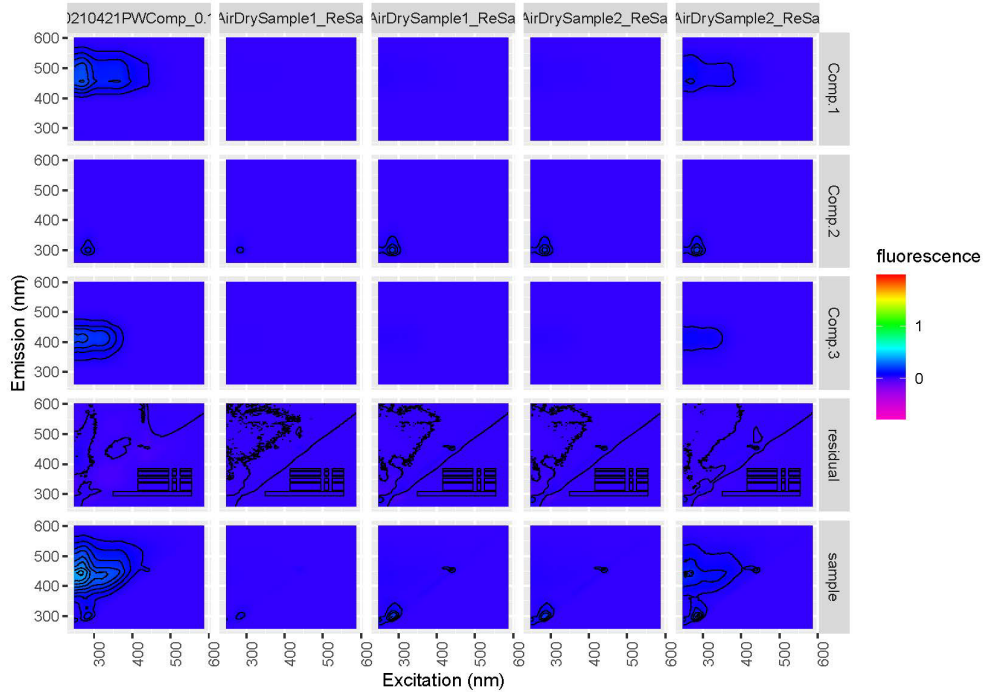


Figure A9. Represents plot of five DOM samples residuals from derived PARAFAC model.

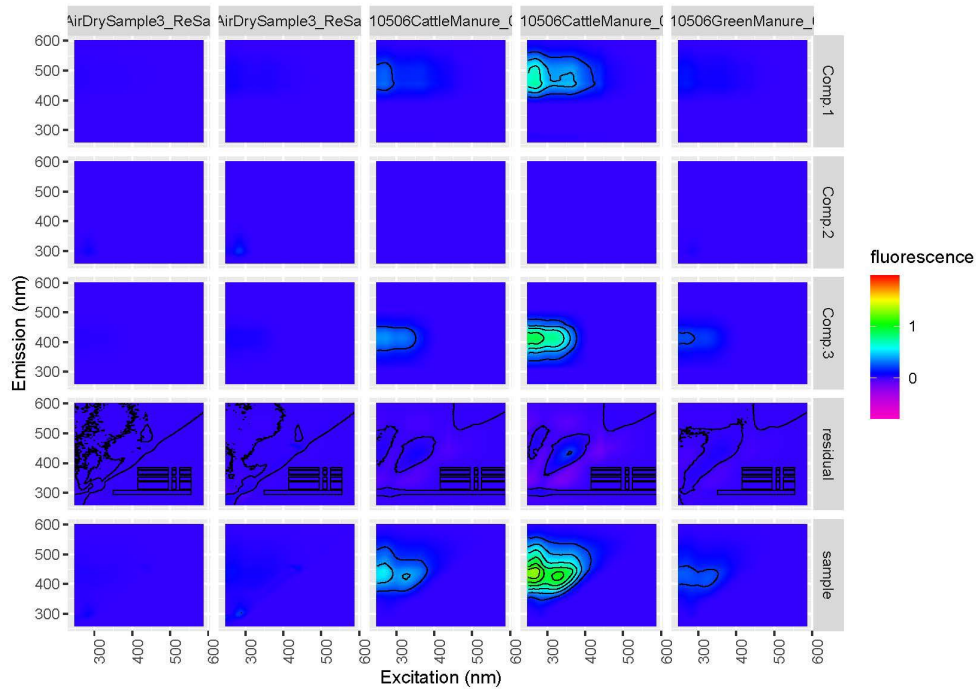


Figure A10. Represents plot of five DOM samples residuals from derived PARAFAC model.

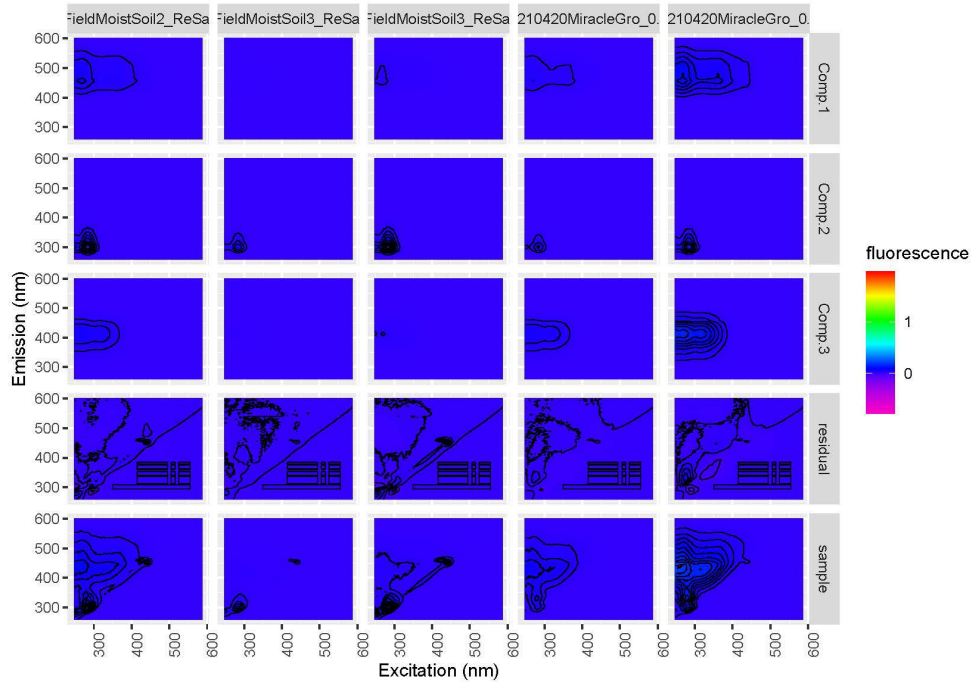


Figure A11. Represents plot of five DOM samples residuals from derived PARAFAC model.

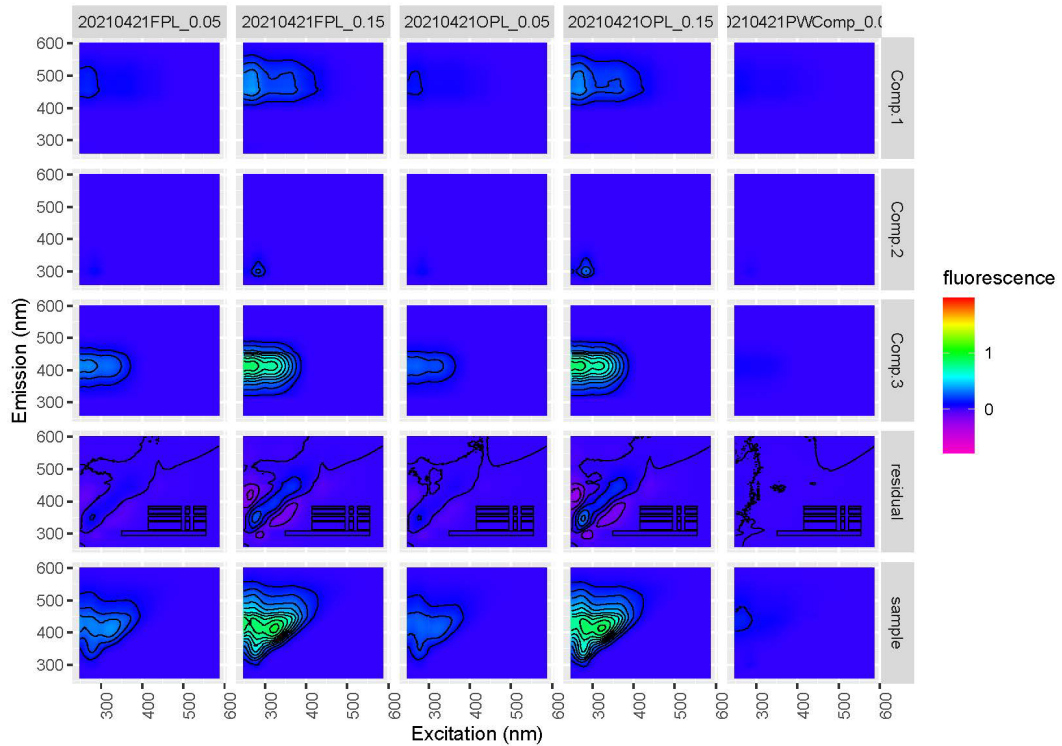


Figure A12. Represents plot of five DOM samples residuals from derived PARAFAC model.

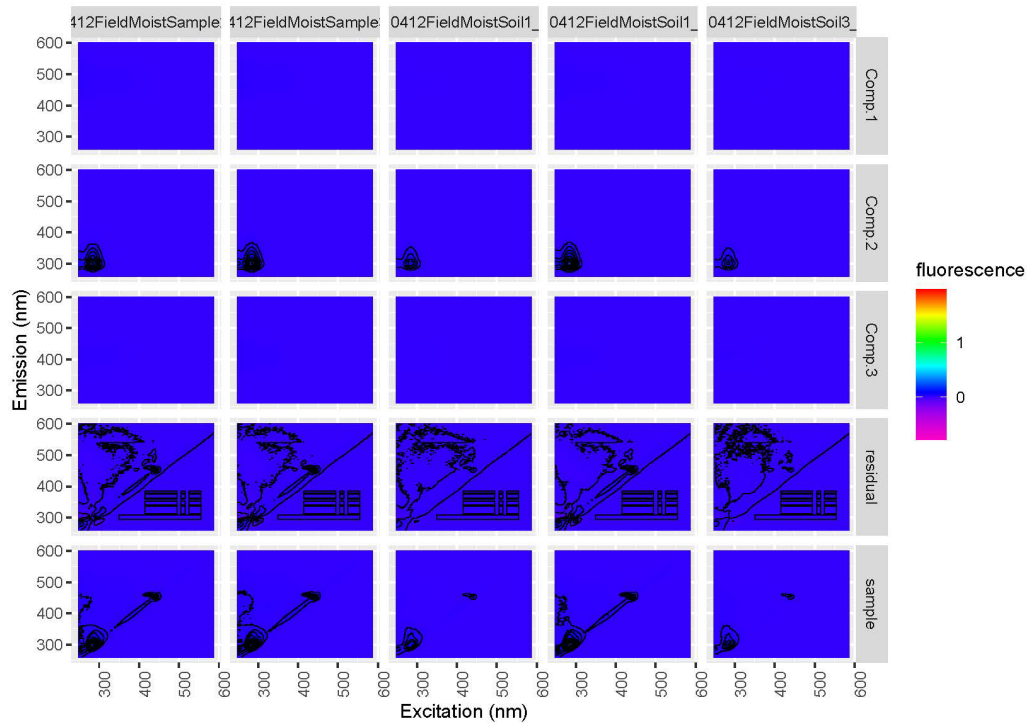


Figure A13. Represents plot of five DOM samples residuals from derived PARAFAC model.

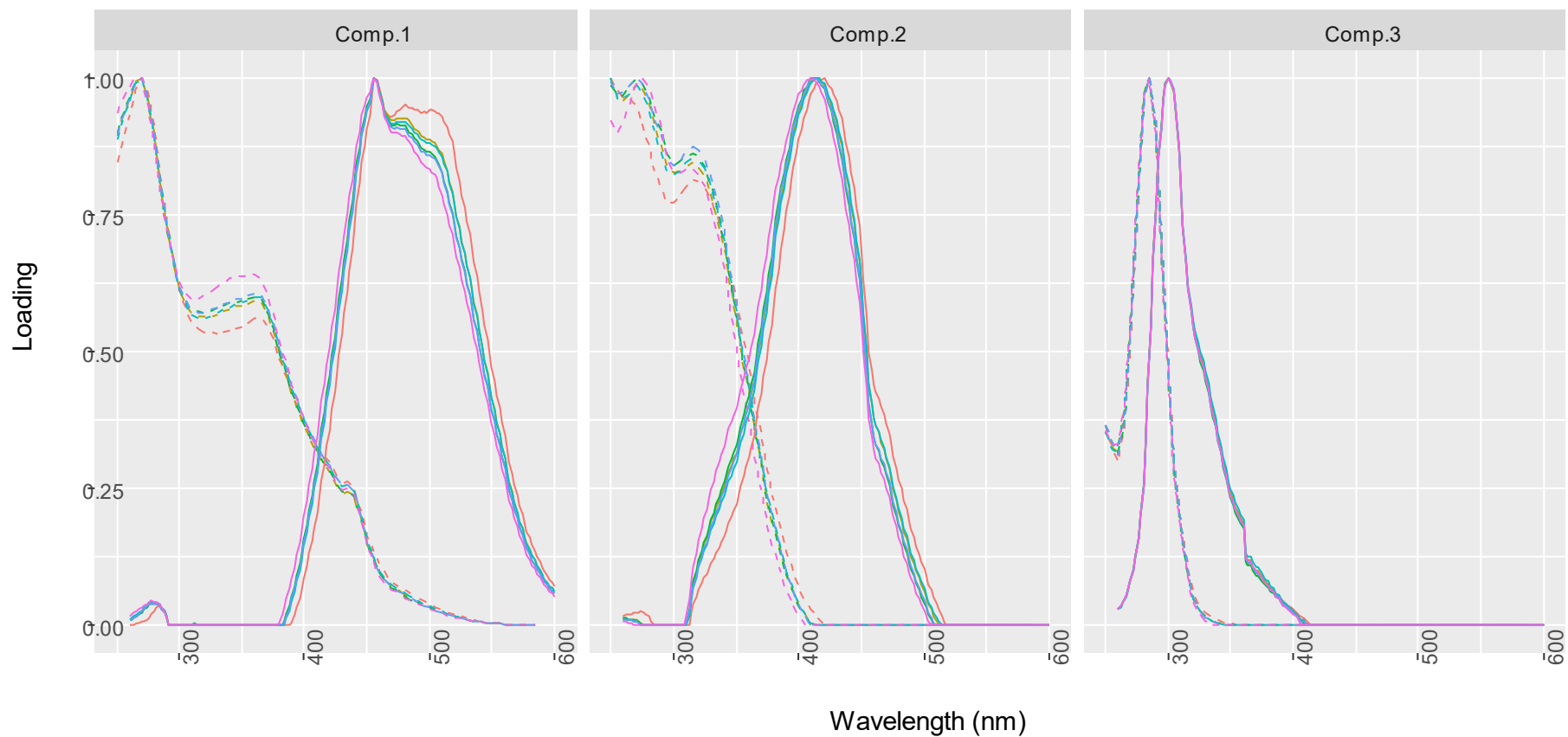


Figure A14. Resulting split-half analysis from validation of 3-component PARAFAC model. Emission is represented by dashed lines while excitation is represented by solid.

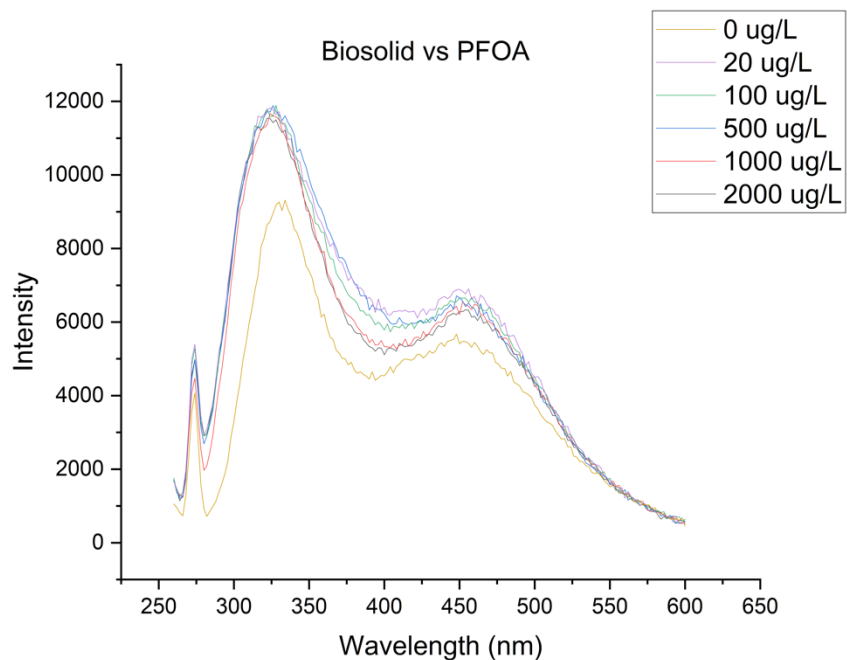


Figure A15. 2-D Fluorescence quenching results for the biosolid DOM vs PFOA at five concentrations. Each line represents the average of three replicates.

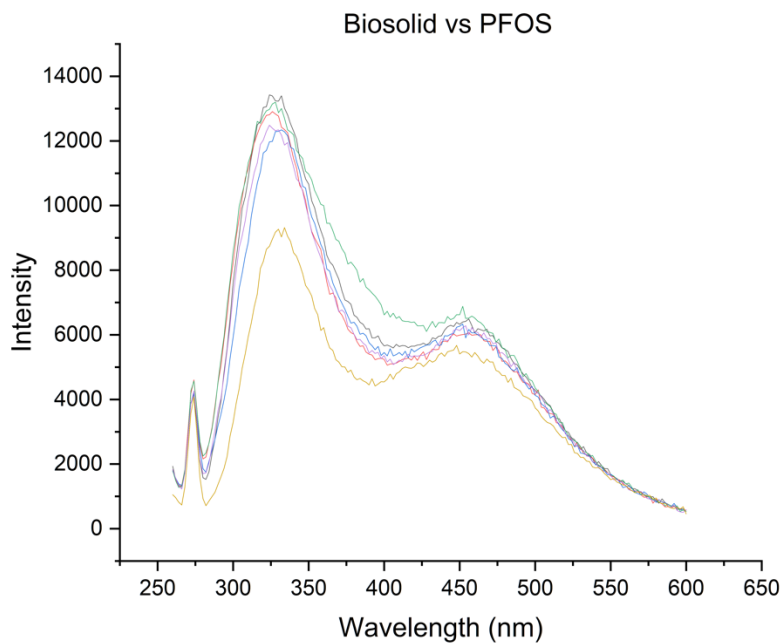


Figure A16. 2-D Fluorescence quenching results for the biosolid DOM vs PFOS at five concentrations. Each line represents the average of three replicates.

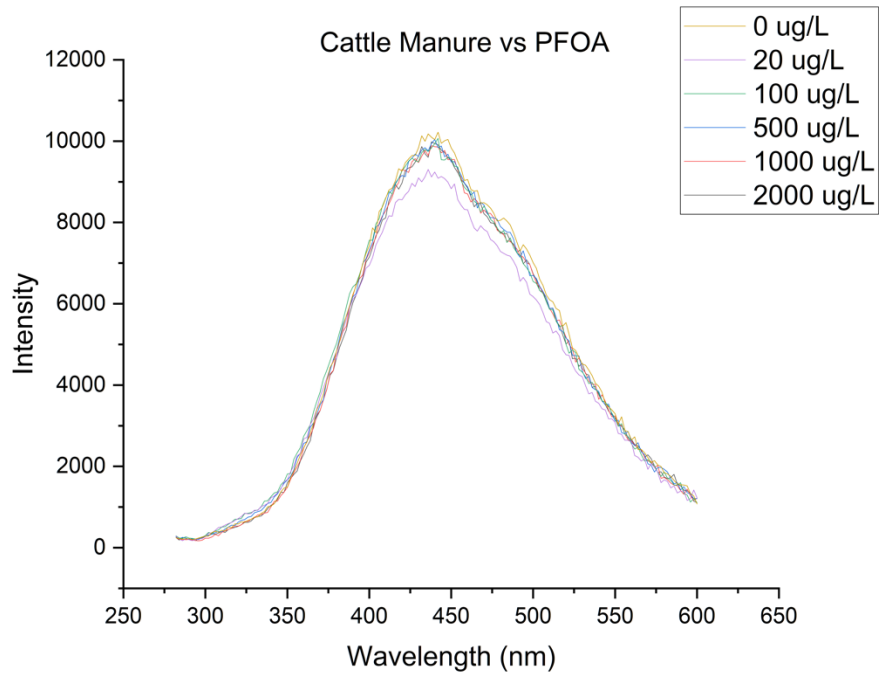


Figure A17. 2-D Fluorescence quenching results for the cattle manure DOM vs PFOA at five concentrations. Each line represents the average of three replicates.

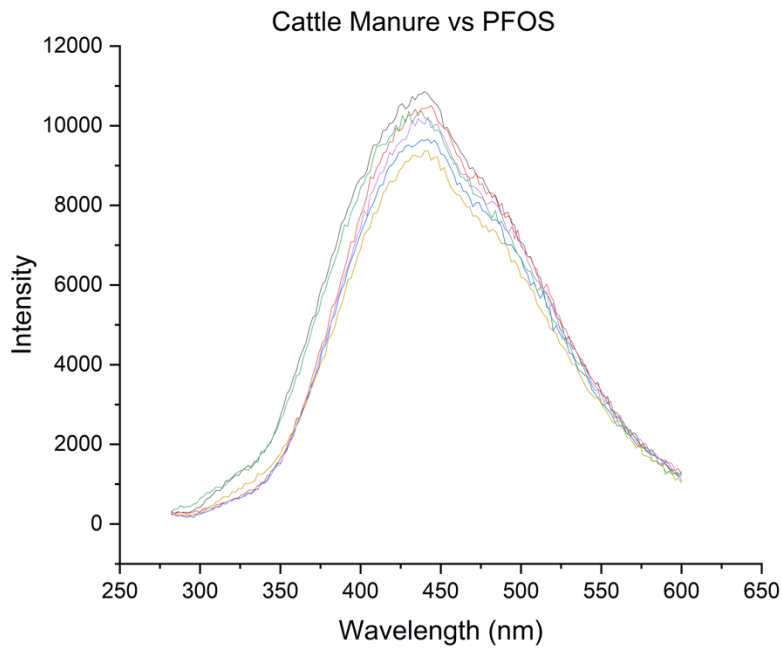


Figure A18. 2-D Fluorescence quenching results for the cattle manure DOM vs PFOS at five concentrations. Each line represents the average of three replicates.

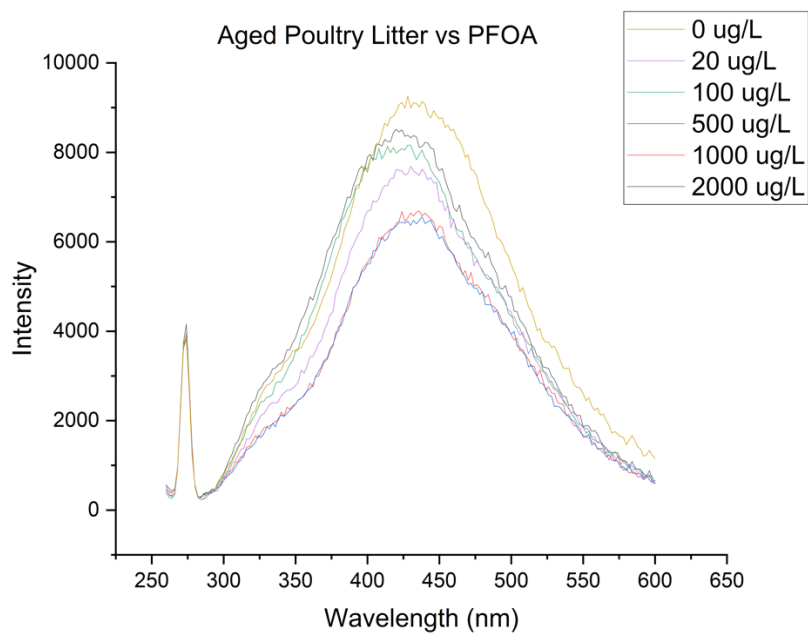


Figure A19. 2-D Fluorescence quenching results for the aged poultry litter DOM vs PFOA at five concentrations. Each line represents the average of three replicates.

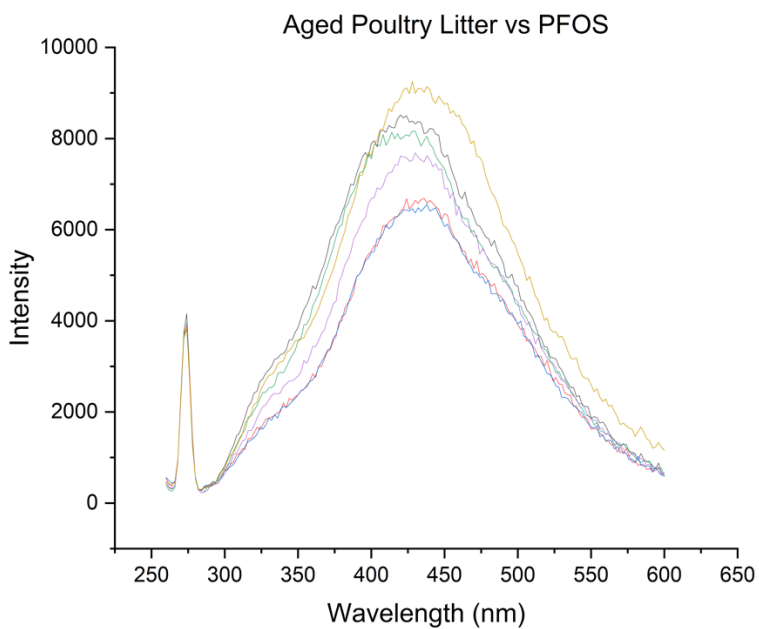


Figure A20. 2-D Fluorescence quenching results for the aged poultry litter DOM vs PFOS at five concentrations. Each line represents the average of three replicates.

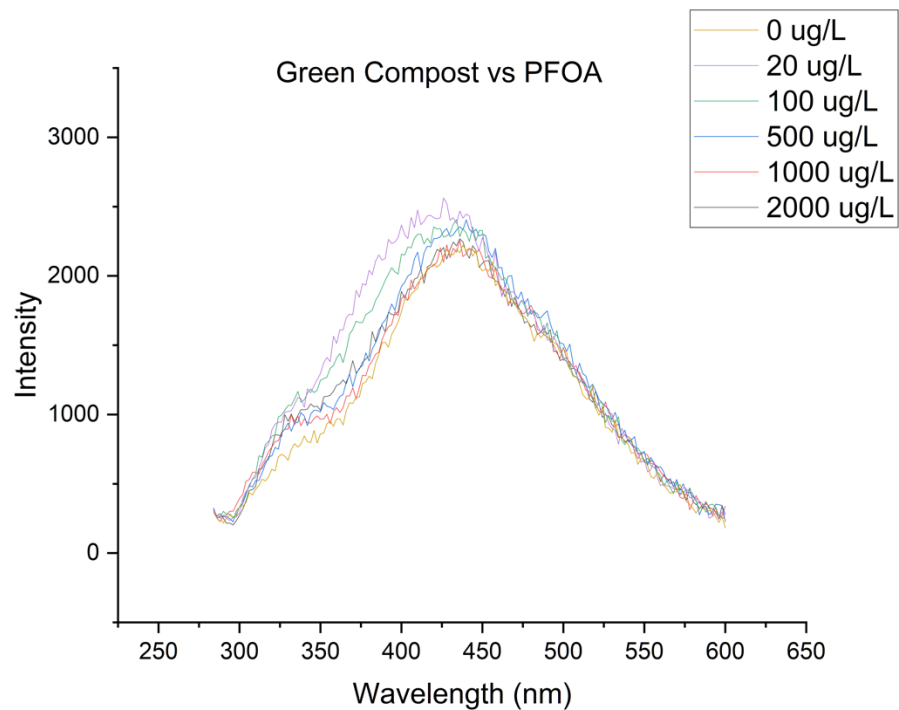


Figure A21. 2-D Fluorescence quenching results for the green compost DOM vs PFOA at five concentrations. Each line represents the average of three replicates.

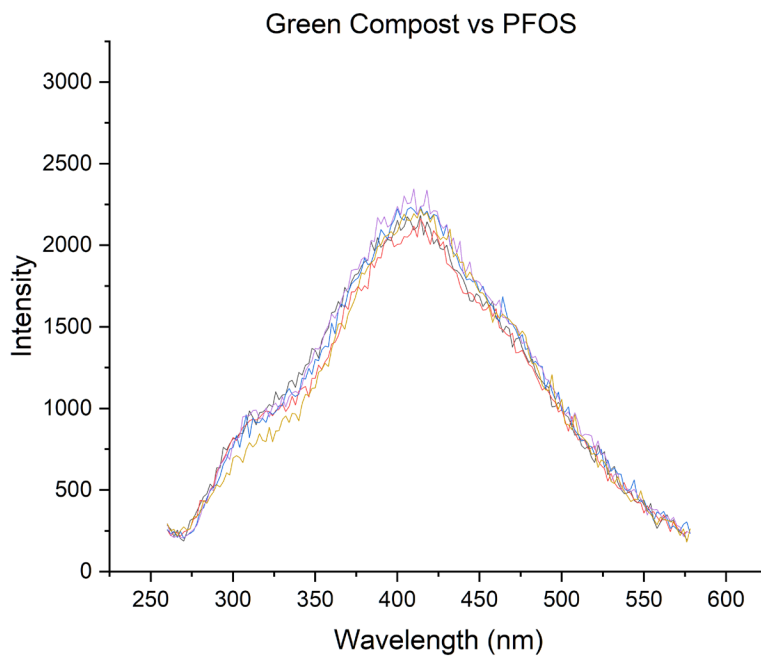


Figure A22. 2-D Fluorescence quenching results for the green compost DOM vs PFOS at five concentrations. Each line represents the average of three replicates.

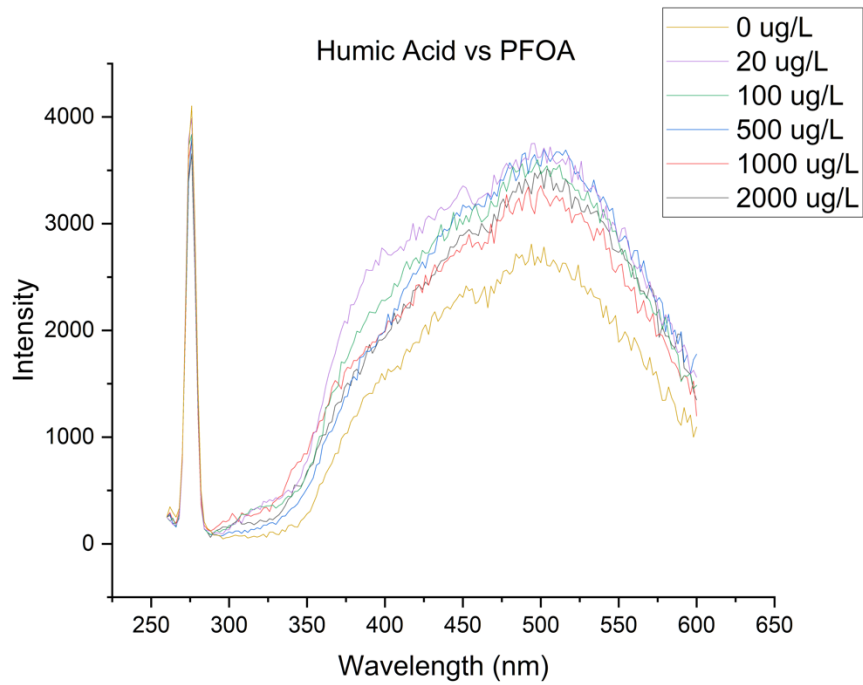


Figure A23. 2-D Fluorescence quenching results for the humic acid DOM vs PFOA at five concentrations. Each line represents the average of three replicates.

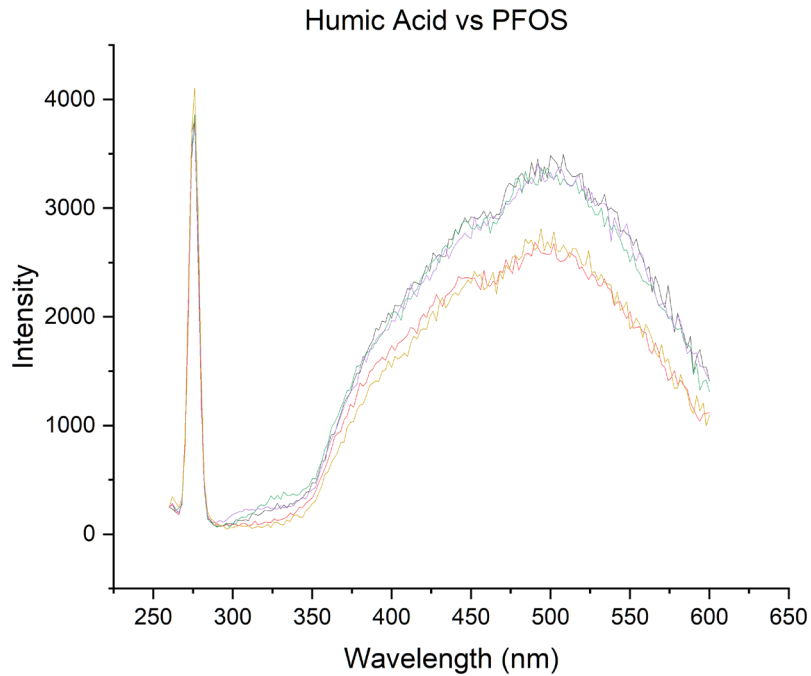


Figure A24. 2-D Fluorescence quenching results for the humic acid DOM vs PFOS at five concentrations. Each line represents the average of three replicates.

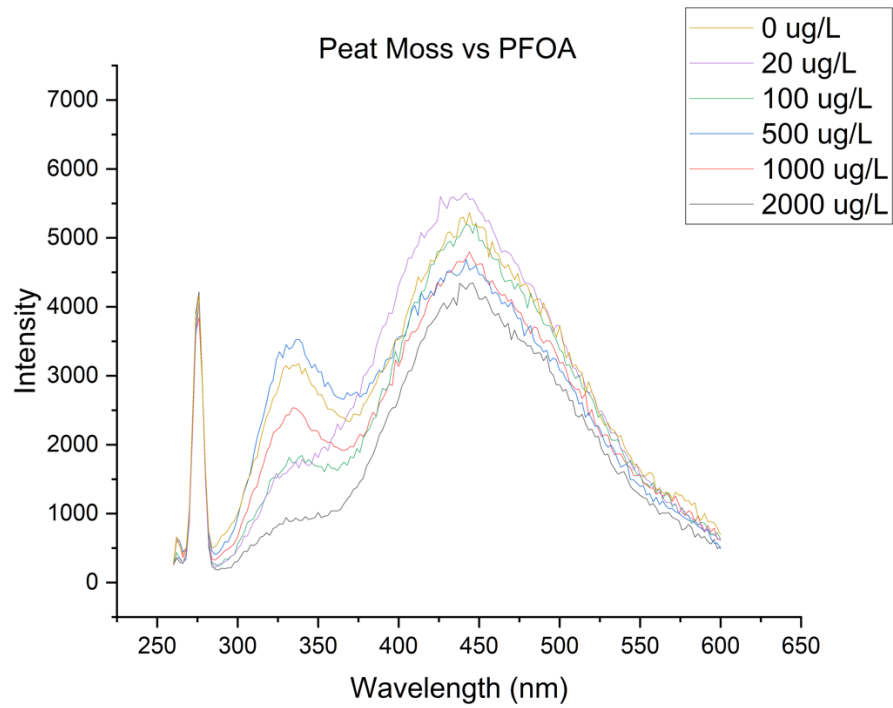


Figure A25. 2-D Fluorescence quenching results for the peat moss DOM vs PFOA at five concentrations. Each line represents the average of three replicates.

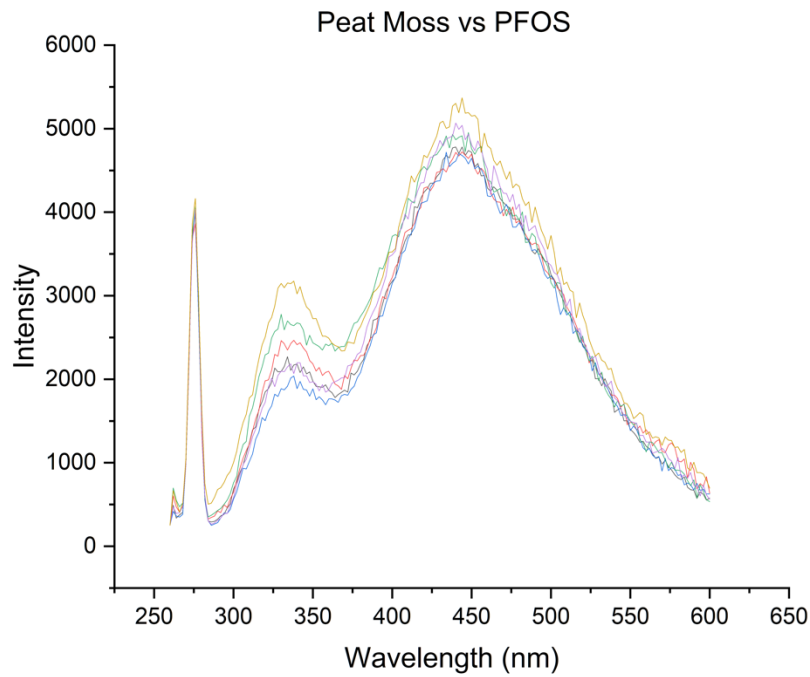


Figure A26. 2-D Fluorescence quenching results for the peat moss DOM vs PFOS at five concentrations. Each line represents the average of three replicates.

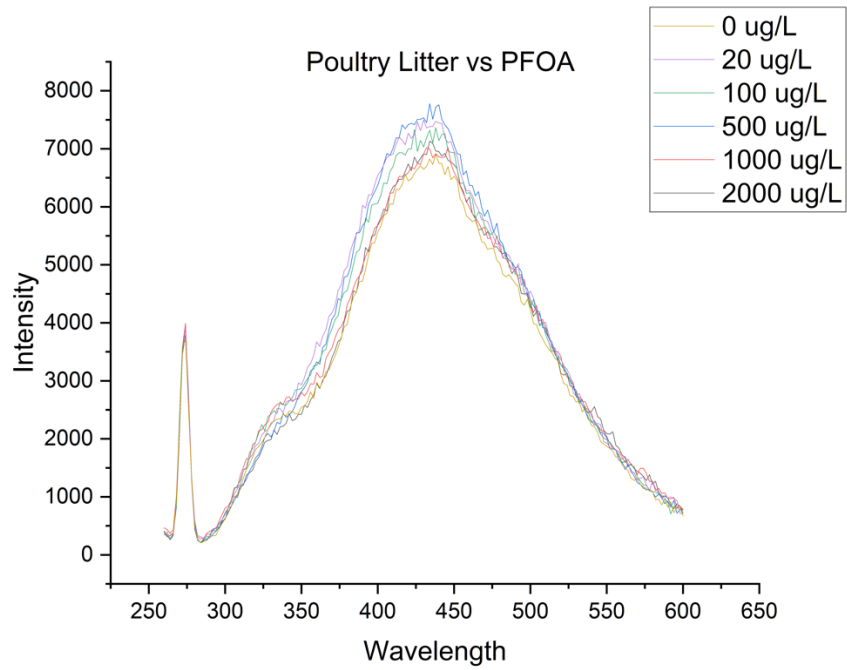


Figure A27. 2-D Fluorescence quenching results for the poultry litter DOM vs PFOA at five concentrations. Each line represents the average of three replicates.

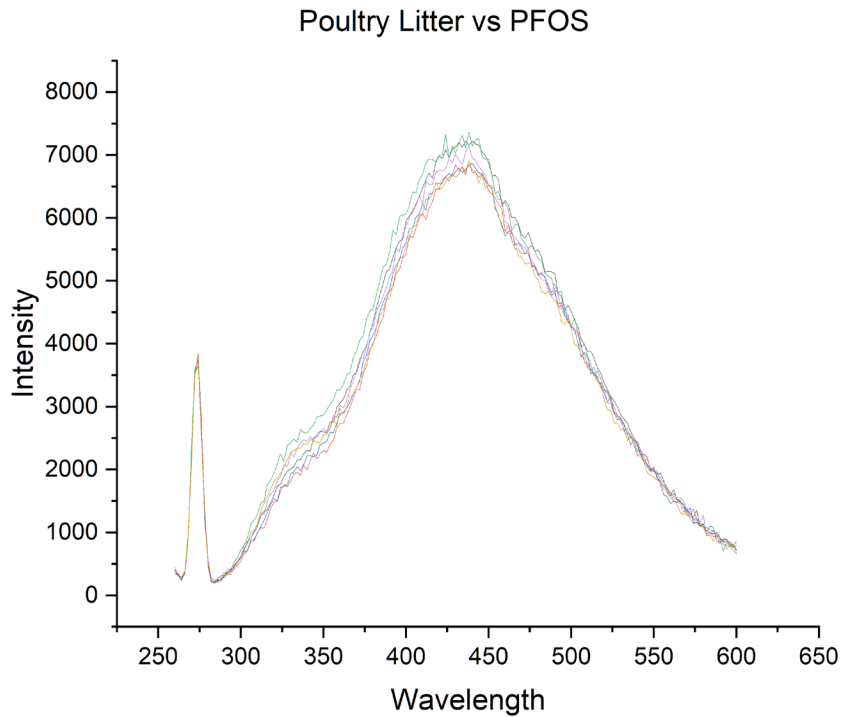


Figure A28. 2-D Fluorescence quenching results for the poultry litter DOM vs PFOS at five concentrations. Each line represents the average of three replicates.

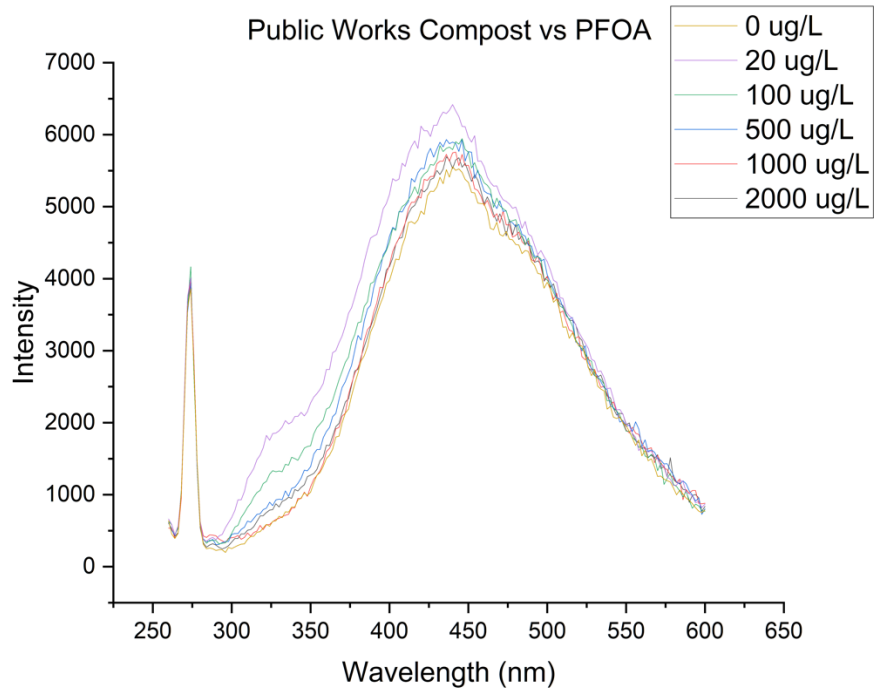


Figure A29. 2-D Fluorescence quenching results for the public works compost DOM vs PFOA at five concentrations. Each line represents the average of three replicates.

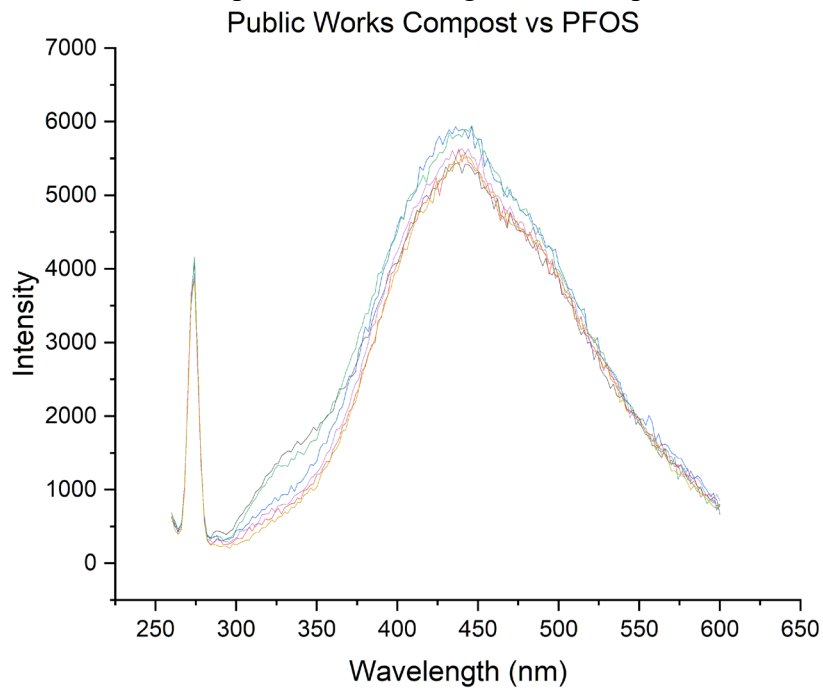


Figure A30. 2-D Fluorescence quenching results for the public works compost DOM vs PFOS at five concentrations. Each line represents the average of three replicates.

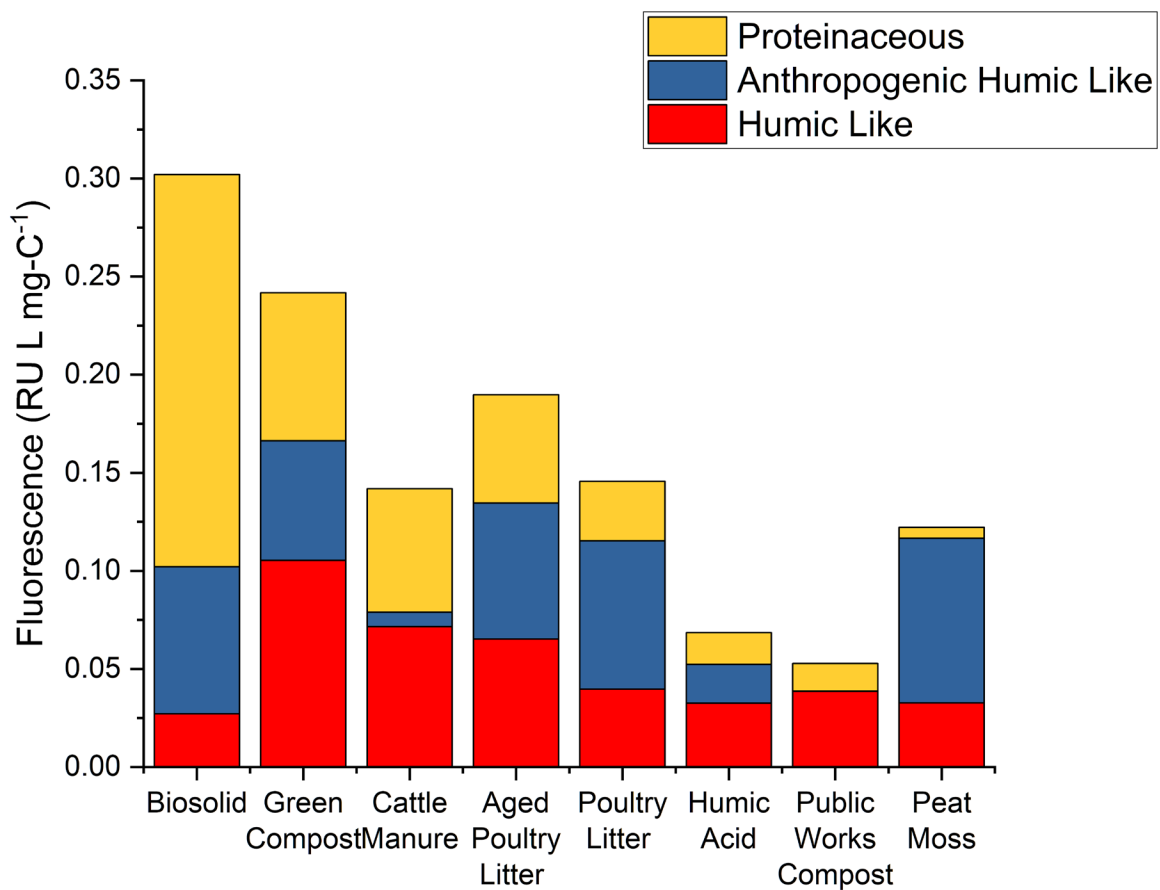


Figure A31. Distribution of PARAFAC components in each of the tested DOM. Image is shown with loadings and standard deviations between replicates in error bars.

Table A1. TOC (mg L⁻¹), texture, as well as PFOA and PFOS (ng g⁻¹) concentrations in DOM extracts. Standard deviation is represented in brackets. DOM samples where no PFOA or PFOS was detected, ND was placed into the corresponding cell.

DOM Sample Name	TOC (mg L ⁻¹)	Texture	Water extractable PFOA (ng g ⁻¹)	Water extractable PFOS (ng g ⁻¹)
Peat Moss	697.6 (14.11)	Finely homogenized material	9.18 (0.24)	6.08 (0.97)
Green Compost	1676 (22.18)	Finely homogenized material	14.5 (0.19)	ND
Cattle Manure	2192 (37.63)	Finely homogenized material	10.8 (0.91)	3.20 (0.46)
Biosolid	560.2 (18.95)	Sludge	134 (6.11)	38.4 (0.51)
Poultry Litter	7643 (42.66)	Particulate with identifiable pine shavings, sawdust, and feathers	21.5 (1.33)	1.08 (0.67)
Aged Poultry Litter	3937 (31.62)	Particulate with identifiable pine shavings and sawdust	22.1 (2.05)	1.34 (0.09)
Public Works Compost	279.1 (19.24)	Finely homogenized material with some identifiable woody debris	0.672 (0.22)	17.9 (0.93)
Humic Acid	1652 (17.59)	Finely ground powder	7.39 (0.79)	29.1 (1.12)

References

- Ahmed, A.A., S. Thiele-Bruhn, S.G. Aziz, R.H. Hilal, S.A. Elroby, et al. 2015. Interaction of polar and nonpolar organic pollutants with soil organic matter: Sorption experiments and molecular dynamics simulation. *Science of The Total Environment* 508: 276–287. doi: [10.1016/j.scitotenv.2014.11.087](https://doi.org/10.1016/j.scitotenv.2014.11.087).
- Andersen, C.M., and R. Bro. 2003. Practical aspects of PARAFAC modeling of fluorescence excitation-emission data. *Journal of Chemometrics* 17(4): 200–215. doi: <https://doi.org/10.1002/cem.790>.
- Anderson, R.H., G.C. Long, R.C. Porter, and J.K. Anderson. 2016. Occurrence of select perfluoroalkyl substances at U.S. Air Force aqueous film-forming foam release sites other than fire-training areas: Field-validation of critical fate and transport properties. *Chemosphere* 150: 678–685. doi: [10.1016/j.chemosphere.2016.01.014](https://doi.org/10.1016/j.chemosphere.2016.01.014).
- Anderson, R.H, D.T. Adamson, and H.F. Stroo. 2019. Partitioning of poly- and perfluoroalkyl substances from soil to groundwater within aqueous film-forming foam source zones. *Journal of Contaminant Hydrology* 220: 59–65. doi: [10.1016/j.jconhyd.2018.11.011](https://doi.org/10.1016/j.jconhyd.2018.11.011).
- Antignac, J.-P., B. Veyrand, H. Kadar, P. Marchand, A. Oleko, et al. 2013. Occurrence of perfluorinated alkylated substances in breast milk of French women and relation with socio-demographical and clinical parameters: Results of the ELFE pilot study. *Chemosphere* 91(6): 802–808. doi: [10.1016/j.chemosphere.2013.01.088](https://doi.org/10.1016/j.chemosphere.2013.01.088).
- van Asselt, E.D., R.P.J.J. Rietra, P.F.A.M. Römkens, and H.J. van der Fels-Klerx. 2011. Perfluorooctane sulphonate (PFOS) throughout the food production chain. *Food Chemistry* 128(1): 1–6. doi: [10.1016/j.foodchem.2011.03.032](https://doi.org/10.1016/j.foodchem.2011.03.032).
- Banzhaf, S., M. Filipovic, J. Lewis, C.J. Sparrenbom, and R. Barthel. 2017. A review of contamination of surface-, ground-, and drinking water in Sweden by perfluoroalkyl and polyfluoroalkyl substances (PFASs). *Ambio* 46(3): 335–346. doi: [10.1007/s13280-016-0848-8](https://doi.org/10.1007/s13280-016-0848-8).
- Barry, V., A. Winqvist, and K. Steenland. 2013. Perfluorooctanoic acid (PFOA) exposures and incident cancers among adults living near a chemical plant. *Environmental Health Perspectives* 121(11–12): 1313–1318. doi: [10.1289/ehp.1306615](https://doi.org/10.1289/ehp.1306615).
- Barzen-Hanson, K.A., and J.A. Field. 2015. Discovery and implications of C2 and C3 perfluoroalkyl sulfonates in aqueous film-forming foams and groundwater. *Environ. Sci. Technol. Lett.* 2(4): 95–99. doi: [10.1021/acs.estlett.5b00049](https://doi.org/10.1021/acs.estlett.5b00049).
- Baylay, A.J., D.J. Spurgeon, C. Svendsen, J.L. Griffin, S.C. Swain, et al. 2012. A metabolomics based test of independent action and concentration addition using the earthworm *Lumbricus rubellus*. *Ecotoxicology* 21(5): 1436–1447. doi: [10.1007/s10646-012-0897-0](https://doi.org/10.1007/s10646-012-0897-0).
- Becker, A.M., S. Gerstmann, and H. Frank. 2008. Perfluorooctane surfactants in waste waters, the major source of river pollution. *Chemosphere* 72(1): 115–121. doi: [10.1016/j.chemosphere.2008.01.009](https://doi.org/10.1016/j.chemosphere.2008.01.009).

- Begley, T.H., K. White, P. Honigfort, M.L. Twaroski, R. Neches, et al. 2005. Perfluorochemicals: Potential sources of and migration from food packaging. *Food Additives & Contaminants* 22(10): 1023–1031. doi: [10.1080/02652030500183474](https://doi.org/10.1080/02652030500183474).
- Bertoncini, E.I., V. D’Orazio, N. Senesi, and M.E. Mattiazzo. 2005. Fluorescence analysis of humic and fulvic acids from two Brazilian oxisols as affected by biosolid amendment. *Anal Bioanal Chem* 381(6): 1281–1288. doi: [10.1007/s00216-005-3054-2](https://doi.org/10.1007/s00216-005-3054-2).
- Blaine, A.C., C.D. Rich, E.M. Sedlacko, K.C. Hyland, C. Stushnoff, et al. 2014. Perfluoroalkyl acid uptake in lettuce (*Lactuca sativa*) and strawberry (*Fragaria ananassa*) irrigated with reclaimed water. *Environ. Sci. Technol.* 48(24): 14361–14368. doi: [10.1021/es504150h](https://doi.org/10.1021/es504150h).
- Birdwell, J.E., and A.S. Engel. 2010. Characterization of dissolved organic matter in cave and spring waters using UV–Vis absorbance and fluorescence spectroscopy. *Organic Geochemistry* 41(3): 270–280. doi: [10.1016/j.orggeochem.2009.11.002](https://doi.org/10.1016/j.orggeochem.2009.11.002).
- Boddy, E., P.W. Hill, J. Farrar, and D.L. Jones. 2007. Fast turnover of low molecular weight components of the dissolved organic carbon pool of temperate grassland field soils. *Soil Biology and Biochemistry* 39(4): 827–835. doi: [10.1016/j.soilbio.2006.09.030](https://doi.org/10.1016/j.soilbio.2006.09.030).
- Bolan, N., D. Adriano, A. Kunhikrishnan, T. James, R. McDowell, et al. 2011. Dissolved organic matter: biogeochemistry, dynamics, and environmental significance in soils. *Advances in Agronomy* 110: 1–75. doi: [10.1016/B978-0-12-385531-2.00001-3](https://doi.org/10.1016/B978-0-12-385531-2.00001-3).
- Bolan, N., B. Sarkar, Y. Yan, Q. Li, H. Wijesekara, et al. 2021. Remediation of poly- and perfluoroalkyl substances (PFAS) contaminated soils – To mobilize or to immobilize or to degrade? *Journal of Hazardous Materials* 401: 123892. doi: [10.1016/j.jhazmat.2020.123892](https://doi.org/10.1016/j.jhazmat.2020.123892).
- Borisover, M., A. Lordian, and G.J. Levy. 2012. Water-extractable soil organic matter characterization by chromophoric indicators: Effects of soil type and irrigation water quality. *Geoderma* 179–180: 28–37. doi: [10.1016/j.geoderma.2012.02.019](https://doi.org/10.1016/j.geoderma.2012.02.019).
- Bouyoucos, G.J. 1962. Hydrometer Method Improved for Making Particle Size Analyses of Soils. *Agronomy Journal* 54(5): 464–465. doi: [10.2134/agronj1962.00021962005400050028x](https://doi.org/10.2134/agronj1962.00021962005400050028x).
- Brusseau, M.L., R.H. Anderson, and B. Guo. 2020. PFAS concentrations in soils: Background levels versus contaminated sites. *Science of The Total Environment* 740: 140017. doi: [10.1016/j.scitotenv.2020.140017](https://doi.org/10.1016/j.scitotenv.2020.140017).
- Buck, R.C., J. Franklin, U. Berger, J.M. Conder, I.T. Cousins, et al. 2011. Perfluoroalkyl and polyfluoroalkyl substances in the environment: Terminology, classification, and origins. *Integr Environ Assess Manag* 7(4): 513–541. doi: [10.1002/ieam.258](https://doi.org/10.1002/ieam.258).
- Campos Pereira, H., M. Ullberg, D.B. Kleja, J.P. Gustafsson, and L. Ahrens. 2018. Sorption of perfluoroalkyl substances (PFASs) to an organic soil horizon – Effect of cation composition and pH. *Chemosphere* 207: 183–191. doi: [10.1016/j.chemosphere.2018.05.012](https://doi.org/10.1016/j.chemosphere.2018.05.012).
- Caricasole, P., M.R. Provenzano, P.G. Hatcher, and N. Senesi. 2010. Chemical characteristics of dissolved organic matter during composting of different organic wastes assessed by ¹³C CPMAS NMR spectroscopy. *Bioresource Technology* 101(21): 8232–8236. doi: [10.1016/j.biortech.2010.05.095](https://doi.org/10.1016/j.biortech.2010.05.095).

- Carmosini, N., and L.S. Lee. 2008. Partitioning of Fluorotelomer Alcohols to Octanol and Different Sources of Dissolved Organic Carbon. *Environ. Sci. Technol.* 42(17): 6559–6565. doi: [10.1021/es800263t](https://doi.org/10.1021/es800263t).
- Chantigny, M.H. 2003. Dissolved and water-extractable organic matter in soils: a review on the influence of land use and management practices. *Geoderma* 113(3–4): 357–380. doi: [10.1016/S0016-7061\(02\)00370-1](https://doi.org/10.1016/S0016-7061(02)00370-1).
- Chefetz, B., Y. Chen, Y. Hadar, and P.G. Hatcher. 1998. Characterization of Dissolved Organic Matter Extracted from Composted Municipal Solid Waste. *Soil Science Society of America Journal* 62(2): 326–332. doi: [10.2136/sssaj1998.03615995006200020005x](https://doi.org/10.2136/sssaj1998.03615995006200020005x).
- Chen, Y., N. Senesi, and M. Schnitzer. 1977. Information Provided on Humic Substances by E4/E6 Ratios. *Soil Science Society of America Journal* 41(2): 352–358. doi: [10.2136/sssaj1977.03615995004100020037x](https://doi.org/10.2136/sssaj1977.03615995004100020037x).
- Chin, Y.-Ping., George. Aiken, and Edward. O’Loughlin. 1994. Molecular Weight, Polydispersity, and Spectroscopic Properties of Aquatic Humic Substances. *Environ. Sci. Technol.* 28(11): 1853–1858. doi: [10.1021/es00060a015](https://doi.org/10.1021/es00060a015).
- Coates, J. 2006. Interpretation of Infrared Spectra, A Practical Approach. In: Meyers, R.A., editor, *Encyclopedia of Analytical Chemistry*. John Wiley & Sons, Ltd, Chichester, UK. p. a5606
- Coble, P.G. 1996. Characterization of marine and terrestrial DOM in seawater using excitation-emission matrix spectroscopy. *Marine Chemistry* 51(4): 325–346. doi: [10.1016/0304-4203\(95\)00062-3](https://doi.org/10.1016/0304-4203(95)00062-3).
- Cory, R.M., and D.M. McKnight. 2005. Fluorescence Spectroscopy Reveals Ubiquitous Presence of Oxidized and Reduced Quinones in Dissolved Organic Matter. *Environ. Sci. Technol.* 39(21): 8142–8149. doi: [10.1021/es0506962](https://doi.org/10.1021/es0506962).
- Costello, M.C.S., and L.S. Lee. 2020. Sources, Fate, and Plant Uptake in Agricultural Systems of Per- and Polyfluoroalkyl Substances. *Curr Pollution Rep.* doi: [10.1007/s40726-020-00168-y](https://doi.org/10.1007/s40726-020-00168-y).
- Cui, D., X. Li, and N. Quinete. 2020. Occurrence, fate, sources and toxicity of PFAS: What we know so far in Florida and major gaps. *TrAC Trends in Analytical Chemistry* 130: 115976. doi: [10.1016/j.trac.2020.115976](https://doi.org/10.1016/j.trac.2020.115976).
- Darrow, L.A., C.R. Stein, and K. Steenland. 2013. Serum Perfluorooctanoic Acid and Perfluorooctane Sulfonate Concentrations in Relation to Birth Outcomes in the Mid-Ohio Valley, 2005–2010.
- Delle Site, A. 2001. Factors Affecting Sorption of Organic Compounds in Natural Sorbent/Water Systems and Sorption Coefficients for Selected Pollutants. A Review. *Journal of Physical and Chemical Reference Data* 30(1): 187–439. doi: [10.1063/1.1347984](https://doi.org/10.1063/1.1347984).
- Du, Z., S. Deng, Y. Bei, Q. Huang, B. Wang, et al. 2014. Adsorption behavior and mechanism of perfluorinated compounds on various adsorbents—A review. *Journal of Hazardous Materials* 274: 443–454. doi: [10.1016/j.jhazmat.2014.04.038](https://doi.org/10.1016/j.jhazmat.2014.04.038).
- EPA. 2016. Drinking Water Health Advisories for PFOA and PFOS. November 2016. <https://www.epa.gov/sdwa/drinking-water-health-advisories-pfoa-and-pfos>.

- EPA. 2019. Per- and Polyfluoroalkyl Substances (PFAS) Action Plan. February 2019. https://www.epa.gov/sites/default/files/2019-02/documents/pfas_action_plan_021319_508compliant_1.pdf.
- EPA. 2022. Lifetime Drinking Water Health Advisories for Four Perfluoroalkyl Substances. June 2022. <https://www.govinfo.gov/content/pkg/FR-2022-06-21/pdf/2022-13158.pdf>
- Fellman, J.B., D.V. D'Amore, E. Hood, and R.D. Boone. 2008. Fluorescence characteristics and biodegradability of dissolved organic matter in forest and wetland soils from coastal temperate watersheds in southeast Alaska. *Biogeochemistry* 88(2): 169–184. doi: [10.1007/s10533-008-9203-x](https://doi.org/10.1007/s10533-008-9203-x).
- Gao, J., C. Liang, G. Shen, J. Lv, and H. Wu. 2017. Spectral characteristics of dissolved organic matter in various agricultural soils throughout China. *Chemosphere* 176: 108–116. doi: [10.1016/j.chemosphere.2017.02.104](https://doi.org/10.1016/j.chemosphere.2017.02.104).
- Garg, S., P. Kumar, V. Mishra, R. Guijt, P. Singh, et al. 2020. A review on the sources, occurrence and health risks of per-/poly-fluoroalkyl substances (PFAS) arising from the manufacture and disposal of electric and electronic products. *Journal of Water Process Engineering* 38: 101683. doi: [10.1016/j.jwpe.2020.101683](https://doi.org/10.1016/j.jwpe.2020.101683).
- Gauthier, T.D., W.Rudolf. Seitz, and C.L. Grant. 1987. Effects of structural and compositional variations of dissolved humic materials on pyrene Koc values. *Environ. Sci. Technol.* 21(3): 243–248. doi: [10.1021/es00157a003](https://doi.org/10.1021/es00157a003).
- Ghisi, R., T. Vamerali, and S. Manzetti. 2019. Accumulation of perfluorinated alkyl substances (PFAS) in agricultural plants: A review. *Environmental Research* 169: 326–341. doi: [10.1016/j.envres.2018.10.023](https://doi.org/10.1016/j.envres.2018.10.023).
- Gong, X., C. Yang, Y. Hong, A.C.K. Chung, and Z. Cai. 2019. PFOA and PFOS promote diabetic renal injury in vitro by impairing the metabolisms of amino acids and purines. *Science of The Total Environment* 676: 72–86. doi: [10.1016/j.scitotenv.2019.04.208](https://doi.org/10.1016/j.scitotenv.2019.04.208).
- Grandjean, P., E.W. Andersen, E. Budtz-Jørgensen, F. Nielsen, K. Mølbak, et al. 2012. Serum Vaccine Antibody Concentrations in Children Exposed to Perfluorinated Compounds. *JAMA* 307(4): 391–397. doi: [10.1001/jama.2011.2034](https://doi.org/10.1001/jama.2011.2034).
- Hansen, K.J., H.O. Johnson, J.S. Eldridge, J.L. Butenhoff, and L.A. Dick. 2002. Quantitative Characterization of Trace Levels of PFOS and PFOA in the Tennessee River. *Environ. Sci. Technol.* 36(8): 1681–1685. doi: [10.1021/es010780r](https://doi.org/10.1021/es010780r).
- Haukås, M., U. Berger, H. Hop, B. Gulliksen, and G.W. Gabrielsen. 2007. Bioaccumulation of per- and polyfluorinated alkyl substances (PFAS) in selected species from the Barents Sea food web. *Environmental Pollution* 148(1): 360–371. doi: [10.1016/j.envpol.2006.09.021](https://doi.org/10.1016/j.envpol.2006.09.021).
- Higgins, C.P., and R.G. Luthy. 2006. Sorption of Perfluorinated Surfactants on Sediments. *Environ. Sci. Technol.* 40(23): 7251–7256. doi: [10.1021/es061000n](https://doi.org/10.1021/es061000n).
- Higgins, C.P., and R.G. Luthy. 2007. Modeling Sorption of Anionic Surfactants onto Sediment Materials: An a priori Approach for Perfluoroalkyl Surfactants and Linear Alkylbenzene Sulfonates. *Environ. Sci. Technol.* 41(9): 3254–3261. doi: [10.1021/es062449j](https://doi.org/10.1021/es062449j).

- Hu, X.C., D.Q. Andrews, A.B. Lindstrom, T.A. Bruton, L.A. Schaider, et al. 2016. Detection of Poly- and Perfluoroalkyl Substances (PFASs) in U.S. Drinking Water Linked to Industrial Sites, Military Fire Training Areas, and Wastewater Treatment Plants. *Environ. Sci. Technol. Lett.* 3(10): 344–350. doi: [10.1021/acs.estlett.6b00260](https://doi.org/10.1021/acs.estlett.6b00260).
- Huang, W., H. Yu, and W.J.W. Jr. 1998. Hysteresis in the sorption and desorption of hydrophobic organic contaminants by soils and sediments 1. A comparative analysis of experimental protocols. : 20.
- Hudson, N., A. Baker, and D. Reynolds. 2007. Fluorescence analysis of dissolved organic matter in natural, waste and polluted waters—a review. *River Research and Applications* 23(6): 631–649. doi: [10.1002/rra.1005](https://doi.org/10.1002/rra.1005).
- Ifon, B.E., C. Kiki, K.H. Lasisi, F. Suanon, B. Adyari, et al. 2022. Effects of bisphenols and perfluoroalkylated substances on fluorescence properties of humic and amino acids substances of dissolved organic matter: EEM-PARAFAC and ATR-FTIR analysis. *Journal of Environmental Chemical Engineering* 10(4): 108186. doi: [10.1016/j.jece.2022.108186](https://doi.org/10.1016/j.jece.2022.108186).
- Ishii, S.K.L., and T.H. Boyer. 2012. Behavior of Reoccurring PARAFAC Components in Fluorescent Dissolved Organic Matter in Natural and Engineered Systems: A Critical Review. *Environ. Sci. Technol.* 46(4): 2006–2017. doi: [10.1021/es2043504](https://doi.org/10.1021/es2043504).
- Jeon, J., K. Kannan, B.J. Lim, K.G. An, and S.D. Kim. 2011. Effects of salinity and organic matter on the partitioning of perfluoroalkyl acid (PFAs) to clay particles. *J. Environ. Monit.* 13(6): 1803. doi: [10.1039/c0em00791a](https://doi.org/10.1039/c0em00791a).
- Jia, C., C. You, and G. Pan. 2010. Effect of temperature on the sorption and desorption of perfluorooctane sulfonate on humic acid. *Journal of Environmental Sciences* 22(3): 355–361. doi: [10.1016/S1001-0742\(09\)60115-7](https://doi.org/10.1016/S1001-0742(09)60115-7).
- Jogsten, I.E., G. Perelló, X. Llebaria, E. Bigas, R. Martí-Cid, et al. 2009. Exposure to perfluorinated compounds in Catalonia, Spain, through consumption of various raw and cooked foodstuffs, including packaged food. *Food and Chemical Toxicology* 47(7): 1577–1583. doi: [10.1016/j.fct.2009.04.004](https://doi.org/10.1016/j.fct.2009.04.004).
- Johnson, G.R., M.L. Brusseau, K.C. Carroll, G.R. Tick, and C.M. Duncan. 2022. Global distributions, source-type dependencies, and concentration ranges of per- and polyfluoroalkyl substances in groundwater. *Science of The Total Environment* 841: 156602. doi: [10.1016/j.scitotenv.2022.156602](https://doi.org/10.1016/j.scitotenv.2022.156602).
- Kaiser, K., and K. Kalbitz. 2012. Cycling downwards – dissolved organic matter in soils. *Soil Biology and Biochemistry* 52: 29–32. doi: [10.1016/j.soilbio.2012.04.002](https://doi.org/10.1016/j.soilbio.2012.04.002).
- Kannan, K., S.H. Yun, and T.J. Evans. 2005. Chlorinated, Brominated, and Perfluorinated Contaminants in Livers of Polar Bears from Alaska. *Environ. Sci. Technol.* 39(23): 9057–9063. doi: [10.1021/es051850n](https://doi.org/10.1021/es051850n).
- Kantiani, L., M. Llorca, J. Sanchís, M. Farré, and D. Barceló. 2010. Emerging food contaminants: a review. *Anal Bioanal Chem* 398(6): 2413–2427. doi: [10.1007/s00216-010-3944-9](https://doi.org/10.1007/s00216-010-3944-9).

- Kierdaszuk, B., I. Gryczynski, A. Modrak-Wojcik, A. Bzowska, D. Shugar, et al. 1995. Fluorescence of Tyrosine and Tryptophan in Proteins Using One- and Two-Photon Excitation. *Photochemistry and Photobiology* 61(4): 319–324. doi: [10.1111/j.1751-1097.1995.tb08615.x](https://doi.org/10.1111/j.1751-1097.1995.tb08615.x).
- Kinniburgh, D.G., W.H. van Riemsdijk, L.K. Koopal, M. Borkovec, M.F. Benedetti, et al. 1999. Ion binding to natural organic matter: competition, heterogeneity, stoichiometry and thermodynamic consistency. *Colloids and Surfaces A: Physicochemical and Engineering Aspects* 151(1–2): 147–166. doi: [10.1016/S0927-7757\(98\)00637-2](https://doi.org/10.1016/S0927-7757(98)00637-2).
- Kothawala, D.N., S.J. Köhler, A. Östlund, K. Wiberg, and L. Ahrens. 2017. Influence of dissolved organic matter concentration and composition on the removal efficiency of perfluoroalkyl substances (PFASs) during drinking water treatment. *Water Research* 121: 320–328. doi: [10.1016/j.watres.2017.05.047](https://doi.org/10.1016/j.watres.2017.05.047).
- Kwok, K.Y., E. Yamazaki, N. Yamashita, S. Taniyasu, M.B. Murphy, et al. 2013. Transport of Perfluoroalkyl substances (PFAS) from an arctic glacier to downstream locations: Implications for sources. *Science of The Total Environment* 447: 46–55. doi: [10.1016/j.scitotenv.2012.10.091](https://doi.org/10.1016/j.scitotenv.2012.10.091).
- Lakowicz, J.R. 2006. *Principles of fluorescence spectroscopy*. Springer, New York, NY.
- Lal, R. 2002. Soil carbon dynamics in cropland and rangeland. *Environmental Pollution* 116(3): 353–362. doi: [10.1016/S0269-7491\(01\)00211-1](https://doi.org/10.1016/S0269-7491(01)00211-1).
- Lau, C., K. Anitole, C. Hodes, D. Lai, A. Pfahles-Hutchens, et al. 2007. Perfluoroalkyl Acids: A Review of Monitoring and Toxicological Findings. *Toxicological Sciences* 99(2): 366–394. doi: [10.1093/toxsci/kfm128](https://doi.org/10.1093/toxsci/kfm128).
- Lau, C., J.L. Butenhoff, and J.M. Rogers. 2004. The developmental toxicity of perfluoroalkyl acids and their derivatives. *Toxicology and Applied Pharmacology* 198(2): 231–241. doi: [10.1016/j.taap.2003.11.031](https://doi.org/10.1016/j.taap.2003.11.031).
- Li, X., Z. Hua, J. Zhang, and L. Gu. 2022. Interactions between dissolved organic matter and perfluoroalkyl acids in natural rivers and lakes: A case study of the northwest of Taihu Lake Basin, China. *Water Research* 216: 118324. doi: [10.1016/j.watres.2022.118324](https://doi.org/10.1016/j.watres.2022.118324).
- Li, Y., D.P. Oliver, and R.S. Kookana. 2018. A critical analysis of published data to discern the role of soil and sediment properties in determining sorption of per and polyfluoroalkyl substances (PFASs). *Science of The Total Environment* 628–629: 110–120. doi: [10.1016/j.scitotenv.2018.01.167](https://doi.org/10.1016/j.scitotenv.2018.01.167).
- Lindstrom, A.B., M.J. Strynar, A.D. Delinsky, S.F. Nakayama, L. McMillan, et al. 2011. Application of WWTP Biosolids and Resulting Perfluorinated Compound Contamination of Surface and Well Water in Decatur, Alabama, USA. *Environ. Sci. Technol.* 45(19): 8015–8021. doi: [10.1021/es1039425](https://doi.org/10.1021/es1039425).
- Liu, C., and J. Liu. 2016. Aerobic biotransformation of polyfluoroalkyl phosphate esters (PAPs) in soil. *Environmental Pollution* 212: 230–237. doi: [10.1016/j.envpol.2016.01.069](https://doi.org/10.1016/j.envpol.2016.01.069).
- Liu, J., and L.S. Lee. 2005. Solubility and Sorption by Soils of 8:2 Fluorotelomer Alcohol in Water and Cosolvent Systems. *Environ. Sci. Technol.* 39(19): 7535–7540. doi: [10.1021/es051125c](https://doi.org/10.1021/es051125c).
- Liu, S., J. Zhou, J. Guo, Z. Gao, Y. Jia, et al. 2022. Insights into the impacts of dissolved organic matter of different origins on bioaccumulation and translocation of per- and polyfluoroalkyl

- substances (PFASs) in wheat. *Environmental Pollution* 293: 118604. doi: [10.1016/j.envpol.2021.118604](https://doi.org/10.1016/j.envpol.2021.118604).
- Longstaffe, J.G., D. Courtier-Murias, and A.J. Simpson. 2016. A nuclear magnetic resonance study of the dynamics of organofluorine interactions with a dissolved humic acid. *Chemosphere* 145: 307–313. doi: [10.1016/j.chemosphere.2015.11.080](https://doi.org/10.1016/j.chemosphere.2015.11.080).
- Lopez, -Espinosa Maria-Jose, D. Mondal, B. Armstrong, M.S. Bloom, and T. Fletcher. 2012. Thyroid Function and Perfluoroalkyl Acids in Children Living Near a Chemical Plant. *Environmental Health Perspectives* 120(7): 1036–1041. doi: [10.1289/ehp.1104370](https://doi.org/10.1289/ehp.1104370).
- Lyu, Y., M.L. Brusseau, W. Chen, N. Yan, X. Fu, et al. 2018. Adsorption of PFOA at the Air–Water Interface during Transport in Unsaturated Porous Media. *Environ. Sci. Technol.* 52(14): 7745–7753. doi: [10.1021/acs.est.8b02348](https://doi.org/10.1021/acs.est.8b02348).
- Margenot, A.J., F.J. Calderón, and S.J. Parikh. 2016. Limitations and Potential of Spectral Subtractions in Fourier-Transform Infrared Spectroscopy of Soil Samples. *Soil Science Society of America Journal* 80(1): 10–26. doi: [10.2136/sssaj2015.06.0228](https://doi.org/10.2136/sssaj2015.06.0228).
- Marschner, B., and K. Kalbitz. 2003. Controls of bioavailability and biodegradability of dissolved organic matter in soils. *Geoderma* 113(3): 211–235. doi: [10.1016/S0016-7061\(02\)00362-2](https://doi.org/10.1016/S0016-7061(02)00362-2).
- Martin, J.W., K. Chan, S.A. Mabury, and P.J. O’Brien. 2009. Bioactivation of fluorotelomer alcohols in isolated rat hepatocytes. *Chemico-Biological Interactions* 177(3): 196–203. doi: [10.1016/j.cbi.2008.11.001](https://doi.org/10.1016/j.cbi.2008.11.001).
- McKnight, D.M., E.W. Boyer, P.K. Westerhoff, P.T. Doran, T. Kulbe, et al. 2001. Spectrofluorometric characterization of dissolved organic matter for indication of precursor organic material and aromaticity. *Limnology and Oceanography* 46(1): 38–48. doi: [10.4319/lo.2001.46.1.0038](https://doi.org/10.4319/lo.2001.46.1.0038).
- Minor, E.C., M.M. Swenson, B.M. Mattson, and A.R. Oyler. 2014. Structural characterization of dissolved organic matter: a review of current techniques for isolation and analysis. *Environ. Sci.: Processes Impacts* 16(9): 2064–2079. doi: [10.1039/C4EM00062E](https://doi.org/10.1039/C4EM00062E).
- Murphy, D.V., A.J. Macdonald, E.A. Stockdale, K.W.T. Goulding, S. Fortune, et al. 2000. Soluble organic nitrogen in agricultural soils. *Biology and Fertility of Soils* 30(5–6): 374–387. doi: [10.1007/s003740050018](https://doi.org/10.1007/s003740050018).
- Murphy, K.R., C.A. Stedmon, D. Graeber, and R. Bro. 2013. Fluorescence spectroscopy and multi-way techniques. *PARAFAC. Anal. Methods* 5(23): 6557. doi: [10.1039/c3ay41160e](https://doi.org/10.1039/c3ay41160e).
- Nelson, J.W., E.E. Hatch, and T.F. Webster. 2010. Exposure to Polyfluoroalkyl Chemicals and Cholesterol, Body Weight, and Insulin Resistance in the General U.S. Population. *Environmental Health Perspectives* 118(2): 197–202. doi: [10.1289/ehp.0901165](https://doi.org/10.1289/ehp.0901165).
- Newton, S., R. McMahan, J.A. Stoeckel, M. Chislock, A. Lindstrom, et al. 2017. Novel Polyfluorinated Compounds Identified Using High Resolution Mass Spectrometry Downstream of Manufacturing Facilities near Decatur, Alabama. *Environ. Sci. Technol.*: 9.

- Ohno, T. 2002. Fluorescence Inner-Filtering Correction for Determining the Humification Index of Dissolved Organic Matter. *Environ. Sci. Technol.* 36(4): 742–746. doi: [10.1021/es0155276](https://doi.org/10.1021/es0155276).
- Ohno, T., and R. Bro. 2006. Dissolved Organic Matter Characterization Using Multiway Spectral Decomposition of Fluorescence Landscapes. *Soil Science Society of America Journal* 70(6): 2028–2037. doi: [10.2136/sssaj2006.0005](https://doi.org/10.2136/sssaj2006.0005).
- Ohno, T., J. Chorover, A. Omoike, and J. Hunt. 2007. Molecular weight and humification index as predictors of adsorption for plant- and manure-derived dissolved organic matter to goethite. *European Journal of Soil Science* 58(1): 125–132. doi: [10.1111/j.1365-2389.2006.00817.x](https://doi.org/10.1111/j.1365-2389.2006.00817.x).
- Ohno, T., Z. He, R.L. Sleighter, C.W. Honeycutt, and P.G. Hatcher. 2010. Ultrahigh Resolution Mass Spectrometry and Indicator Species Analysis to Identify Marker Components of Soil- and Plant Biomass-Derived Organic Matter Fractions. ACS Publications. doi: [10.1021/es101089t](https://doi.org/10.1021/es101089t).
- Omoike, A., and J. Chorover. 2006. Adsorption to goethite of extracellular polymeric substances from *Bacillus subtilis*. *Geochimica et Cosmochimica Acta* 70(4): 827–838. doi: [10.1016/j.gca.2005.10.012](https://doi.org/10.1016/j.gca.2005.10.012).
- Peuravuori, J., and K. Pihlaja. 1997. Molecular size distribution and spectroscopic properties of aquatic humic substances. *Analytica Chimica Acta* 337(2): 133–149. doi: [10.1016/S0003-2670\(96\)00412-6](https://doi.org/10.1016/S0003-2670(96)00412-6).
- Pizzurro, D.M., M. Seeley, L.E. Kerper, and B.D. Beck. 2019. Interspecies differences in perfluoroalkyl substances (PFAS) toxicokinetics and application to health-based criteria. *Regulatory Toxicology and Pharmacology* 106: 239–250. doi: [10.1016/j.yrtph.2019.05.008](https://doi.org/10.1016/j.yrtph.2019.05.008).
- Pucher, M., U. Wünsch, G. Weigelhofer, K. Murphy, T. Hein, et al. 2019. staRdom: Versatile Software for Analyzing Spectroscopic Data of Dissolved Organic Matter in R. *Water* 11(11): 2366. doi: [10.3390/w11112366](https://doi.org/10.3390/w11112366).
- Qi, Y., H. Cao, W. Pan, C. Wang, and Y. Liang. 2022. The role of dissolved organic matter during Per- and Polyfluorinated Substance (PFAS) adsorption, degradation, and plant uptake: A review. *Journal of Hazardous Materials* 436: 129139. doi: [10.1016/j.jhazmat.2022.129139](https://doi.org/10.1016/j.jhazmat.2022.129139).
- Qin, X., B. Yao, L. Jin, X. Zheng, J. Ma, et al. 2020. Characterizing Soil Dissolved Organic Matter in Typical Soils from China Using Fluorescence EEM–PARAFAC and UV–Visible Absorption. *Aquat Geochem* 26(1): 71–88. doi: [10.1007/s10498-019-09366-7](https://doi.org/10.1007/s10498-019-09366-7).
- R Core Team. 2020. R: A Language and Environment for Statistical Computing. <https://www.r-project.org/>.
- Resch-Genger, U., and P.C. DeRose. 2010. Fluorescence standards: Classification, terminology, and recommendations on their selection, use, and production (IUPAC Technical Report). *Pure and Applied Chemistry* 82(12): 2315–2335. doi: [10.1351/PAC-REP-09-09-02](https://doi.org/10.1351/PAC-REP-09-09-02).
- Riffaldi, R., R. Levi-Minzi, and A. Saviozzi. 1983. Humic fractions of organic wastes. *Agriculture, Ecosystems & Environment* 10(4): 353–359. doi: [10.1016/0167-8809\(83\)90086-5](https://doi.org/10.1016/0167-8809(83)90086-5).
- R. Murphy, K., C. A. Stedmon, D. Graeber, and R. Bro. 2013. Fluorescence spectroscopy and multi-way techniques. PARAFAC. *Analytical Methods* 5(23): 6557–6566. doi: [10.1039/C3AY41160E](https://doi.org/10.1039/C3AY41160E).

- Rochette, P., and E.G. Gregorich. 1998. Dynamics of soil microbial biomass C, soluble organic C and CO₂ evolution after three years of manure application. *Can. J. Soil. Sci.* 78(2): 283–290. doi: [10.4141/S97-066](https://doi.org/10.4141/S97-066).
- Santos, F.T.D., C. Fehmberger, C.M. Aloisio, I.R. Bautitz, and E. Hermes. 2021. Composting of swine production chain wastes with addition of crude glycerin: organic matter degradation kinetics, functional groups, and carboxylic acids. *Environ Sci Pollut Res* 28(36): 50542–50553. doi: [10.1007/s11356-021-14063-6](https://doi.org/10.1007/s11356-021-14063-6).
- Schwarzenbach René P., P.M. Gschwend, and D.M. Imboden. 2003. *Environmental Organic Chemistry*. John Wiley & Sons, New York, NY.
- Shin, H.-M., V.M. Vieira, P.B. Ryan, R. Detwiler, B. Sanders, et al. 2011. Environmental Fate and Transport Modeling for Perfluorooctanoic Acid Emitted from the Washington Works Facility in West Virginia. *Environ. Sci. Technol.* 45(4): 1435–1442. doi: [10.1021/es102769t](https://doi.org/10.1021/es102769t).
- Sigmund, G., H.P.H. Arp, B.M. Aumeier, T.D. Bucheli, B. Chefetz, et al. 2022. Sorption and Mobility of Charged Organic Compounds: How to Confront and Overcome Limitations in Their Assessment. *Environ. Sci. Technol.* 56(8): 4702–4710. doi: [10.1021/acs.est.2c00570](https://doi.org/10.1021/acs.est.2c00570).
- Smith, B. 1998. *Infrared spectral interpretation: A systematic approach*. CRC Press, Boca Raton, FL.
- Stedmon, C.A., and R. Bro. 2008. Characterizing dissolved organic matter fluorescence with parallel factor analysis: a tutorial. *Limnology and Oceanography: Methods* 6(11): 572–579. doi: [10.4319/lom.2008.6.572](https://doi.org/10.4319/lom.2008.6.572).
- Stedmon, C.A., and S. Markager. 2005. Resolving the variability in dissolved organic matter fluorescence in a temperate estuary and its catchment using PARAFAC analysis. *Limnology and Oceanography* 50(2): 686–697. doi: <https://doi.org/10.4319/lo.2005.50.2.0686>.
- Steenland, K., L. Zhao, A. Winquist, and C. Parks. 2013. Ulcerative Colitis and Perfluorooctanoic Acid (PFOA) in a Highly Exposed Population of Community Residents and Workers in the Mid-Ohio Valley. *Environmental Health Perspectives* 121(8): 900–905. doi: [10.1289/ehp.1206449](https://doi.org/10.1289/ehp.1206449).
- Sumner, M.E., and W.P. Miller. 1996. Cation Exchange Capacity and Exchange Coefficients. *Methods of Soil Analysis*. John Wiley & Sons, Ltd. p. 1201–1229
- Sunderland, E.M., X.C. Hu, C. Dassuncao, A.K. Tokranov, C.C. Wagner, et al. 2019. A review of the pathways of human exposure to poly- and perfluoroalkyl substances (PFASs) and present understanding of health effects. *J Expo Sci Environ Epidemiol* 29(2): 131–147. doi: [10.1038/s41370-018-0094-1](https://doi.org/10.1038/s41370-018-0094-1).
- Taniyasu, S., N. Yamashita, H.-B. Moon, K.Y. Kwok, P.K.S. Lam, et al. 2013. Does wet precipitation represent local and regional atmospheric transportation by perfluorinated alkyl substances? *Environment International* 55: 25–32. doi: [10.1016/j.envint.2013.02.005](https://doi.org/10.1016/j.envint.2013.02.005).
- Tittlemier, S.A., K. Pepper, L. Edwards, and G. Tomy. 2005. Development and characterization of a solvent extraction–gas chromatographic/mass spectrometric method for the analysis of perfluorooctanesulfonamide compounds in solid matrices. *Journal of Chromatography A* 1066(1–2): 189–195. doi: [10.1016/j.chroma.2005.01.069](https://doi.org/10.1016/j.chroma.2005.01.069).

- Venkatesan, A.K., and R.U. Halden. 2013. National inventory of perfluoroalkyl substances in archived U.S. biosolids from the 2001 EPA National Sewage Sludge Survey. *Journal of Hazardous Materials* 252–253: 413–418. doi: [10.1016/j.jhazmat.2013.03.016](https://doi.org/10.1016/j.jhazmat.2013.03.016).
- Veum, K.S., K.W. Goyne, R.J. Kremer, R.J. Miles, and K.A. Sudduth. 2014. Biological indicators of soil quality and soil organic matter characteristics in an agricultural management continuum. *Biogeochemistry* 117(1): 81–99. doi: [10.1007/s10533-013-9868-7](https://doi.org/10.1007/s10533-013-9868-7).
- Viticoski, R.L., D. Wang, M.A. Feltman, V. Mulabagal, S.R. Rogers, et al. 2022. Spatial distribution and mass transport of Perfluoroalkyl Substances (PFAS) in surface water: A statewide evaluation of PFAS occurrence and fate in Alabama. *Science of The Total Environment* 836: 155524. doi: [10.1016/j.scitotenv.2022.155524](https://doi.org/10.1016/j.scitotenv.2022.155524).
- Wang, Z., J.C. DeWitt, C.P. Higgins, and I.T. Cousins. 2017. A Never-Ending Story of Per- and Polyfluoroalkyl Substances (PFASs)? *Environ. Sci. Technol.* 51(5): 2508–2518. doi: [10.1021/acs.est.6b04806](https://doi.org/10.1021/acs.est.6b04806).
- Wang, K., W. Li, X. Gong, Y. Li, C. Wu, et al. 2013. Spectral study of dissolved organic matter in biosolid during the composting process using inorganic bulking agent: UV–vis, GPC, FTIR and EEM. *International Biodeterioration & Biodegradation* 85: 617–623. doi: [10.1016/j.ibiod.2013.03.033](https://doi.org/10.1016/j.ibiod.2013.03.033).
- Wang, K., X. Li, C. He, C.-L. Chen, J. Bai, et al. 2014. Transformation of dissolved organic matters in swine, cow and chicken manures during composting. *Bioresource Technology* 168: 222–228. doi: [10.1016/j.biortech.2014.03.129](https://doi.org/10.1016/j.biortech.2014.03.129).
- Wang, F., K. Shih, R. Ma, and X. Li. 2015. Influence of cations on the partition behavior of perfluoroheptanoate (PFHpA) and perfluorohexanesulfonate (PFHxS) on wastewater sludge. *Chemosphere* 131: 178–183. doi: [10.1016/j.chemosphere.2015.03.024](https://doi.org/10.1016/j.chemosphere.2015.03.024).
- Wang, W., G. Rhodes, J. Ge, X. Yu, and H. Li. 2020. Uptake and accumulation of per- and polyfluoroalkyl substances in plants. *Chemosphere* 261: 127584. doi: [10.1016/j.chemosphere.2020.127584](https://doi.org/10.1016/j.chemosphere.2020.127584).
- Wang, Y., X. Zhang, X. Zhang, Q. Meng, F. Gao, et al. 2017. Characterization of spectral responses of dissolved organic matter (DOM) for atrazine binding during the sorption process onto black soil. *Chemosphere* 180: 531–539. doi: [10.1016/j.chemosphere.2017.04.063](https://doi.org/10.1016/j.chemosphere.2017.04.063).
- Washington, J.W., H. Yoo, J.J. Ellington, T.M. Jenkins, and E.L. Libelo. 2010. Concentrations, Distribution, and Persistence of Perfluoroalkylates in Sludge-Applied Soils near Decatur, Alabama, USA. *Environ. Sci. Technol.* 44(22): 8390–8396. doi: [10.1021/es1003846](https://doi.org/10.1021/es1003846).
- Weber, A.K., L.B. Barber, D.R. LeBlanc, E.M. Sunderland, and C.D. Vecitis. 2017. Geochemical and Hydrologic Factors Controlling Subsurface Transport of Poly- and Perfluoroalkyl Substances, Cape Cod, Massachusetts. *Environ. Sci. Technol.* 51(8): 4269–4279. doi: [10.1021/acs.est.6b05573](https://doi.org/10.1021/acs.est.6b05573).
- Wei, C., X. Song, Q. Wang, and Z. Hu. 2017. Sorption kinetics, isotherms and mechanisms of PFOS on soils with different physicochemical properties. *Ecotoxicology and Environmental Safety* 142: 40–50. doi: [10.1016/j.ecoenv.2017.03.040](https://doi.org/10.1016/j.ecoenv.2017.03.040).

- Weishaar, J.L., G.R. Aiken, B.A. Bergamaschi, M.S. Fram, R. Fujii, et al. 2003. Evaluation of Specific Ultraviolet Absorbance as an Indicator of the Chemical Composition and Reactivity of Dissolved Organic Carbon. *Environ. Sci. Technol.* 37(20): 4702–4708. doi: [10.1021/es030360x](https://doi.org/10.1021/es030360x).
- Xia, X., Z. Dai, A.H. Rabearisoa, P. Zhao, and X. Jiang. 2015. Comparing humic substance and protein compound effects on the bioaccumulation of perfluoroalkyl substances by *Daphnia magna* in water. *Chemosphere* 119: 978–986. doi: [10.1016/j.chemosphere.2014.09.034](https://doi.org/10.1016/j.chemosphere.2014.09.034).
- Xiao, F., B. Jin, S.A. Golovko, M.Y. Golovko, and B. Xing. 2019. Sorption and Desorption Mechanisms of Cationic and Zwitterionic Per- and Polyfluoroalkyl Substances in Natural Soils: Thermodynamics and Hysteresis. *Environ. Sci. Technol.* 53(20): 11818–11827. doi: [10.1021/acs.est.9b05379](https://doi.org/10.1021/acs.est.9b05379).
- Xiao, F., M.F. Simcik, T.R. Halbach, and J.S. Gulliver. 2015. Perfluorooctane sulfonate (PFOS) and perfluorooctanoate (PFOA) in soils and groundwater of a U.S. metropolitan area: Migration and implications for human exposure. *Water Research* 72: 64–74. doi: [10.1016/j.watres.2014.09.052](https://doi.org/10.1016/j.watres.2014.09.052).
- Xu, D., C. Li, Y. Wen, and W. Liu. 2013. Antioxidant defense system responses and DNA damage of earthworms exposed to Perfluorooctane sulfonate (PFOS). *Environmental Pollution* 174: 121–127. doi: [10.1016/j.envpol.2012.10.030](https://doi.org/10.1016/j.envpol.2012.10.030).
- Yamashita, Y., R. Jaffé, N. Maie, and E. Tanoue. 2008. Assessing the dynamics of dissolved organic matter (DOM) in coastal environments by excitation emission matrix fluorescence and parallel factor analysis (EEM-PARAFAC). *Limnology and Oceanography* 53(5): 1900–1908. doi: [10.4319/lo.2008.53.5.1900](https://doi.org/10.4319/lo.2008.53.5.1900).
- You, C., C. Jia, and G. Pan. 2010. Effect of salinity and sediment characteristics on the sorption and desorption of perfluorooctane sulfonate at sediment-water interface. *Environmental Pollution* 158(5): 1343–1347. doi: [10.1016/j.envpol.2010.01.009](https://doi.org/10.1016/j.envpol.2010.01.009).
- Young, C.J., V.I. Furdui, J. Franklin, R.M. Koerner, D.C.G. Muir, et al. 2007. Perfluorinated Acids in Arctic Snow: New Evidence for Atmospheric Formation. *Environ. Sci. Technol.* 41(10): 3455–3461. doi: [10.1021/es0626234](https://doi.org/10.1021/es0626234).
- Yu, Q., R. Zhang, S. Deng, J. Huang, and G. Yu. 2009. Sorption of perfluorooctane sulfonate and perfluorooctanoate on activated carbons and resin: Kinetic and isotherm study. *Water Research* 43(4): 1150–1158. doi: [10.1016/j.watres.2008.12.001](https://doi.org/10.1016/j.watres.2008.12.001).
- Zareitalabad, P., J. Siemens, F. Wichern, W. Amelung, and R. Georg Joergensen. 2013. Dose-dependent reactions of *Aporrectodea caliginosa* to perfluorooctanoic acid and perfluorooctanesulfonic acid in soil. *Ecotoxicology and Environmental Safety* 95: 39–43. doi: [10.1016/j.ecoenv.2013.05.012](https://doi.org/10.1016/j.ecoenv.2013.05.012).
- Zhao, H., B. Qu, Y. Guan, J. Jiang, and X. Chen. 2016. Influence of salinity and temperature on uptake of perfluorinated carboxylic acids (PFCAs) by hydroponically grown wheat (*Triticum aestivum* L.). *SpringerPlus* 5(1): 541. doi: [10.1186/s40064-016-2016-9](https://doi.org/10.1186/s40064-016-2016-9).
- Zhao, L., L. Zhu, L. Yang, Z. Liu, and Y. Zhang. 2012. Distribution and desorption of perfluorinated compounds in fractionated sediments. *Chemosphere* 88(11): 1390–1397. doi: [10.1016/j.chemosphere.2012.05.062](https://doi.org/10.1016/j.chemosphere.2012.05.062).

- Zhao, S., S. Fang, L. Zhu, L. Liu, Z. Liu, et al. 2014. Mutual impacts of wheat (*Triticum aestivum* L.) and earthworms (*Eisenia fetida*) on the bioavailability of perfluoroalkyl substances (PFASs) in soil. *Environmental Pollution* 184: 495–501. doi: [10.1016/j.envpol.2013.09.032](https://doi.org/10.1016/j.envpol.2013.09.032).
- Zheng, G., E. Schreder, J.C. Dempsey, N. Uding, V. Chu, et al. 2021. Per- and Polyfluoroalkyl Substances (PFAS) in Breast Milk: Concerning Trends for Current-Use PFAS. *Environ. Sci. Technol.* 55(11): 7510–7520. doi: [10.1021/acs.est.0c06978](https://doi.org/10.1021/acs.est.0c06978).
- Zhi, Y., and J. Liu. 2019. Column chromatography approach to determine mobility of fluorotelomer sulfonates and polyfluoroalkyl betaines. *Science of The Total Environment* 683: 480–488. doi: [10.1016/j.scitotenv.2019.05.149](https://doi.org/10.1016/j.scitotenv.2019.05.149).
- Zsolnay, Á. 2003. Dissolved organic matter: artefacts, definitions, and functions. *Geoderma* 113(3): 187–209. doi: [10.1016/S0016-7061\(02\)00361-0](https://doi.org/10.1016/S0016-7061(02)00361-0).